Michigan State University

This is to certify that the

dissertation entitled

Characterization of the Donor To
The Reaction Center in Photosystem II
By Electron Nuclear Double Resonance
(Endor) Spectroscopy

presented by

Ivan D. Rodriguez

has been accepted towards fulfillment
of the requirements for

Ph.D. degree in Chemistry

Gerald T. Babcock
Major professor

Date 10/30/89.

CHARACTERIZATION OF THE DONOR TO THE REACTION CENTER IN PHOTOSYSTEM II BY ELECTRON NUCLEAR DOUBLE RESONANCE (ENDOR) SPECTROSCOPY

By

Iván David Rodriguez

A DISSERTATION

Submitted to
Michigan State University
in partial fulfillment of the requirements
for the degree of

DOCTOR OF PHILOSOPHY

Department of Chemistry

1989

ABSTRACT

CHARACTERIZATION OF THE DONOR TO THE REACTION CENTER IN PHOTOSYSTEM II BY ELECTRON NUCLEAR DOUBLE RESONANCE (ENDOR) SPECTROSCOPY

By

Iván David Rodriguez

In photosystem II(PSII) of green plants, two tyrosine free radicals are involved in the oxygen process, along with P680, the reaction center chlorophyll. The Y_Z^+ species functions as an electron carrier between the oxygen evolving complex and P680. Y_D^+, the other tyrosyl radical present in this photosystem, has an unknown function in the photosynthetic apparatus. A characteristic, partially resolved EPR signal is a common feature for both of these radicals. Even though Y_Z^+ and Y_D^+ are functionally different, their chemical structure and orientation in the membrane appear to be essentially the same. Only in their EPR power saturation behavior do Y_Z^+ and Y_D^+ show a difference. The EPR lines of these protein bound radicals are broadened owing to unresolved hyperfine structure, making it difficult to extract information from these poorly resolved spectra. Under these conditions additional spectroscopic techniques, such as electron nuclear double resonance (ENDOR), must be used to extract the different proton hyperfine tensor components that contribute to the EPR spectrum. In the work presented here we have used ENDOR spectroscopy to measure the hyperfine couplings for the Y_D^+ species and to explore the environment surrounding the radical. The hyperfine couplings corresponding to the β-protons are used to determine the geometry of the methylene group at the 1-position of the tyrosine phenol group.

The ar
relative
protons
addition
mined b
the diff
a way to
in PSII
which la
with the
been ab
oriented
from the
plane w
membran
ENDOR
radical an
usually we
so-called
determine
region. A
characteris
using g-ani

The analysis shows that the dihedral angles of the two methylene group protons relative to the phenol ring are not identical. As a result only one of the two protons interacts strongly with the unpaired electron spin of the radical. In addition the hyperfine tensor components of the ring protons have been determined by using two-dimensionally oriented samples. The hyperfine couplings for the different set of protons measured from the Y_D^+ ENDOR spectrum provided a way to calculate the unpaired spin density distribution for the tyrosine radical in PSII. The proposed unpaired spin density distribution for the Y_D^+ radical, in which large spin density is localized at the 1,3 and 5 position, is in agreement with the expected unpaired spin density for phenoxy type radicals. We have also been able to determine the orientation of the tyrosine ring plane by using oriented PSII membranes, chemical models and EPR simulations. The results from these studies show that the orientation of the Y_D^+ tyrosyl aromatic ring plane with respect to the membrane plane is such that the angle between the membrane plane and the line through carbons one and four is about 60°. ENDOR is also able to probe more subtle interactions that occur between the radical and its protein environment. The protons of nearby amino acids are usually weakly coupled to the unpaired spin and contribute resonances in the so-called matrix region. The solvent accessibility of the Y_D^+ binding site has been determined by using H_2O/D_2O exchange and analyzing the matrix ENDOR region. A hydrogen-bond to the Y_D^+ radical has been observed and its spatial characteristics with respect to the tyrosine ring plane have been determined by using g-anisotropy and physical sample orientation techniques.

To my wife, Norma Lourdes, my niece, Ivonne Marie, and my nephews, Gustavo Emanuel, Etien Rafael, and Andres Rafael.

ACKNOWLEDGMENTS

I would like to thank Dr. Gerald T. Babcock for his guidance and financial support. I would also like to thank all my fellow lab members for their friendship and camaraderie. Drs. O'Malley and Chandrashekar have my appreciation for teaching me how to run the EPR/ENDOR spectrometer. Special thanks go to my friend, Dr. Juan Lopez-Garriga, who on more than one occasion provided me a place to live. I am deeply grateful to my parents Teofilo and Irma and to all the members of my family for their support and encouragement. Finally, I would like to thank my wife, Norma, for her love, help, patience and encouragement.

TABLE OF CONTENTS

LIST OF TABLES

LIST OF FIGURES

A

$\tilde{A}$

a

BChl

Bph

Chl

D

EDTA

ENDOR

EPR

F_x, F_y, F

G

g

$\tilde{g}$

g_n

H

$\tilde{H}$

Hepes

HPLC

LIST OF ABBREVIATIONS AND SYMBOLS

A	acceptor
$\hat{\tilde{A}}$	hyperfine coupling tensor
a	isotropic hyperfine coupling constant
BChl	Bacteriochlorophyll
Bph	Bacteriopheophytin
Chl	Chlorophyll
D	donor
EDTA	ethylene diamine tetracetate
ENDOR	electron nuclear double resonance
EPR	electron paramagnetic resonance
F_X, F_A, F_B	3 iron-sulfur centers in PSI
G	gauss
g	g-value
$\hat{\tilde{g}}$	electron g tensor
g_n	nuclear g-value
H	magnetic field
$\vec{H}$	external Zeeman magnetic field vector
Hepes	2-hydroxyethyl-1-peperazineethanesulfonic acid
HPLC	high pressure liquid chromatography

b

I

Γ

İ

L_{mon}

L_{tot}

Mes

M_n

M_n

NADP

NMR

OEC

PSI

PSII

P_{680}

P_{700}

PQ

pH

Q_a, Q_b

S

Ṡ

$S_n (n=0-4)$

Ṫ

h	Planck's constant
I	nuclear spin
I^-	reduced first intermediate occeptor in PSI
$\hat{I}$	nuclear spin operator
L_{ENDOR}	number of resonance lines in ENDOR
L_{ESR}	number of resonance lines in ESR
Mes	4-morpholine-ethanosulphonic acid
M_I	nuclear spin quantum number
M_s	electron spin quantum number
NADP	nicotidamide adenine dinucleotide phosphate
NMR	nuclear magnetic resonance
OEC	oxygen evolving complex
PSI	photosystem I
PSII	photosystem II
P_{680}	reaction center chlorophyll in PSII
P_{700}	reaction center chlorophyll in PSI
PQ	plastoquinone
pH	$-\log[H^+]$
Q_a, Q_b	acceptor quinones
S	spin of an electron
$\hat{S}$	electron spin operator
S_n(n=0-4)	states of charge accumulating system on the donor side of PSII
$\hat{T}$	dipolar hyperfine tensor

T_{1e}	electron spin-lattice relaxation time
T_{1n}	nuclear spin-lattice relaxation time
Tris	tris(hydroxymethyl) amino methane
T_x	cross relaxation time
Y_z^+, Y_D^+	oxidized tyrosine radicals in PSII
β	Bohr magneton
β_n	nuclear magneton
μ_s	magnetic moment associated with the spin of an electron
$\psi_{(o)}$	electron wave function

CHAPTER 1
INTRODUCTION

Photosynthesis is the energy conversion process on which all life on earth depends. All our fossil fuel and all our food are products of photosynthetic reactions and the presence of oxygen in the earth's atmosphere is a direct result of the photosynthetic reactions of higher plants and algae. The photosynthetic process in this type of organism can be described with the following reaction:

$$H_2O + CO_2 \xrightarrow{h\nu} CH_2O + O_2 \qquad (1)$$

Much progress has been made in understanding the photosynthetic process since the above reaction was proposed, but many aspects of the molecular mechanisms of the reactions in photosynthesis are still obscure.

The ability to perform photosynthesis is shared by some bacteria, although photosynthetic bacteria utilize light of appreciably longer wavelength than algae and higher plants. The photosynthetic system of bacteria uses only one light reaction to move an electron from the ultimate donor to the final acceptor. In contrast, algae and higher plants use two photoreactions in series to transport electrons from water, which is oxidized to O_2 (Equation 1), to the final acceptor, nicotinamide adenine dinucleotide phosphate ($NADP^+$). Since the primary charge separation process and subsequent stabilization steps correspond to

transfer of an unpaired electron, magnetic resonance techniques such as electron paramagnetic resonance (EPR) and electron nuclear double resonance (ENDOR) are powerful tools to investigate the structure and function of photosynthetic systems.

At a molecular level there are some properties common to all photosynthetic organisms. Each photosystem contains a unit called the reaction center, in which the primary process, a light induced charge separation, takes place. The products of these charge separations are stabilized in subsequent electron transfer reactions. Another feature of the photosynthetic process common to bacteria, higher plants, and algae is that all reaction centers are associated with the so-called antenna pigments, of which chlorophyll (Chl) and bacteriochlorophyll (BChl) are the most important. Upon photoexcitation of one of the antenna molecules, the energy absorbed is eventually transferred to the primary donor of the reaction center. Once the primary donor (D) is excited it transfers an electron to an acceptor (A), which produces the primary charge separation (1-6)

$$DA \xrightarrow{h\nu} D^{+}A^{-} \qquad (2)$$

In higher plants and algae there are two different photosystems, Photosystem I (PSI) and Photosystem II (PSII), which are connected through a series of redox components. These two photosystems work in series to drive electrons from the oxygen evolving complex (OEC) in PSII to the reducing site of $NADP^{+}$ in PSI. Figure 1.1 shows the so called Z-scheme for higher plants and algae.

Figure 1.1. Flow of electrons through the oxygen evolving complex (OEC) in Photosystem II to Photosystem I.

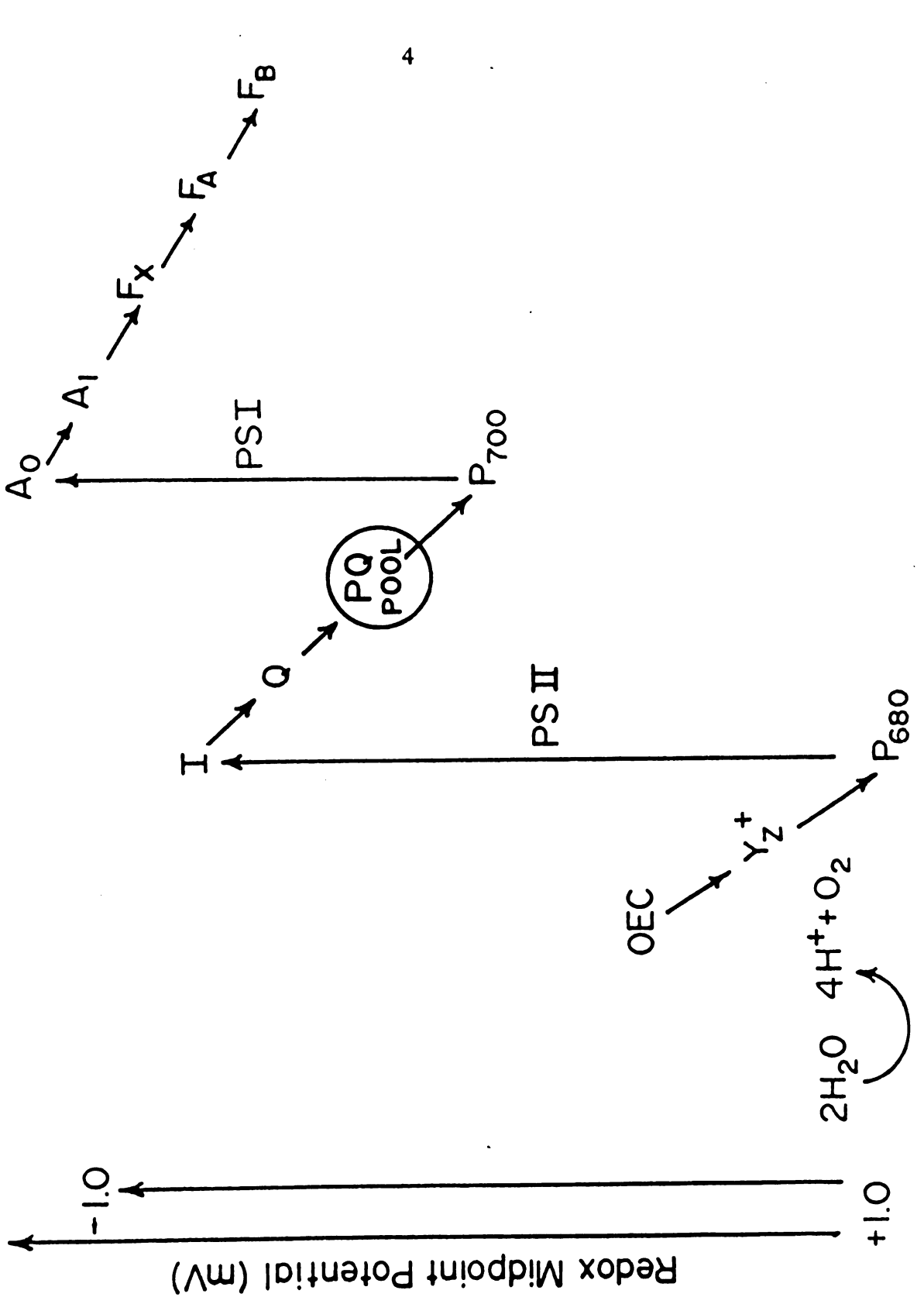
Redox Midpoint Potential (mV)
+1.0
-1.0
2H2O 4H+ + O2
OEC
YZ+
P680
PS II
I
Q
PQ POOL
P700
PSI
A0
A1
FX
FA
FB

(7-11).

to a h

recent

(16) th

and the

trons th

mangan

PSI of g

difficult

ms (22).

prepara

centrati

through

acceptor

F_v, F_x)

this pho

B

thetic re

the struc

understo

because

been crys

The first intermediary acceptor, I, in PSII is a pheophytin molecule (7-11). The secondary acceptor Q is a plastoquinone and is magnetically coupled to a high spin iron ion (12-14). The secondary donor of PSII, known as Z, but recently renamed Y_z^+ owing to its tyrosine origin (15), serves to reduce rapidly (16) the primary donor in the reaction center of PSII, P_{680} (P stands for pigment and the subscript refers to the wavelength of maximum absorption). The electrons that reduce Y_z^+ come from the oxidation of water that takes place at the manganese ensemble in the OEC (17-21). As opposed to the primary donor in PSI of green plants or to the cation radicals of bacterial systems, P_{680} has been difficult to trap in its oxidized state. Even at low temperatures its lifetime is 3-4 ms (22). However, the transient P_{680} EPR signal has been observed in PSII preparations under conditions where the electron transfer is inhibited by concentrations of ferricyanide greater than 3mM (23). PSI and PSII are connected through a plastoquinone pool, which funnels electrons from PSII to PSI. The acceptor side of PSI is composed of a Chl *a* molecule, 3 iron-sulfur centers (F_x, F_A, F_B) and possibly a quinone (24); $NADP^+$ is the ultimate electron acceptor in this photosystem.

Bacterial photosynthetic reactions are less complex than plant photosynthetic reactions due to the fact that they involve only one photosystem. Hence, the structure of the reaction center of the photosynthetic purple bacteria is better understood than that of the reaction centers in plant photosystems, particularly because the reaction center complexes from two photosynthetic bacteria have been crystallized (24-29). X-ray diffraction analysis of crystallized reaction

center
about
the fir
accept
sulfur
sulfur
similar
bacteria

Donor S

T

(i.e., BC

molecul

species

thesis d

EPR si

the EPR

(i.e., √2

suggests

values f

radical s

hypothes

resonanc

centers of *Rhodospseudomonas virides* (24-30) has given detailed information about the organization of the electron transfer components. In purple bacteria the first intermediary acceptor is a bacteriopheophytin (BPh) molecule, secondary acceptors are two quinone molecules complexed to an iron. However, in green sulfur bacteria the acceptor side contains a BChl c molecule (33-34) and two iron sulfur centers (35). Thus, the acceptor side of the green sulfur bacteria is similar to that of PSI in plant photosynthesis and the acceptor side of purple bacteria is more like the acceptor side of PSII in plant photosynthesis.

EPR and ENDOR in Photosynthesis

Donor Side

The primary donor in plant and bacterial photosynthesis is a (B)Chl a (*i.e.*, BChl a for bacterial systems and Chl a for plant systems) molecule or molecules. In principle, EPR provides a way of determining the structure of this species but the EPR signal of the primary donors in bacteria and plant photosynthesis does not show resolved hyperfine structure. However, the linewidth of the EPR signal does contain some information. The reduction of the linewidth in the EPR signal of the primary donor in photosynthetic bacteria by a factor of 1.4 (*i.e.*, $\sqrt{2}$) relative to that of chemically oxidized monomeric BChl a *in vitro* suggests the dimeric structure proposed by Norris and co-workers (34). Accurate values for the electron spin density on the carbon atoms of the conjugated radical species making up the primary donor would provide a direct test of this hypothesis. Such information can be obtained through electron nuclear double resonance (ENDOR).

By using ENDOR spectroscopy Feher and co-workers (35) showed that the hyperfine splittings, which are directly related to the unpaired spin density distribution on the π-system of the carbon framework of BChl a in the primary donor, were half of those of the corresponding hyperfine splittings of BChl a *in vitro*. This provided strong support for the idea that the primary donor in bacterial systems is a BChl dimer (or special pair in Norris terminology (34)). The assignment of the observed ENDOR lines to protons of the BChl molecule took some effort. There are 4 classes of protons in BChl a (Figure 1.2): a) the CH_3 groups on rings I and III, b) the four β-protons (one carbon away from the conjugated system) in rings II and IV and the β-proton at C10, c) the α-protons on the three methine positions, d) δ-protons, two carbons away from the conjugated rings.

Even though the protons of the CH_3 groups are β-protons, they can be distinguished from other β-protons because of the rapid rotation of the CH_3 groups, even at temperatures below 80K (35). The α-protons have very strong anisotropic hyperfine splittings and are difficult to observe due to line broadening. The δ-protons have very small hyperfine splittings and their ENDOR lines will be grouped close to the free proton frequency; because their hyperfine splittings are dependent on geometry they will be difficult to detect in the frozen state. The β-protons on the ring are coupled to the unpaired electron spin densities on the adjacent ring carbons, but their ENDOR lines may be broadened because of differences in their position with respect to the Chl plane. The hyperfine splitting of a β-proton is given by (36)

Figure 1.2. Chlorophylls and bacteriochlorophylls. Molecules without the central Mg, atom are called (bacterio) pheophytin.

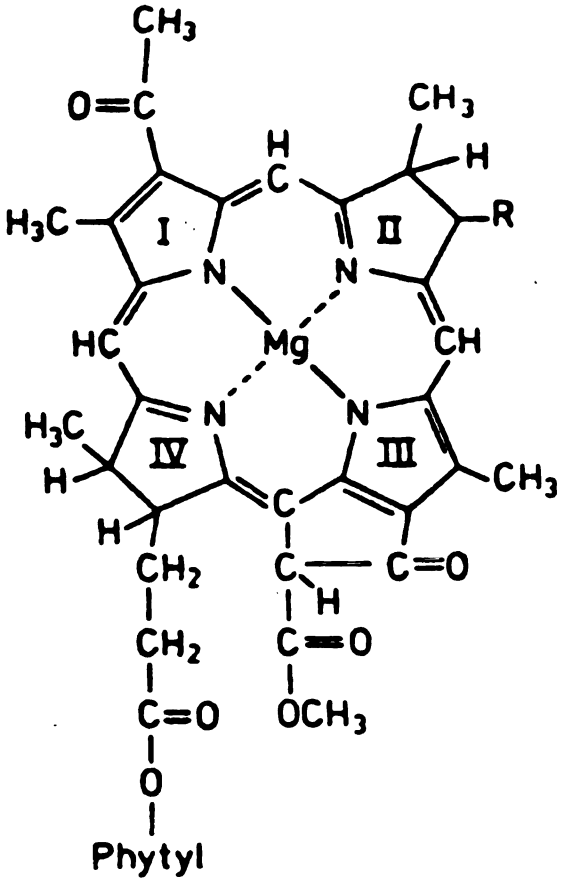

Bacteriochlorophyll *a*: R = H−CH_2−CH_3

Bacteriochlorophyll *b*: R = =CH−CH_3

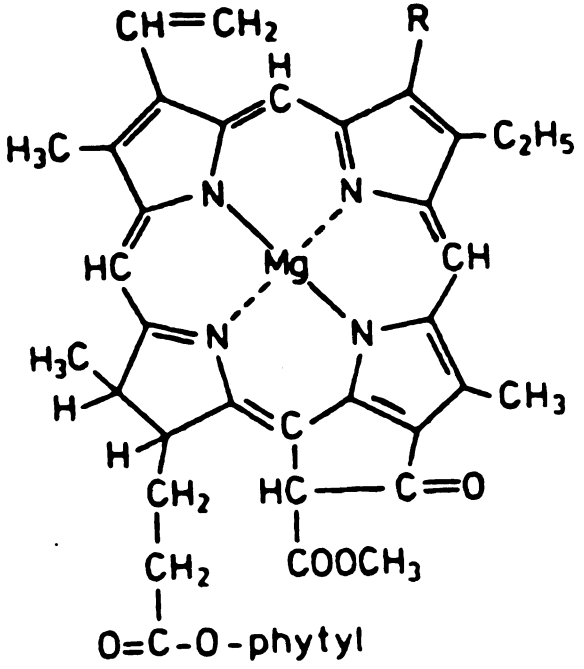

Chlorophyll *a*; R = CH_3

Chlorophyll *b*; R = CHO

$$a_\beta = (B_0 + B_1 COS^2\theta)\rho \qquad (3)$$

where B_0 and B_1 are constants ($B_1/B_0 \approx 10$), θ is the dihedral angle between the C_α-C_β-H plane and the p_z orbital at the C_α, and ρ is the spin density on the C_α atom. For rotating CH_3 groups $<\cos^2\theta> = 1/2$ and $a_\beta \approx (B_0 + 1/2B_1)\rho$.

By using the above guidelines and *in vitro* model compound studies, the ENDOR lines of the BChl a in the primary donor were assigned (37-40). In addition, the use of triple ENDOR techniques (40) permitted the determination of the sign of the hyperfine splittings, strengthening the assignment of various lines to α and β-protons.

As we have seen, for the bacterial photosystem the proposed special pair hypothesis was strongly supported by proton ENDOR experiments. For the primary donor in plant photosynthesis, however, the results were less unambigious (35,37,41). Norris and co-workers (37,41) obtained a low temperature ENDOR spectrum of the chemically oxidized algae *S. lividus* (37) and *C. vulgaris* (41) PSI reaction center chlorophylls and compared them with the low temperature spectrum of Chl a cation radical in solution, oxidized with I_2 or $FeCl_3$. They made assignments by selective deuteration and chemical modification *in vitro* (37,39,42) of Chl a. Based on their findings they concluded that the unpaired electron was delocalized between two Chl a molecules of the *in vivo* special pair. However, ENDOR experiments on PSI particles made from spinach chloroplasts (43) led to similar data but different conclusions. O'Malley and

Babcock (44) compared the proton ENDOR spectra of the primary donor in PSI from spinach chloroplasts and PSI particles to the corresponding ENDOR spectrum of monomeric Chl a cation radicals. They interpreted the hyperfine splittings of the radical *in vivo* in terms of a Chl a cation radical monomer. The reduction in the α-carbon hyperfine splittings, and hence the α-carbon unpaired spin densities observed for the *in vivo* species when compared to the *in vitro* radical, was attributed to differences in the composition of the ground state orbital of the two systems (44). For the primary donor in PSI in plants, a mixture of 75% D_0 and 25% D_1, where D_0 and D_1 represent the ground and first excited state orbitals calculated by Petke and co-workers for Chl a cation radical (45), gave good agreement between calculated and experimental spin density reduction factors. The following interactions of the pigment ion with its protein environment were given as possible factors responsible for lowering the D_1 level *in vivo:* ligation of the central Mg atom with its protein surroundings, hydrogen bonding to the 9-keto carbonyl group (Figure 1.2) and electrostatic interactions with charged amino acid residues. O'Malley and co-workers proposed that the primary donors of PSII and PSI in plants were both monomeric Chl a species in which the D_1 orbital makes a significant contribution to the unpaired spin density distribution. Up to this date whether the primary donors in plant photosynthesis are monomeric or dimeric structures is an open question.

The secondary donor to the oxidized reaction center (B)Chl depends on each photosystem: Y_z for PSII in plants, a cytochrome for bacteria, and plastocyanin for PSI. Here we focus on Y_z^+, the intermediate electron carrier

between the Mn complex in the OEC and the reaction center in PSII (Figure 1) (46) . This radical was first observed by EPR in PSII that had lost the ability to evolve oxygen (47). Based on EPR (48,49) and optical (19,50) data it was suggested that the $Y_z^{\bullet}$ was a plastoquinone cation radical. However, it has been recently postulated that $Y_z^{\bullet}$ species corresponds to a tyrosine residue in PSII (15,51). Another cofactor known as $Y_D^{\bullet}$ (15,16,51) shows a similar EPR signal to that of $Y_z^{\bullet}$ but different kinetic behavior. The similarity of their EPR spectra suggests that both radicals have the same molecular structure and probably the same orientation within the protein structure. In oxygen evolving material the $Y_z^{\bullet}$ EPR signal decays in about 1 msec (52), whereas the $Y_D^{\bullet}$ EPR signal is stable for hours. The role of this latter radical in the oxygen evolving process is not clear, but recently Rutherford *et al.* (53) suggested that Y_D may be involved in maintaining the integrity of the manganese complex in the OEC.

Joliot and co-workers (54) noted that four flashes were needed before O_2 could be released. This observation led to Kok's S-state model. (55) which is well accepted:

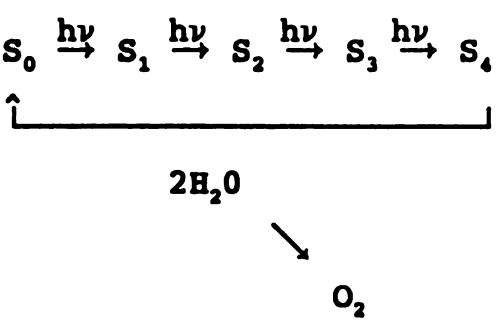

(4)

In this model S represents the water splitting center, the subscripts indicate the number of stored oxidizing equivalents and O_2 evolution occurs only after the S_4

state has

and the

transitior

four Mn

Even tho

and valer

experime

UV-VIS

resonance

been attri

suggested

spectral si

observed

(71-73) ha

excited sta

that magne

the Mn ion

with a g =

this species

Rutherford

multiline ar

the S_2 state

like Mn_4O_4

state has been reached. A manganese cluster has been associated with the OEC and the water splitting process (56-58). It has been suggested that the S-state transitions correspond to valence changes in this Mn cluster. A stoichiometry of four Mn per PSII in O_2 evolving PSII membranes has been determined (59). Even though the stoichiometry for the Mn is well established, the organization and valence states of these ions remain uncertain. At least four different experimental approaches have been used to address this question: X-ray (60-62), UV-VIS (20,21,63), extraction/quantitation techniques (64-66) and magnetic resonance (67-78). Focusing on the latter technique, a multiline EPR signal has been attributed to the Mn ensemble that is in the S_2 state (67). The authors suggested Mn_2(III,IV) or Mn_4[$(III)_3$,(IV)] structures for this Mn species from spectral simulations (68). However, Hansson and co-workers explained the observed EPR spectrum with a Mn_2(II,III) model (69,70). Brudvig and dePaula (71-73) have suggested that the S = 1/2 multiline EPR signal arises from an excited state in an envelope of states of different spin multiplicities. This implies that magnetic exchange interactions occur between at least three or all four of the Mn ions in the OEC and explains the observation of another EPR signal with a g = 4.1 (74,75) also associated with the OEC. The spectral properties of this species are characteristic of an S = 3/2 state. Brudvig and co-workers and Rutherford *et al.* have provided experimental support to indicate that both the multiline and the g = 4.1 EPR signals originate from different configurations of the S_2 state in the OEC (76,77). Brudvig and Crabtree (78) proposed a cubane-like Mn_4O_4 cluster as the structure of the manganese ensemble in the lower

S-states and suggested that the S-state transitions involve mainly a Mn(III) to Mn(IV) valence changes in the Mn cluster.

Acceptor Side

The observed EPR signal of the reduced acceptor components of the green bacteria are similar to those of PSI and the reduced acceptor components of the purple bacteria are quite similar to those of PSII. In PSI, A_o displays an EPR signal with g = 2.0017 and linewidth of 11.5 G and the A_1 EPR signal has a g = 2.0054 and linewidth of 10.8 G; A_0 is believed to be a Chl anion radical. The lower g-value and broader linewidth of the A_o EPR signal as compared to a Chl a anion radical *in vitro* has been explained in terms of magnetic interactions between the nearby iron sulfur centers (33).

The g-value and linewidth of A_1 are not characteristic of an anion of Chl. It was suggested that A_1, the intermediate that give rise to the EPR signal with g = 2.0054 and linewidth of 10.8 G, was a phylloquinone anion radical (79-81). Anions of semiquinone usually show a near gaussian EPR signal with a linewidth of 5-15 G at X-band (82-85). Semiquinone anion radicals can be differentiated from Chl anion radicals by their higher g-value which is close to 2.005. Based on EPR and optical work it was suggested that the A_1 radical was a phylloquinone anion radical (86). This was also supported by ENDOR studies on model and biological samples (87). However, recent experiments by Barry *et al.* (88) concluded that the EPR spectrum attributed to A_1 does not arise from a phylloquinone. These authors suggested that an amino acid in the PSI protein structure could be responsible for this signal.

has a

accept

has g

so-call

linewi

cryoge

coupli

compl

only o

state.

broad

later

plaine

Remo

after

reacti

(89).

the s

signa

and

iron

The analog to the acceptor side of PSII in plants, *i.e.*, the purple bacteria, has a BPh as primary acceptor (11) and an iron quinone complex as secondary acceptor. This primary acceptor shows two different EPR signals. The first one has g = 2.003 and a linewidth of about 13 G (89). The second signal is the so-called split pheophytin EPR signal (10,89-98), which shows g = 2.003 and a linewidth varying from 60-100 G. The second signal can be only detected at cryogenic temperatures (less than 10K) and is probably due to a magnetic coupling interaction between the pheophytin anion and the reduced quinone-iron complex. Such interactions are consistent with the fact that the split signal is only observed when the iron-quinone complex is in its reduced, paramagnetic state.

The quinone-iron complex also shows an EPR signal with g = 1.87 and a broad linewidth (≈100 G). This signal was first observed in bacteria (94-97) and later on in PSII particles (90,91,98,99). The observed broad line can be explained by a coupling between the quinone and the high spin iron ion (100-101). Removal of the iron by detergents in bacteria (102) results in an EPR signal, after reduction, that is characteristic of a quinone anion radical (103). PSII reaction centers depleted of iron were first reported by Klimov and co-workers (89). They measured the amount of iron present in the centers by monitoring the split pheophytin anion signal. They found that when the split pheophytin signal was diminished after photoreduction a small EPR signal with g = 2.0044 and linewidth of 9.2 G was formed. This signal is similar to the one found in the iron uncoupled quinone acceptors in bacteria.

In a

acceptor I

generated

with horse-

were simila

(105,106) p

BChl a, b a

temperatur

showed EN

and for BPh

parameters

possible to d

ever, they do

dimer. The

data (107,108

possibility of

picosecond op

These authors

primary donor

decrease of the

the I⁻ EPR sign

acceptor capable

In an effort to identify the EPR signal from the primary intermediate acceptor I^-, Feher (104) performed a low temperature ENDOR study of I^- generated in reaction centers of *Rps. Sphaeroides* R-26 that were supplemented with horse-heart cytochrome c. Some of the ENDOR lines in the sample *in vivo* were similar to those observed in the BPh a anion radical *in vitro*. Fajer (105,106) performed ENDOR experiments on the anion radicals of BPh a, b and BChl a, b and reaction center of *Rps. viridis* at high (liquid state) and low temperature (frozen solutions). At 170K the reaction centers of *Rps. viridis* showed ENDOR resonances similar to those observed for BChl b anion radical and for BPh b anion radicals *in vitro*. It is clear from the EPR and ENDOR parameters (g-values, linewidth and hyperfine splitting values) that it is not possible to distinguish between BPh a and BChl a anion radicals for I^-. However, they do indicate that the species involved certainly is a monomer and not a dimer. The identification of this molecule as BPh a is concluded from optical data (107,108), which is also consistent with the ENDOR and EPR data. The possibility of more than one intermediary besides BPh a was ruled out by picosecond optical experiments (109) performed on *C. vironsum* and *Rps. viridis*. These authors also measured the decrease of the triplet EPR intensity of the primary donor as a function of illumination at 80K. They found that the decrease of the triplet state of the primary donor was matched by an increase of the I^- EPR signal intensity. They concluded that there is no other intermediary acceptor capable of triplet state generation via back reaction.

Feher and co-workers performed ENDOR studies in the solid state (*i.e.*, frozen solutions) on reaction centers of *Rps. sphaeroides* (110,111) where the iron was substituted by zinc. These authors were able to identify the ENDOR lines arising from the methyl, methylene and exchangeable hydrogens that are believed to bond to the carbonyl oxygens (112). Several sets of ENDOR lines corresponding to small hyperfine splittings (matrix ENDOR (112)) were also observed in the ENDOR spectra of both Q_A^- and Q_B^- (the acceptor quinones), indicating dipolar interactions with residues from the surrounding protein. In addition to these lines, ENDOR transitions from nitrogens, most likely from the imidazole of histidine, were observed.

In these studies it was found that the quinone binding site was asymmetric, making the two carbonyl oxygens on the quinone nonequivalent. They found that in Q_B^- the nonequivalence of the oxygens was less pronounced than in Q_A^-. These conclusions were based on experiments performed with reaction centers in which the native quinone was substituted with model quinones and from ^{17}O hyperfine splittings. This asymmetry of the two oxygens was attributed to either different strengths of the hydrogen bonded protons or to the presence of the positive charge on Zn^{2+} that had been substituted into the Fe^{2+} site. The difference in the observed hyperfine splittings of Q_A^- and Q_B^- is presumably related to the change in redox potential that leads to the electron transport for Q_A^- and Q_B^-. Also by using a simple dipole-dipole approximation these authors estimated the bond lengths of the hydrogen bonded protons in both Q_A^- and Q_B^-.

A

experim

not beer

spectra

give son

(113,11

more in

the func

radical

chlorop

(116).

with de

spectru

the PQ

a high

posed

(49,118

resolve

group

of the

PQ cati

Although a great deal of information has been obtained from these experiments the picture is not completed yet. The matrix ENDOR lines have not been explored in detail, in particular, the difference between the ENDOR spectra of Q_A^- and Q_B^-. Also a study of the pH dependence of the spectra may give some information about the proposed proton uptake by the semiquinones (113,114). The ENDOR spectra from metal-free reaction centers may provide more information about the structure of the metal complex, the binding site, and the function of the Fe^{2+} or other divalent ions substituted into this site (110).

Description of Work to be Presented

It was first suggested by Weaver that Y_D^+ was a plastoquinone (PQ) radical (115). Kohl and Wood tested this hypothesis by extracting PQ from chloroplasts from green plants and reconstituting them with deuterated PQ (116). The narrowing of the Y_D^+ EPR signal as a result of the reconstitution with deuterated PQ gave support to Weaver's idea. EPR simulations of the Y_D^+ spectrum based on a plastosemiquinone anion radical also provided support to the PQ model for the species Y_D^+ (117). However, based on the requirement of a high redox potential for Y_Z^+ and on its spectroscopic properties it was proposed that the species responsible for Y_Z^+ and Y_D^+ was a PQ cation radical (49,118). EPR on oriented membranes was used to assign the major, partially resolved hyperfine splittings in the Y_D^+ and Y_Z^+ EPR spectra to the 2-methyl group of the plastoquinone molecule. It was also suggested that the orientation of the radical with respect to the membrane plane was such that the ring of the PQ cation radical was perpendicular to the membrane plane (49). An indirect

way to

determi

using h

was do

experin

extract

1.15.

plastoc

Y_2^* an

a) Y_2

ation c

organi

3, in w

with o

center

results

to the

using

Y_D^* E

sample

α-proto

them h

way to test the hypothesis that Y_z and Y_D are plastoquinone molecules is by determining quantitatively the amount of plastoquinone in the PSII system by using high performance liquid chromatography (HPLC). Such a determination was done by Takahashi and Katoh (119) and by deVitry *et al.* (120). In their experiments they extracted PQ from PSII preparations and analyzed the organic extract by HPLC. The former group found 2 PQ/PSII while the latter found only 1.15. If Y_z^+ and Y_D^+ are both plastoquinone molecules there should be 4 plastoquinone molecules per reaction center, one for Q_A and one for Q_B, one for Y_z^+ and one for Y_D^+. There are some possible explanations for their results: a) Y_z and Y_D are covalently bound; b) Y_z and Y_D are trapped by the denaturation of the membrane which collapses around these species upon addition of organic solvent; c) Y_z or Y_D are not quinones. The results presented in Chapter 3, in which the PSII membranes were digested or "open" prior to the extraction with organic solvents, shows that there are only about 2 quinones per reaction center, suggesting that Y_D^+ and Y_z^+ are not plastoquinones molecules. These results agree with those presented by other workers (119,120) and give support to the tyrosine origin proposed by Barry and co-workers (15).

A more direct way of determining the structure of these radicals is by using ENDOR spectroscopy. In Chapter 4, I assign the main couplings of the Y_D^+ ENDOR spectrum by using oriented PSII membranes. By using these samples we have been able to obtain the ENDOR signal corresponding to the α-protons at the 3-5 positions. These signals possess a high anisotropy making them hard to detect; by using oriented samples, however, the relative

concentr

powder

the tyros

for each

these ca

tyrosine

the meth

observed

between

positions

plane wa

A

exchange

After inc

change w

trum was

sample a

the excha

solvents

so-called

attributed

amino ac

D_2O exch

concentration of the sample is increased as compared to an unoriented or powder sample. A complete picture of the unpaired spin density distribution on the tyrosine aromatic ring was obtained by using the hyperfine coupling constants for each set of protons. The unpaired spin density distribution obtained from these calculations is in agreement with the expected spin density distribution in tyrosine model compounds. I have calculated the dihedral angle (Equation 3) for the methylene protons within the tyrosine model. The apparent quartet structure observed in the $Y_D^{\bullet}$ EPR spectrum can be explained in terms of near degeneracy between one of the β-methylene protons and the two α-protons at the 3-5 positions. Also the orientation of the $Y_D^{\bullet}$ radical with respect to the membrane plane was elucidated.

A second approach to study this radical and its environment was to try to exchange any exchangeable hydrogen with deuterium in the radical binding site. After incubating the PSII membranes isolated from chloroplasts no noticeable change was observed in the $Y_D^{\bullet}$ EPR spectrum. But when the ENDOR spectrum was analyzed, several differences were observed between the exchanged sample and the control sample (*i.e.*, one that had received the same treatment as the exchanged sample but for which protonated solvents instead of deuterated solvents were used). We found that changes occurred more quickly in the so-called matrix region. This region around the free proton frequency has been attributed to dipole-dipole interactions between the radical and the more distant amino acid protons in the binding site (121). Under conditions in which the D_2O exchange is not complete (as described in Chapter 5) several resonances

are absent in this matrix region indicating a rapid exchange. A pH effect was observed: samples at different pH's (*e.g.*, pH = 6.0 compared to pH = 7.5) show different intensities and ENDOR transitions after the exchange process. Because the matrix region contains resonances from protons more remote from the radical, it is not surprising that it responds more rapidly to the conditions in bulk water.

If the samples are incubated for 6 hours at pD = 7.5, freeze dried and resuspended in D_2O a more complete exchange was obtained. With the help of previous work on model quinones (122) we assigned two resonances (3.5 and 7.1 MHz) to a hydrogen bonded proton. The axial nature of the hyperfine tensor and the fact that it is essentially traceless support this conclusion. Also we conclude that the binding site for $Y_D^{\bullet}$ and probably for $Y_Z^{\bullet}$ is well shielded from the bulk water (as indicated by the slow exchange). In addition by using a dipole-dipole approximation we have calculated the bond length for the hydrogen bonded proton.

It will be shown that in combination with computer simulation of the oriented EPR spectra, the use of oriented PSII membranes, theoretical calculation, D_2O/H_2O exchange, and ENDOR spectroscopy, detailed information about the structure, unpaired spin density distribution and the orientation of the tyrosine radical in the membrane can be obtained.

1.

2.

3.

4.

5.

6.

7.

8.

9.

10.

11.

12.

13.

14.

15.

16.

References

1. The Photosynthetic Bacteria (Clayton, R.K. and Sistrom, W.W., eds.) 1979 Plenum Press, New York.

2. Kaufmann, K.J., Dutton, P.L., Netzel, T.L., Leigh, J.S., Jr. and Rentzepis, P.M. (1975) Science 188, 1301.

3. Rockley, M.G., Windsor, M.W. Cogdell, R.J. and Parson, W.W. (1975) Proc. Nat'l. Acad Sci. USA 72, 2251.

4. Shuvalov, V.A., Dolan, E. and Ke, B. (1979) Proc. Nat'l. Acad Sci. USA 76, 770.

5. Shuvalov, V.A. Klvanik, A.V.,Sharkov, A.V. Kryukov, P.G. and Ke, B. (1979) FEBS Lett. 107, 313.

6. Fenton, J.M., Pellin, M.J. Govindijee and Kaufmann, K.J. (1979) FEBS Lett. 100, 1.

7. Klimov, V.V., Allakhverdiev, S.I., Demeter, S. and Kranovsky, A.A. (1979) Dokl. Akad USSR 249, 227.

8. Klimov, V.V., Klevanik, A.V., Shuvalov, V.A. and Kranovsky, A.A. (1977) FEBS Lett. 82, 183.

9. Klimov, V.V., Allakhverdiev, S.I., Shutilova, N.I. and Krasnovsky, A.A. (1980) Sov. Plant Physiol. 27, 102.

10. Klimov, V.V., Dolan, E. and Ke, B. (1980) FEBS Lett. 112, 97.

11. Klimov, V.V. and Krasnousky, A.A. (1982) Biophysics, 27, 186.

12. Nugent, J.H.A., Diner, B.A. and Evans, M.C.W. (1981) FEBS Lett., 124, 241.

13. Rutherford, A.W. and Zimmermann, J.L. (1984) Biochim. Biophys. Acta 767, 168.

14. Rutherford, A.W. (1985) Biochim. Biophys. Acta 807, 189.

15. Barry, B.A. and Babcock, G.T. (1987) Proc. Nat'l. Acad Sci. USA 84, 7099.

16. Hoganson, C.W. and Babcock, G.T. (1988) Biochemistry, in press.

17.

18.

19.

20.

21.

22.

23.

24.

25.

26.

27.

28.

29.

30.

31.

32.

33.

17. Kok, B., Forbush, B. and McGloin, M. (1970) Photochem. Photobiol. 11, 457.

18. Dekker, J.P., Plijter, J.J., Ouwehand, L. and Van Gorkom, H.J. (1984) Biochim. Biophys. Acta 767, 176.

19. Dekker, J.P., Van Gorkom, H.J., Brok, M. and Ouwehand, L. (1984) Biochim. Biophys. Acta 764, 301.

20. Dekker, J.P., Van Gorkom, H.J., Wensick, J. and Ouwehand, L. (1984) Biochim. Biophys. Acta 767, 1.

21. Velthuys, B.R. (1981) In: Photosynthesis; Photosynthetic Electron Transport and Photophosphoryllation (Akoyanoglou, G. ed.) Vol.2, pp 75, Balaban Int'l. Science Series, Philadelphia, PA.

22. Mathis, P. (1977) in: Primary Processes of Photosynthesis (Barber J. ed.) pp 269, Elsevier, Amsterdam.

23. Hoganson, C.W. and Babcock, G.T. (1988) Biochemistry, submitted.

24. Setif, P. Mathis, P. and Vaenngaard, T. (1984) Biochim. Biophys. Acta 767, 404.

25. Michel, H.J. (1982) Molec. Biol. 158, 562.

26. Gast, P., Wasielewski, M.R., Schiffer, M. and Norris, J.R. (1983) Nature, 305, 451.

27. Michel, H. Deisenhofer, J., Mik, K. and Lottspeich, F. (1983) in: Structure and Function of Membrane Proteins (Quagliariello, E. and Palmiero, F. eds.) pp 191. Elsevier Science Publisher, B.V.

28. Ozawa, T. (1984) J. Bioenerg. Biomembranes 16, 321.

29. Michel, H. (1983) Trends in Biochemical Sciences 8, 56.

30. Allen, J.P. and Feher, G. (1984) Proc. Nat'l. Acad Sci. USA 81, 4795.

31. Nuys, A.M., Van Dorsen, R.J., Duysens, L.N.M. and Amesz, J. (1985) Proc. Nat'l. Acad Sci. USA 82, 6865.

32. Braumann, T., Vasmel, H. Grimme, L.H. and Amesz, J. (1986) Biochim. Biophys. Acta 848, 83.

33. Swathoff, T., Gast, P. Hoff, A.J. and Amesz, J. (1981) FEBS lett. 130, 93.

34. Norris, J.R., Uphaus, R.D., Crespi, H.L. and Katz, J.J. (1971) Proc. Nat'l. Acad Sci. USA , 68, 625.

35. Feher, G., Hoff, A.J., Isaacson, R.A. and Ackerson, L.C. (1975) Ann. N.Y. Acad. Sci. 244, 239.

36. Carter, M.V. and Vincow, G. (1967) J. Chem. Phys. 47, 302.

37. Norris, J.F., Scheer, H. and Katz, J.J. in: The Porphyrins (Dolphin, D., ed.) p. 4159. Academic Press, New York.

38. Scheer, H. Katz, J.J. and Norris, J.R. (1977) J. Am. Chem. Soc. 99, 1372.

39. Borg, D.C., Forman, A. and Fajer, J. (1976) J. Am. Chem. Soc. 98, 6889.

40. Hoff, A.J. and Mobius, K. (1978) Proc. Nat'l. Acad Sci. USA 75, 2296.

41. Norris, J.R., Druyan, M.E., and Katz, J.J. (1973) J. Am. Chem. Soc. 95, 1680.

42. Norris, J.R., Scheer, H. Druyan, M.E. and Katz, J.J. (1974) Proc. Nat'l. Acad Sci. USA 71, 4897.

43. Feher, G., Hoff, A.J., Isaacson, R.A. and Lozier (1979) Physics Reports 54, 75.

44. O'Malley, P.J. and Babcock, G.T. (1983) in: Proc. of the 6th Intl. Congress in Photosyn. Sybesman, C. ed.) Vol 1 pp. 697. Junk, Amsterdam.

45. Petke, J.D. Maggiora, G.M., Shipman, L.L. and Christoffersen, R.E. (1980) Photochem. Photobiol. 31, 243.

46. Babcock, G.T. (1987) in: New Comprehensive Biochemistry: Photosynthesis (Amesz, J. ed.) pp. 125. Elsevier, Amsterdam.

47. Babcock, G.T. and Sauer, K. (1975) Biochim. Biophys. Acta 376, 315.

48. Ghanotakis, D.F., O'Malley, P.J., Babcock, G.T. and Yocum, C.F. (1983) in: The Oxygen Evolving System of Photosynthesis (Inoue, Y. et al. eds.) pp 99. Academic Press, Tokyo.

49. O'Malley, P.J. and Babcock, G.T. (1984) Biochim. Biophys. Acta 765, 370.

50. Diner, B.A. and DeVitry, C. (1984) in: Advances in Photosynthesis Research (Sybeama, C., ed.) Vol 1, pp 407. Martinus Nijhoff/Dr. W. Junk, The Hague.

51.

52.

53.

54.

55.

56.

57.

58.

59.

60.

61.

62.

63.

64.

65.

66.

67.

51. Debus, R.J., Barry, B.A., Babcock, G.T. and McIntosh, L. (1988) Proc. Nat'l. Acad. Sci. USA 85, 427.

52. Blankenship, R.E., Babcock, G.T., Warden, J.T. and Sauer, K. (1975) FEBS Lett. 51, 287.

53. Styring, S. and Rutherford, A.W. (1987) Biochemistry, 27, 4915.

54. Joliot, P., Barbier, G. and Chabaud, R. (1969) Photochem. Photobiol. 10, 309.

55. Kok, B., Forbush, B. and McGloin, M. (1970) Photochem. Photobiol. 11, 457.

56. Cheniae, G. (1980) Methods in Enzymol., 69, 349.

57. Amesz, J. (1983) Biochim. Biophys. Acta 726, 1.

58. Radmer, R. and Cheniae, G.M. (1977) in: Primary Processes of Photosynthesis (Barber, J. ed) pp 303, Elsevier, Amsterdam.

59. Ghanotakis, D.F., Babcock, G.T. and Yocum, C.F. (1984) Biochim. Biophys. Acta 765, 388.

60. Kirby, J.A., Goodin, D.B., Wydrzynski, T., Robertson, A.S. and Klein, M.P. (1981) J. Am. Chem. Soc., 103, 5537.

61. Goodin, D.B., Yachandra, V.K., Britt, R.D., Sauer, K. and Klein, M.P. (1984) Biochim. Biophys. Acta, 767, 209.

62. Yachandra, V.K., Guites, R.D., McDermott, A., Britt, R.D., Dexheimer, S.L., Sauer, K. and Klein, M.P. (1986) Biochim. Biophys. Acta, 850, 324.

63. Velthyus, B.R. (1980) Ann. Rev. Plant Physiol. 31, 545.

64. Lozier, R., Baginsky, M. and Butler, W.L. (1971) Photochem. Photobiol. 14, 323.

65. Blankenship, R.E. and Sauer, K. (1974) Biochim. Biophys. Acta 357, 252.

66. Yocum, C.F. Yerkes, C.T., Blankenship, R.E., Sharp, R.R. and Babcock, G.T. (1981) Proc. Nat'l Acad. Sci. USA 78, 7507.

67. Dismukes, G.C. and Siderer, Y. (1981) Proc. Nat'l. Acad Sci. USA 72, 274.

68.

69.

70.

71.

72.

73.

74.

75.

76.

77.

78.

79.

80.

81.

82.

83.

84.

85.

86.

68. Dismukes, G.L., Ferris, K. and Watnick, P. (1982) Photochem. Photobiol. 3, 243.

69. Hansson, O. and Andreasson, L.E. (1982) Biochim. Biophys. Acta 679, 261.

70. Andreasson, L.E., Hansson, O. and Vanngard, T. (1983) Chem. Scripta 21, 71.

71. Beck, W.F., de Paula, J.C. and Brudvig, G.W. (1985) Biochemistry 24, 3035.

72. de Paula, J.C. and Brudvig, G.W. (1985) J. Am. Chem. Soc. 107, 2643.

73. de Paula, J.C., Beck, W.F. and Brudvig, G.W. (1986) J. Am. Chem. Soc. 108, 4002.

74. Zimmermann, J.L. and Rutherford, A.W. (1984) Biochim. Biophys. Acta 767, 160.

75. Casey, J.L. and Sauer, K. (1984) Biochim. Biophys. Acta 762, 21.

76. Zimmermann, J.L. and Rutherford, A.W. (1985) Physiol. Veg. 23, 425.

77. Volker, M., Renger, G. and Rutherford, A.W. (1986) Biochim. Biophys. Acta 851, 424.

78. Brudvig, G.W. and Crabtree, R.H. (1986) Proc. Nat'l. Acad Sci. USA 83, 4586.

79. Malkin, R. (1986) FEBS Letts 208, 343.

80. Schoeder, H.U. and Lockau, W. (1986) FEBS Letts. 199, 23.

81. Takahashi, Y., Hirota, K. and Katoh, S. (1985) Photosyn. Res. 6, 183.

82. Hales, B.J. (1975) J. Am. Chem. Soc. 97, 5993.

83. Hales, B.J. (1978) J. Chem. Phys. 65, 3767.

84. Hales, B.J. (1975) J. Am. Chem. Soc. 98, 7350.

85. Hales, B.J. and Case, B.O. (1981) Biochim. Biophys. Acta 637, 291.

86. Bonnerja, J. and Evans, M.C.W. (1982) FEBS Letts. 148, 313.

87.

88.

89.

90.

91.

92.

93.

94.

95.

96.

97.

98.

99.

100.

101.

102.

103.

87. Bender, C.J., Rodriguez, I.D., Lockau, W. and Babcock, G.T. (1987) Biophys. J. 51, 393.

88. Barry, B.A., Bender, C.J. McIntosh, L., Ferguson-Miller, S. and Babcock, G.T. (1988) Isr. J. chem., Submitted.

89. Klimov, V.V., Dolan, E., Shaw, E.R. and Ke, B. (1980) Proc. Nat'l. Acad Sci. USA 77, 7227.

90. Nuget, J.H.A., Diner, B.A. and Evans, M.C.W. (1981) FEBS Letts. 124, 241.

91. Rutherford, A.W. and Mathis, P. (1983) FEBS Letts. 154 328.

92. Tiede, D.M., Prince, R.C., Reed, G.H. and Dutton, P.L. (1976) FEBS Letts. 65, 301.

93. Tiede, D.M., Prince, R.C. and Dutton, P.L. (1976) Biochim. Biophys. Acta 449, 447.

94. Mc ElRoy, J.D., Feher, G. and Mauzerall, D. (1970) Biophys. J. 10, 204a.

95. Leigh, J.S. and Dutton, D.L. (1976) Biochem. Biophys. Res. Com. 46, 414.

96. Dutton, P.L. and Leigh, J.S. (1973) Biochim. Biophys. Acta 314, 178.

97. Dutton, P.L., Leigh, J.S. and Reed, D.W. (1973) Biochim. Biophys. Acta 292, 654.

98. Rutherford, A.W., Zimmermann, J.L. and Mathis, P. (1984) in: Proc. 6th Int'l. Cong. Photosyn. (Sybesma, C. ed.) Voll, pp 443. M. Nijhoff, W. Junk Publishers, The Hague.

99. Rutherford, A.W. and Zimmermann, J.L. (1984) Biochim. Biophys. Acta 767, 168.

100. Butler, G.C., Calvo, R., Fredkin, D.R., Isaacson, R.A., Okamura, M.Y. and Feher, G. (1984) Biophys. J. 45, 947.

101. Dismukes, G.C., Frank, H.A., Friesner, R. and Sauer, K. (1984) Biochim. Biophys. Acta 764, 253.

102. Loach, P.A. and Hull, R.L. (1972) Proc. Nat'l. Acad Sci. USA 69, 786.

103. Feher, G., Okamura, M.Y. and Mc Elroy, J.D. (1972) Biochim. Biophys. Acta 267, 222.

104.

105.

106.

107.

108.

109.

110.

111.

112.

113.

114.

115.

116.

117

118

119

120

121

104. Feher, G., Isaacson, R.A. and Okamura, M.Y. (1977) Biophys. J. 17, 149a.

105. Fajer, J., Davis, M.S., Brune, D.C., Forman, A. and Thornber, J.P. (1978) J. Am. Chem. Soc. 100, 1918.

106. Fajer, J., Davis, M.S. and Forman, A. (1977) Biophys. J. 17, 149a.

107. Holten, D., Windsor, M.W., Parson, W.W. and Thornber, J.P. (1978) Biochim. Biophys. Acta 501, 112.

108. Clayton, R.K. and Yamamoto, T. (1976) Biophys. J. 16, 222a.

109. Netzel, T.L., Rentzepis, P.M., Tiede, D.M., Prince, R.C. and Dutton, P.L. (1977) Biochim. Biophys. Acta 460, 467.

110. Debus, R.J., Feher, G. and Okamura, M.Y. (1986) Biochem. 25, 2276.

111. Feher, G., Isaacson, R.A., Okamura, M.Y. and Lubitz, W. (1985) in: Antennas and Reaction Centers of Photosynthetic Bacteria (Michele-Beyerle, ME, ed.) Vol. 42, pp 174. Springer-Verlag, Berlin.

112. Feher, G., Okamura, M.Y. and Mc Elroy, I.D. (1972) Biochim. Biophys. Acta 267, 222.

113. Prince, R.C. and Dutton, P.L. (1978) in: The Photosynthetic Bacteria, Clayton, (R.K. and Sistrom, W.R. ed.) Chapter 24 p 439. Plenum, N.Y.

114. Rutherford, A.W. and Evans, C.W. (1980) FEBS Letts.110, 257.

115. Weaver, E.C. (1962) Arch. Biochem. Biophys. 99, 193.

116. Kohl, D.H. and Wood, P.M. (1969) Plant Physiol. 44, 1439.

117. Hales, B.J. and das Gupta, A. (1981) Biochim. Biophys. Acta 637, 303.

118. O'Malley, P.J. Babcock, G.T. and Prince, R.C. (1984) Biochim. Biophys. Acta 766, 243.

119. Takahashi, Y. and Katoh, S. (1986) Biochim. Biophys. Acta 842, 183.

120. DeVitry, C., Carles, C. and Diner, B.A. (1986) FEBS Letts. 196, 203.

121. Chandrashekar, T.K., O'Malley, P.J., Rodriguez, I.D. and Babcock, G.T. (1986) in: Prog. in Photosyn. Res. (J. Biggins, ed.) vol. 1 pp 423, Martinos Nihoff, Dordrecht.

122 O
m
M

122. O'Malley, P.J., Chandrashekar, T.K. and Babcock, G.T. (1985) in: Antennas and Reaction Centers of Photosynthetic Bacteria (Michelle-Beyerle, M.E. ed.) Vol. 42, pp 259, Springer-Verlag, Berlin.

CHAPTER 2
EPR AND ENDOR SPECTROSCOPY

Introduction

In electron paramagnetic resonance (EPR) spectroscopy electron spin transitions between different electronic Zeeman levels are stimulated. The coupling of the unpaired electron(s) with magnetic nuclei leads to the splitting of these levels into hyperfine sublevels, thus increasing the number of EPR transitions. Delocalization of the unpaired electron in an organic π-radical results in the coupling between this unpaired electron and all magnetic nuclei within the π-system creating in this way a multispin ensemble. If the coupling constants are the same for the different interacting nuclei of the same spin the number of resonance lines L_{ESR} is given by (1):

$$L_{ESR} = 2IN + 1 \qquad (1)$$

where N is the number of nuclei with spin I. The relative intensities, C, for the case of I=1/2 follows the binomial series:

$$C = \frac{N!}{(N-K)!\ K!} \qquad (2)$$

where K = 0, 1, 2, $\cdots$ N.

If, on the other hand, the coupling constants for the different nuclei are different, as for example the radical of triphenylmethyl with one set of three equivalent protons and two sets of six equivalent protons, then the number of resonance lines is given by:

$$L_{ESR} = (2N_1I_1 + 1)(2N_2I_2 + 1)\cdot\cdot\cdot(2N_k I_k + 1)$$

$$= \prod_{i=1}^{k} (2N_iI_i + 1) \qquad (3)$$

Therefore the number of lines increases multiplicatively with the number of non-equivalent nuclei and it may increase to such an extent that the individual lines can no longer be resolved. For our example of triphenylmethyl we would expect theoretically 4x7x7 = 196 lines. This high density of spectra lines is one of the limitation in EPR spectroscopy. This limits the utility of this technique in the investigation of large organic radicals because of its insufficient resolving power.

One way of improving the resolution in EPR is offered by double resonance methods in which the sample is simultaneously irradiated with two resonant fields. Electron nuclear double resonance (ENDOR) was first used by Feher in the study of solids (2) and later applied by Hyde and Maki to organic radicals in solution (3). This technique overcomes the resolution problem in EPR by introducing additional selection rules. If we consider just the isotropic interactions between the unpaired electron(s) and the magnetic nuclei we have

seen that the number of lines in EPR increases multiplicatively (Equation 3) whereas in ENDOR they increase additively:

$$L_{ENDOR} = 2M \qquad (4)$$

where M is the number of nonequivalent groups of protons. If we compared the EPR and ENDOR spectra of the bis (biphenylylene) allyl radical we see that from the 1250 lines expected in the EPR spectrum (5x5x5x5x2) only about 400 are observed. The ENDOR spectrum, on the other hand, shows all five possible line pairs, one for each set of equivalent protons (see Figure 2.1). The hyperfine coupling constants can be extracted without too much difficulty. However, unequivocal assignments of this coupling constants to individual groups can only be achieved by selective isotopic labelling.

Electron Paramagnetic Resonance

The magnetic moment μ_s associated with the spin of an electron is given by the following equation:

$$\mu_s = -g\beta S \qquad (5)$$

where β is the Bohr magneton, g is the so-called g value for the free electron equal to 2.0023; S is the spin of the electron which is equal to 1/2, meaning that the spin angular momentum is equal to $\pm$ 1/2 ($h/2\pi$) where h is Planck's constant. In an homogeneous magnetic field, the direction of the spin angular

Figure 2.1. EPR Spectrum in CCl_4 (T=293K) and ENDOR spectrum in mineral oil (T=330K) of bis (biphenylylene) allyl radical. From reference 11.

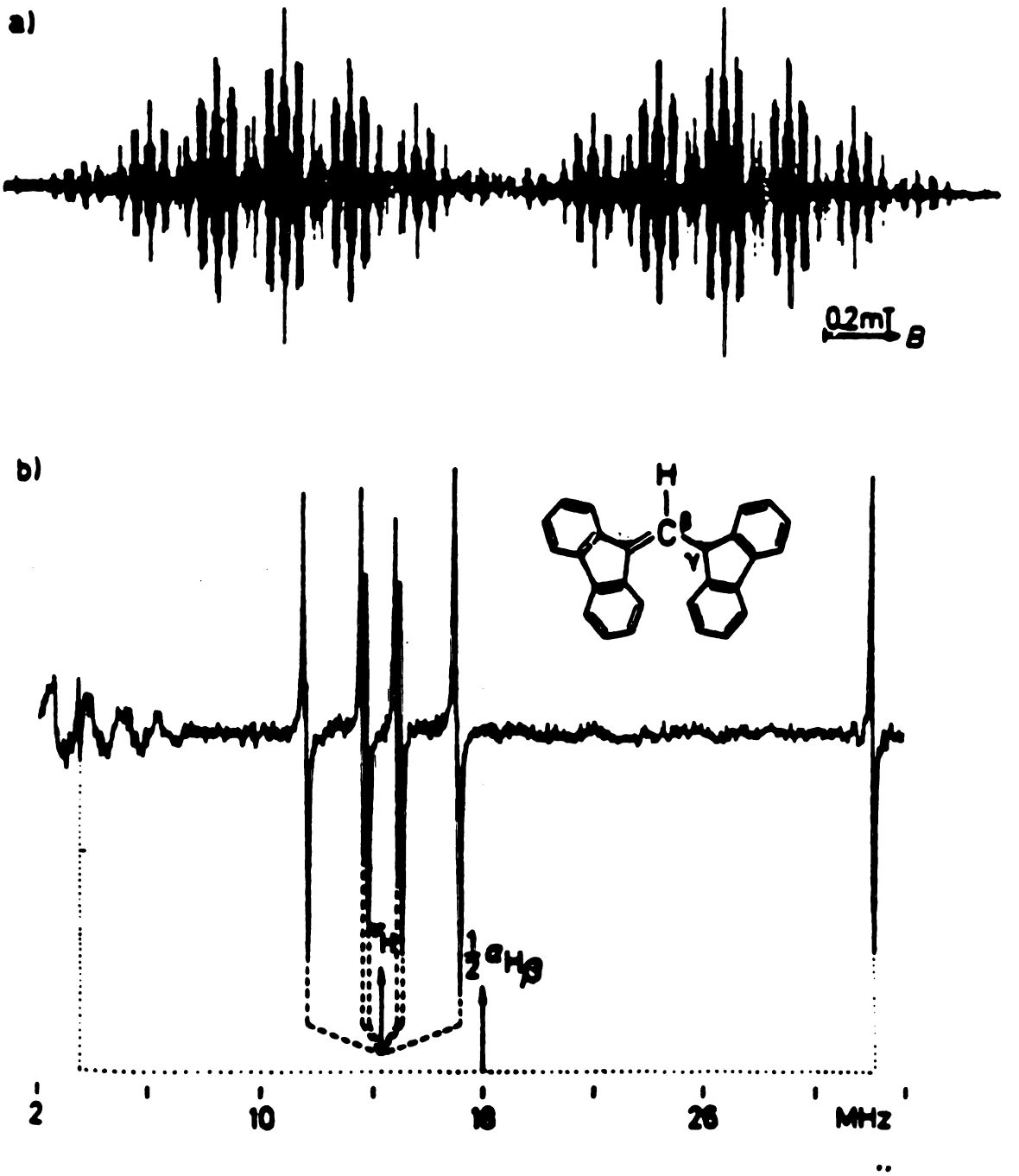
a)
0.2mT
B
b)
H
C
γ
$\frac{1}{2}a_{Hg}$
2
10
18
26
MHz

momentum is restricted to ± 1/2 (h/2π). This means that there are two possible configuration for the alignment of the spin magnetic moment with respect to the magnetic field: a parallel and an antiparallel configuration, which correspond to the Zeeman levels of the unpaired electron. The energies associated with these levels are ± 1/2 gβH and the resonance condition for these two Zeeman components is given by:

$$h\nu = g\beta H \tag{6}$$

where H is the magnetic field and ν is the resonance frequency. The electron paramagnetic resonance experiment is performed by placing a sample in a microwave cavity in the presence of an homogeneous magnetic field of several thousands gauss and constant microwave frequency. The magnetic field is swept until Equation 6 is satisfied and an EPR signal is recorded. However, the situation is not as simple as it appears from the above discussion. The EPR spectra usually do not consist of a simple absorption line but is a more complex, multiline spectra. This observation leads to the conclusion that the magnetic field experience by the unpaired electron can be described by:

$$H = H_0 + H_1 \tag{7}$$

where H_0 is the external applied magnetic field and H_1 is a perturbing field originating in the sample itself. H_1 gives rise to the observed hyperfine interaction between the unpaired electron and a nearby nucleus. This perturbing

field can be divided into two different parts: an isotropic or orientationally independent part and an anisotropic part which arises from dipolar interactions. In solution, where molecules tend to be tumbling rapidly (see discussion below), the anisotropic part of H_1 averages to zero and therefore the EPR spectrum is a result or measure of isotropic interactions. When the radical is immobilized the dipolar interactions are no longer averaged to zero and the contribution to the spectra from the anisotropic part of H_1 can be observed. However extracting the principal anisotropic elements of the H_1 tensor from this immobilized spectra may be difficult due to the fact that all possible orientations of the radical with respect to the external magnetic field are present. But studying immobilized radicals by ENDOR both the isotropic and anisotropic parts of H_1 can be obtained. This will be discussed in more detail in the next sections.

Electron Nuclear Hyperfine Interaction

The interaction between the electron and magnetic dipole gives rise to the hyperfine splitting observed in an EPR spectrum. The direction of the components of the electron and nuclear-spin angular momenta in a magnetic field are defined by M_s and M_I where $M_s = \pm 1/2$ and M_I can have 2I+1 values between –I and I. The splitting of the electronic Zeeman levels, which are defined by M_s, into sublevels defined by M_I, is a direct result of this hyperfine interaction. This hyperfine splitting is governed by the selection rules $\Delta M_s = \pm 1$ and $\Delta M_I = 0$. A single proton (I = 1/2) will split each Zeeman level into two sublevels giving rise to a two line spectrum. In general, the number of resonances lines are given by Equations 1 and 3.

Spin Hamiltonian

The spin Hamiltonian for the simplest case of a radical with one unpaired electron (S = 1/2) and one magnetic nucleus (I = 1/2), *e.g.,* a proton is:

$$H = \beta \hat{S} \cdot \hat{\bar{g}} \cdot \bar{H} + h\hat{S} \cdot \hat{\bar{A}} \cdot \hat{I} - g_N \beta_N \hat{I} \cdot \bar{H} \qquad (8)$$

where β = Bohr magneton

$\hat{S}$ = electron spin operator

$\hat{\bar{g}}$ = electron g tensor

$\bar{H}$ = external Zeeman magnetic field vector

h = Planck's constant

$\hat{\bar{A}}$ = hyperfine coupling tensor

$\hat{I}$ = nuclear spin operator

g_N = nuclear g value

β_N = nuclear magneton

The first item in this equation is called the electron-Zeeman term and describes the interaction between the applied magnetic field and the unpaired electron. The magnitude of the Zeeman splitting is dictated by the g-tensor which describes one of the orientation dependent magnetic interaction encountered in an EPR experiment. The third term is called the nuclear-Zeeman term and it has little effect at X-band frequencies (4). If the orbital angular momentum of the unpaired electron were completely quenched, the g-tensor would be isotropic and equal to the free electron g-value, 2.0023. However, deviations from this g-value have been observed and interpreted in terms of spin orbit interactions

betw

unpa

appl

σ-bo

posi

cons

freq

odd

g-shi

this

than

grea

prom

requ

and

for t

unpa

as th

inter

tensc

indep

intera

between ground and excited states of the radical (5,6). If the orbital of the unpaired electron is a carbon $2P_z$ orbital, the observed g-shifts when the field is applied perpendicular to the z axis are a result of the following: promotion of a σ-bonding electron to pair with the odd electron in the π-orbital, which gives a positive g-shift approximately equal to $2\xi/\nu_1$ where ξ is the spin orbit coupling constant and ν_1 is the frequency of the electronic transition ("promotional frequency"). The other effect which is reflected as a g-shift is a promotion of the odd electron from the π-orbital into an antibonding orbital to give a negative g-shift approximately equal to $-2\xi/\nu_2$, where ν_2 is the promotional frequency of this transition. In general the promotional energy corresponding to ν_2 is greater than that corresponding to ν_1 and therefore g_{xx} and g_{yy} are expected to be greater than the free electron g-value. The value of g_{zz} can only be affected by promotion of a σ-bonding electron to an antibonding state. The high energy required for this transition means that g_{zz} will be close to the free electron value, and therefore the z axis is expected to be the direction of the minimum g-value for the radical.

The second term in Equation 8 describes the interaction between the unpaired electron and a nucleus of non-zero spin. This interaction is referred to as the electron-nuclear hyperfine interactions. This term represents the hyperfine interaction between the electronic and nuclear spins, which is described by the tensor $\hat{\mathbf{A}}$. This term is usually divided into two parts: the orientation-independent part (isotropic), which describes the so-called Fermi contact interaction (7), and the orientation-dependent part (anisotropic), which arises

from dipolar interactions between the electronic and nearby nuclear magnetic moments. Therefore the hyperfine interaction can be described by the following equation:

$$\hat{S} \cdot \hat{\bar{A}} \cdot \hat{I} = a \cdot \hat{S} \cdot \hat{I} + \hat{S} \cdot \hat{\bar{T}} \cdot \hat{I} \qquad (9)$$

where a is the isotropic hyperfine coupling constant and $\hat{\bar{T}}$ is the dipolar hyperfine tensor. The first term in this equation is known as the Fermi contact term and the second term is known as the dipolar coupling term.

Isotropic Hyperfine Interaction

The first term in Equation 9 can be written as:

$$a\hat{S} \cdot \hat{I} = \left\langle \frac{8\pi}{3} \right\rangle g\beta g_N \beta_N |\psi_{(o)}|^2 \hat{S} \cdot \hat{I} \qquad (10)$$

where $\psi_{(o)}$ is the electron wave functions evaluated at the nucleus. This equation predicts that the hyperfine splitting can only be observed if the probability of finding the unpaired electron at the interacting nucleus is different than zero. It is apparent from this equation that the isotropic hyperfine interaction will only be nonzero if $|\psi_{(o)}|^2$ is nonzero *i.e.*, if the orbital of the unpaired electron has s-character. For a proton the differences in magnitude of the isotropic coupling can be as large as 500 gauss in the hydrogen atom and as small as a few milligauss for some proton in organic radicals. Why should $|\psi_{(o)}|^2$ vary so much? We can find the answer to this by analyzing the shape of the atomic and molecular orbitals: p and d atomic orbitals and π-molecular orbitals have zero density at the nucleus (*i.e.*, $|\psi_{(o)}|^2$ vanishes) and orbitals of

this type can not give rise to isotropic splitting. Therefore, $|\psi_{(o)}|^2$ depends on the amount of s-character of the orbital or in a molecule the amount of a sigma character.

Anisotropic Hyperfine Interaction

The second term in Equation 9 corresponds to the anisotropic or direction dependent part of the effective Hamiltonian. This term can be written as:

$$\hat{S} \cdot \hat{\bar{T}} \cdot \hat{I} = [g\beta g_N \beta_N (3\cos^2\theta - 1)/r^3]\hat{S} \cdot \hat{I} \qquad (11)$$

where r is the vector between the electron and the nucleus, θ is the dipolar angle between r and the applied magnetic field. This is an oversimplification of the dipolar Hamiltonian and it only holds true under the following conditions:

1) The g-value is isotropic
2) The dominant energy term is the electronic Zeeman term allowing the quantization of $\hat{S}$ to be along the applied magnetic field, also $\hat{I}$ is assumed to be quantized in this direction (taken to be the z axis).
3) The x and y components of the $\hat{S}$ and $\hat{I}$ matrices are neglected because they are assumed to be quantized along the z axis.
4) Assume that a p-orbital on the interacting nucleus is the one that interacts with the unpaired electron.

When a radical is tumbling fast in solution, *i.e.*, at a rate faster than the reciprocal of the hyperfine frequency (see Equation 12 below) then the field at the electron due to the nuclear dipolar interaction will average to zero.

Therefore we may expect to see dipolar hyperfine interaction only in a viscous liquid, a solid or an immobilized radical. In these types of systems collision are so infrequent that all orientations in space can not become magnetically equivalent during a time shorter than the reciprocal hyperfine frequency $\Delta\nu$:

$$\Delta\nu = \frac{g\beta\Delta H}{h} \qquad (12)$$

where ΔH is the hyperfine splitting. A splitting of 1 gauss, at g = 2.0 will give a frequency of about 2.8 MHz which corresponds to a time of 3.5×10^{-7} sec. The characteristic time for random tumbling of a molecule in a liquid is in the order of 10^{-10} sec., that is, sufficiently fast relative to the limit imposed by the magnitude of most hyperfine interactions.

ENDOR

The derivation given here follows that given by Wertz and Bolton (8). Before going into a detailed description of the ENDOR processes, let us look briefly at a simple ENDOR experiment on an immobilized radical with S = 1/2 and I = 1/2. Figure 2.2 shows a general block diagram of an EPR-ENDOR spectrometer. Suppose that we have two hyperfine lines with resonant field at H_k and H_n as pictured in Figure 2.3 with an arbitrary g-value and a coupling of 20 MHz. An ENDOR experiment will proceed in the following way:

1) A sample is placed in the ENDOR cavity; the EPR signal is optimized by adjusting several spectrometer parameters and the field is locked at the desired position, let us say H_k.

Figure 2.2. General block diagram of an EPR-ENDOR spectrometer. From reference 11.

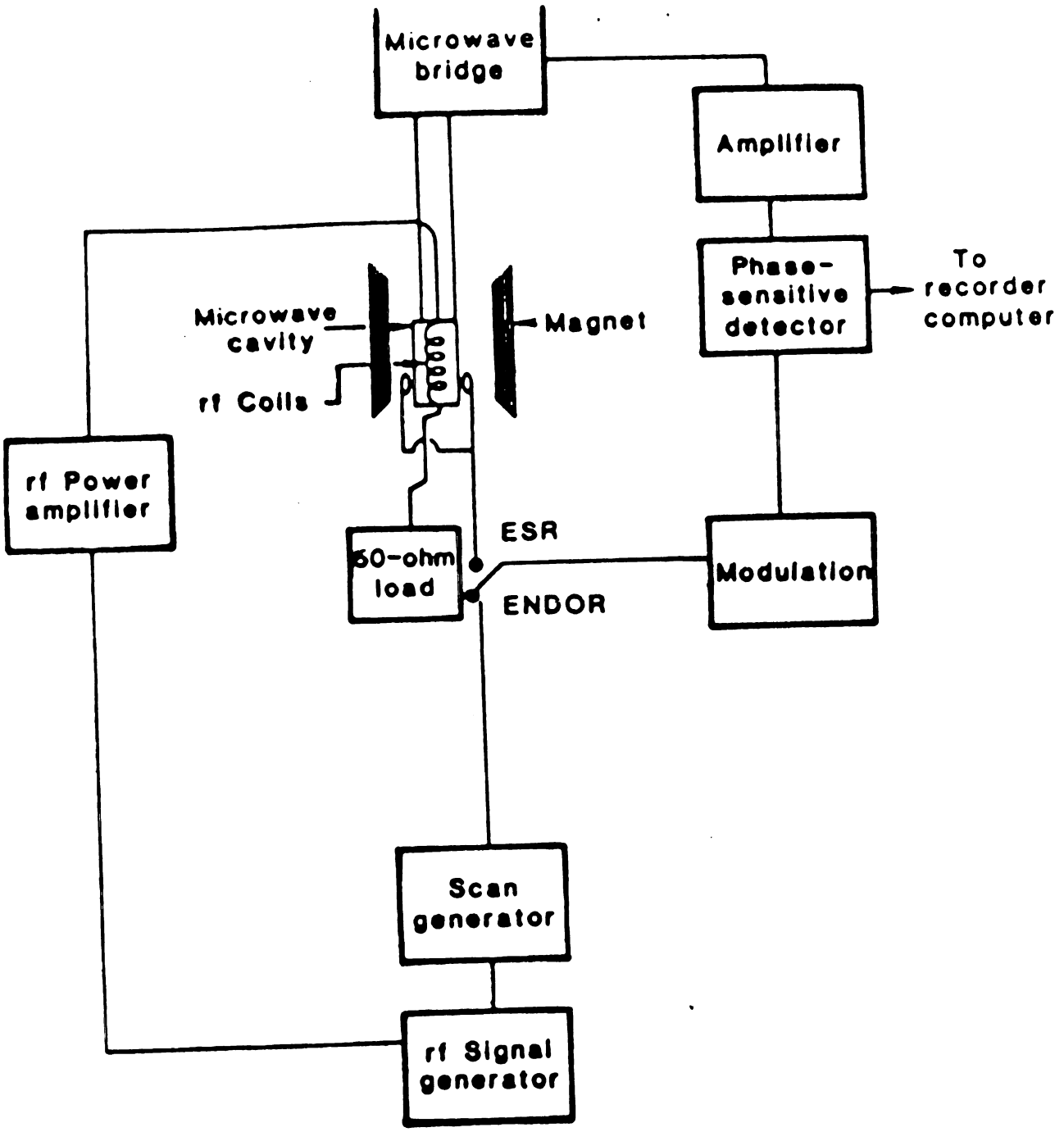
Microwave bridge
Amplifier
Phase-sensitive detector
To recorder computer
Microwave cavity
Magnet
rf Coils
rf Power amplifier
ESR
50-ohm load
ENDOR
Modulation
Scan generator
rf Signal generator

Figure 2.3. **Energy levels of** a system with S = 1/2 at constant magnetic field (a) and **with a variable** magnetic field (b). From reference 8.

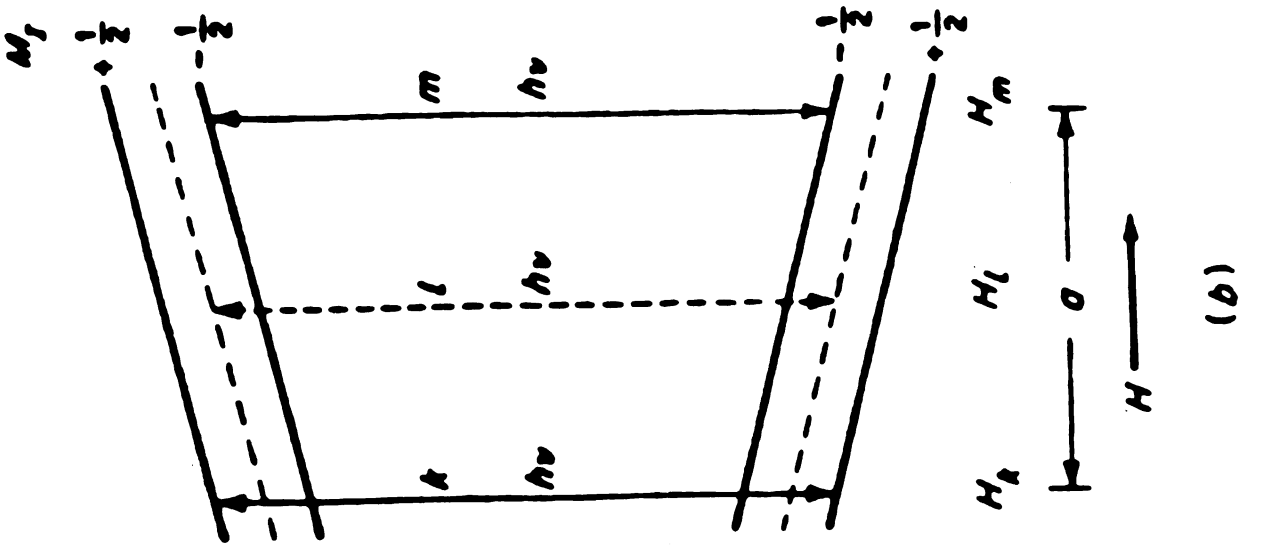

(b)

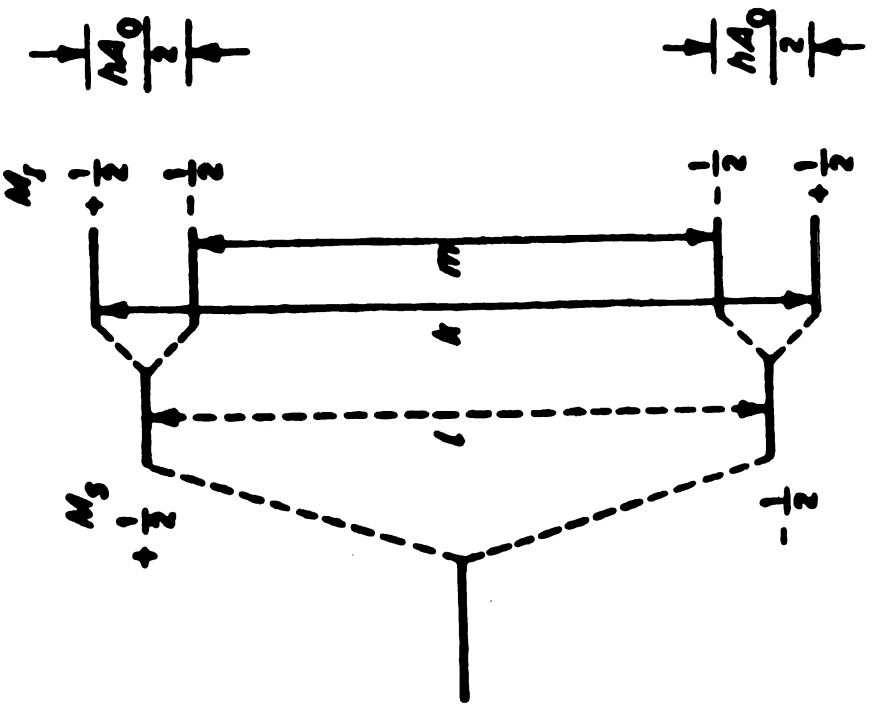

(a)

2) The microwave power is then increased to partially saturate the EPR signal in part 1.

3) An oscillating radio frequency is applied to the sample by means of a frequency generator. This creates a magnetic field H_{rf} on the sample. With the frequency generator, the 10-20 MHz region is scanned while the intensity of the EPR signal is recorded. Besides noise, the base line should be constant indicating a constant EPR absorption. The horizontal axis will be a measure of the frequency of the rf generator.

At frequencies ν_{n1} and ν_{n2} of the rf generator two signals will be recorded (Figure 2.4), one for the electron coupled parallel to the applied magnetic field and the other with it antiparallel. These signals represent changes in the EPR absorption intensity which is the ENDOR spectrum. If we measured the frequencies of these lines at the maximum of each peak we will see that the difference between ν_{n1} and ν_{n2} is numerically equal to the hyperfine coupling, that is 20 MHz that we obtained from the EPR spectrum in our example but measured with a greater precision. Also the mean of the absolute frequencies of ν_{n1} and ν_{n2} will be close to the NMR frequency (ν_N) of the nucleus in the field H_k. Since $\nu_N = g_N\beta_N H_k/h$, if the nucleus responsible for the hyperfine splitting had been uncertain, it would have been possible to establish its identity from the value of g_N. If we repeat the experiment, but setting this time the magnetic field at H_m instead of H_k, an ENDOR spectrum similar to the one previously described would be recorded. However, the relative intensities of the two

Figure 2.4. Changes in the EPR signal amplitude i.e. ENDOR lines for a system with S = 1/2 and I = 1/2 as the rf generator is scanned through the region including the frequencies ν_{n1} and ν_{n2}. From reference 11.

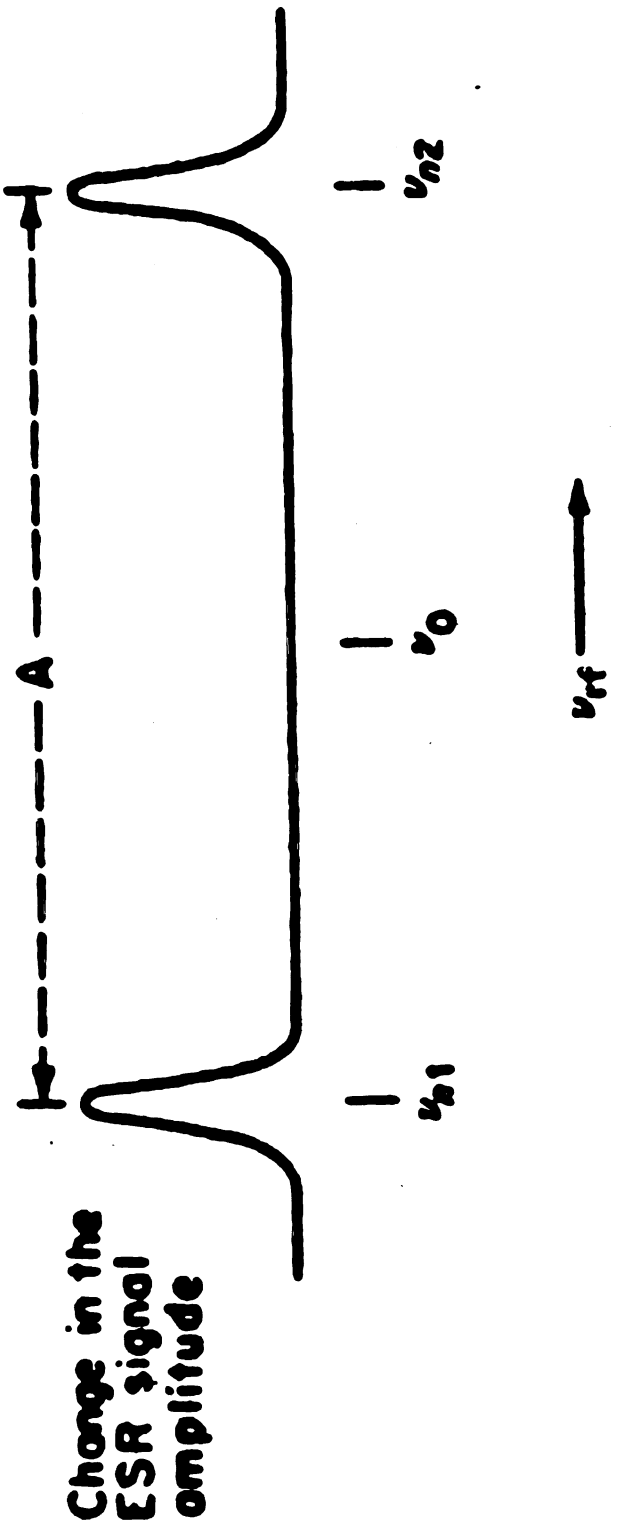
Change in the ESR signal amplitude
A
ν_{n1}
ν_0
ν_{n2}
ν_{rf}

ENDOR lines may not be the same in the two spectra. The ENDOR lines typically represent a change of about one percent of the EPR line intensity, therefore a spectrometer with high sensitivity is required. Even though sensitivity may be a problem in ENDOR spectroscopy, the information that can be retrieved from an unresolved EPR spectrum, *e.g.*, hyperfine coupling constant, identity of an unknown interacting nucleus, quadrupole couplings in a system with $I \geq 1$, is invaluable. Before considering the so-called steady state ENDOR experiment in detail, let us look at the energy levels and possible transitions of this system.

ENDOR Levels and ENDOR Transitions

To obtain a full description of the lines observed in an ENDOR spectrum we need to return to the full Hamiltonian including the nuclear Zeeman term (and quadrupole term if $I \geq 1$). We also need to consider each state at low microwave power and during or immediately after going through one of the frequencies ν_{n1} or ν_{n2} at high rf power. The relative populations of each state depends on the relaxation mechanisms within the system, which in turn affects directly the behavior of the ENDOR resonances in the spectrum. These relaxation processes will be considered in more detail in the next section.

An effective spin Hamiltonian describing the interaction between a nucleus ($I = 1/2$) and an electron ($S = 1/2$) in a magnetic field was presented earlier (Equation 8). This Hamiltonian can be simplified by assuming a fixed magnetic field and a fixed orientation of a single crystal such that effective g and A values may be used. Therefore Equation 8 becomes:

$$H = \beta \cdot \hat{S} g \bar{H} + hA\hat{S} \cdot \hat{I} - g_N \beta_N \hat{I} \cdot \bar{H} \qquad (13)$$

The first-order energy levels (W_{M_S,M_I}) obtained from this Hamiltonian are:

$$W_{1/2,1/2} = 1/2\ g\beta H + 1/4\ hA - 1/2_N g_N \beta_N H \qquad (14a)$$

$$W_{1/2,-1/2} = 1/2\ g\beta H - 1/4\ hA + 1/2\ g_N \beta_N H \qquad (14b)$$

$$W_{-1/2,-1/2} = -1/2\ g\beta H + 1/4\ hA + 1/2\ g_N \beta_N H \qquad (14c)$$

$$W_{-1/2,1/2} = -1/2\ g\beta H - 1/4\ hA - 1/2\ g_N \beta_N H \qquad (14d)$$

where g = electronic g-value

β = Bohr magneton

H = external magnetic field

h = Planck's constant

A = hyperfine coupling constant

g_N = nuclear g-value

β_N = nuclear magneton

These energy levels are schematically represented in Figure 2.5a and b; the nuclear transitions at frequencies ν_{n1} and ν_{n2} are also shown. These nuclear transitions are determined by the selection rules $\Delta M_s = 0$ and $\Delta M_I = \pm 1$. In an ENDOR experiment we do not try to look directly at the absorption of rf power

Figure 2.5. Energy levels of a system with S = 1/2 in a constant magnetic field. The EPR transitions are shown with wide arrows. The solid line represents nuclear transitions which will give rise to ENDOR lines. Microwave saturation of the transition M_I = + 1/2 ($h\nu_{e1}$) (a). Microwave saturation of the transition M_I = - 1/2 ($h\nu_{e2}$) (b). Energy levels at constant microwave frequency (c). From reference 11.

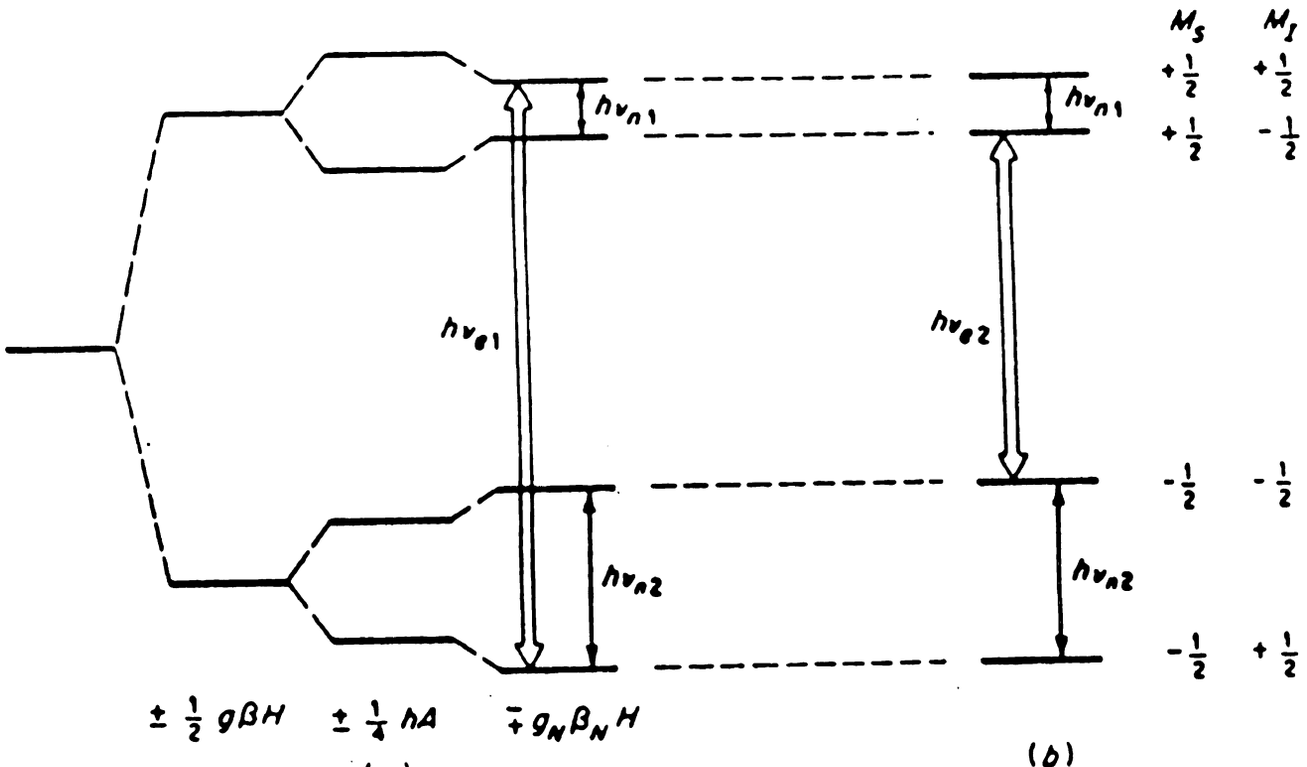
M_S M_I
$+\frac{1}{2}$ $+\frac{1}{2}$
$+\frac{1}{2}$ $-\frac{1}{2}$
$-\frac{1}{2}$ $-\frac{1}{2}$
$-\frac{1}{2}$ $+\frac{1}{2}$
$h\nu_{n1}$
$h\nu_{n1}$
$h\nu_{e1}$
$h\nu_{e2}$
$h\nu_{n2}$
$h\nu_{n2}$
$\pm \frac{1}{2} g\beta H$ $\pm \frac{1}{4} hA$ $\mp g_N \beta_N H$
(a)
(b)

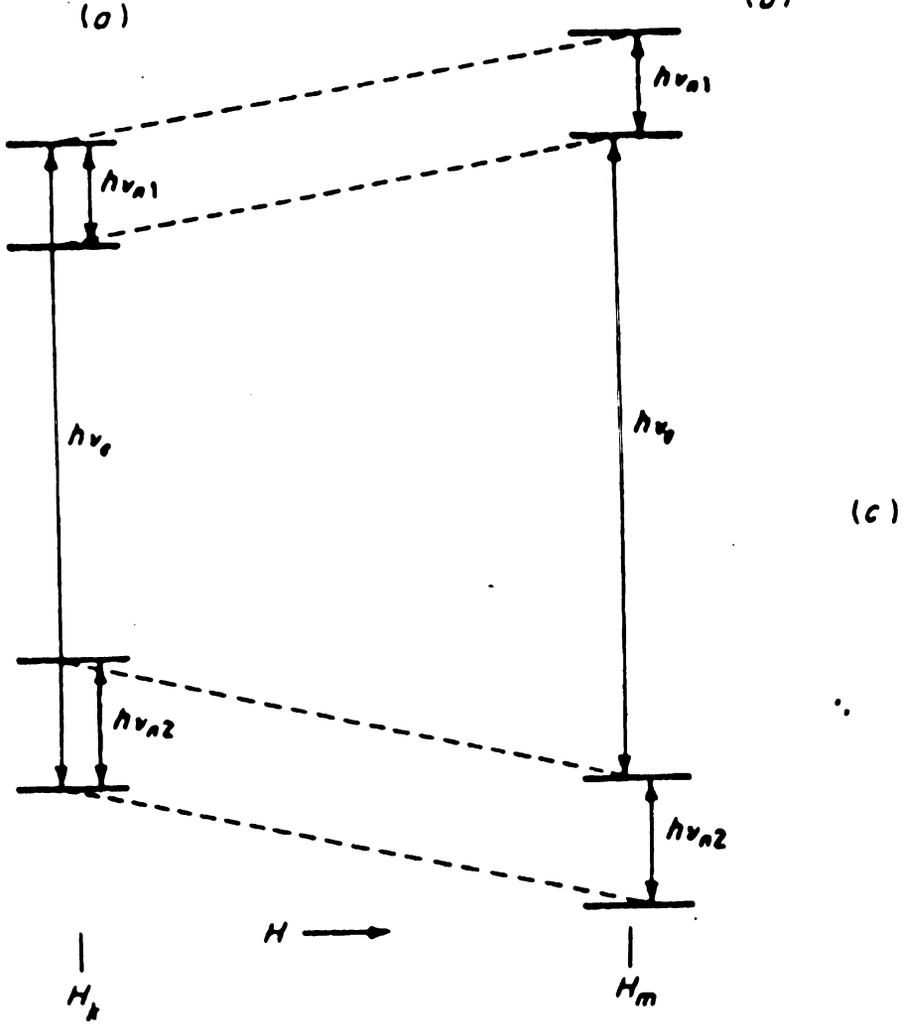
$h\nu_{n1}$
$h\nu_{n1}$
$h\nu_e$
$h\nu_e$
$h\nu_{n2}$
$h\nu_{n2}$
H
H_k
H_m
(c)

at ν_{n1} and ν_{n2} but we look for the changes in the EPR transitions as the population of various states is redistributed. The energy difference for the allowed transitions can be obtained from Equations 14a and 14b:

$$|W_{1/2,1/2} - W_{1/2,-1/2}| = h\nu_{n1} = |hA/2 - g_N\beta_N H| \quad (15)$$

Equation 15 can be rewritten as:

$$\nu_{n1} = |A/2 - g_N\beta_N H/h| = |A/2 - \nu_N| \quad (16)$$

In the same way we obtain for ν_{n2} the following equation:

$$\nu_{n2} = |A/2 + g_N\beta_N H/h| = |A/2 + \nu_N| \quad (17)$$

The reason why absolute magnitude are used in Equations 15, 16 and 17 is because the order of the energy levels can not be established because an oscillating rf field is used in the ENDOR experiment and we can obtain only the energy difference between the energy levels, *i.e.*, we are unable to determine information on the sign of A from the simple ENDOR experiment we consider here. The principal results obtained from the magnitudes of ν_{n1} and ν_{n2} are the determination of the hyperfine coupling A from

$$|A| = \nu_{n1} \pm \nu_{n2} \quad (18)$$

where minus sign applies when $|A|/2 < \nu_n$. An inhomogeneously broadened EPR line is composed of an envelope of many single spin packets; a spin packet is defined as a homogeneously broadened line. The spin-spin relaxation time T_{2e} is the main cause of the inhomogeneous broadening observed in the EPR line. In an ENDOR experiment one spin packet of width $\Gamma \approx 1/T_{2e}$ is saturated and only spins with this packet take part in the ENDOR transitions. In addition to T_{2e}, anisotropy of the g-tensor and hyperfine interactions contribute to EPR line broadening. ENDOR will only depend on the anisotropy of their hyperfine interactions. The net result is that resonance lines are usually narrower in an ENDOR spectrum than in an inhomogeneously broadened EPR spectrum which facilitates the measurement of the hyperfine coupling from ENDOR frequencies. ENDOR lines often have linewidths of about 10 KHz, but they have been observed to range from 3 KHz to 1 MHz.

The concentration of the nuclei present in most EPR and ENDOR experiments is usually too low to permit their NMR detection; that is why ENDOR is used instead of performing an NMR experiment at the nuclear resonance frequency. This greater sensitivity of the ENDOR experiment over regular NMR is due to the following: 1) since the energy of the EPR quantum is greater than that of the NMR quantum, one may have much greater difference in population for the more widely spaced levels. 2) The fact that the nucleus is not only acting in the applied magnetic field but also in the magnetic field of the electron (which is usually on the order of 10^5 to 10^6 gauss at the nucleus) increases the effectiveness of the interacting nucleus in changing the intensity of

an EPR line during an ENDOR experiment. Therefore a greater population difference can be induced than if only an external magnetic field determines these population differences.

Relaxation Processes in Steady-State ENDOR

Even in our simple four level system (Figure 2.5), there are at least three different relaxation times that govern the distribution of population among the energy levels in an ENDOR experiment. These relaxation times not only dictate the temperature range over which the experiment can be performed, but also other experimental conditions such as microwave power; furthermore, these relaxation times determine the nature of the observed ENDOR spectrum. Besides T_{1e}, the spin-lattice relaxation time, one is concerned with T_{1n}, the nuclear spin-lattice relaxation time and T_x, the cross relaxation time. When there are no microwave or rf fields present, the reciprocal of these relaxation times, T_{1e}, T_{1n} and T_x, represent the transition rates between the levels which they connect (see Figure 2.6a). T_{1n} is associated with the nuclear transitions ($\Delta M_s = 0$, $\Delta M_I = \pm 1$) and the cross relaxation times T_x is associated with the "spin flips", that is, processes for which $\Delta(M_s + M_I) = 0$. In general, $T_{1e} << T_x << T_{1n}$. Usually to do an ENDOR experiment in the solid-state one has to work at very low temperature ($\approx$4K). Under these conditions microwave power saturation can be achieved without too much problem because T_{1e} is relatively long. A longer T_{1e} also means that the nuclear transitions (*i.e.*, $\Delta M_I = \pm 1$) will be able to compete with the electronic (*i.e.*, $\Delta M_s = \pm 1$) transitions. One may define the relaxation time T_{2e} based on the width of a normalized line:

Figure 2.6. Relaxation paths for a system with S = 1/2 and I = 1/2 and are labeled by their relaxation times as described in the text (a). Relative state population in the absence of a microwave magnetic field (b). From reference 11.

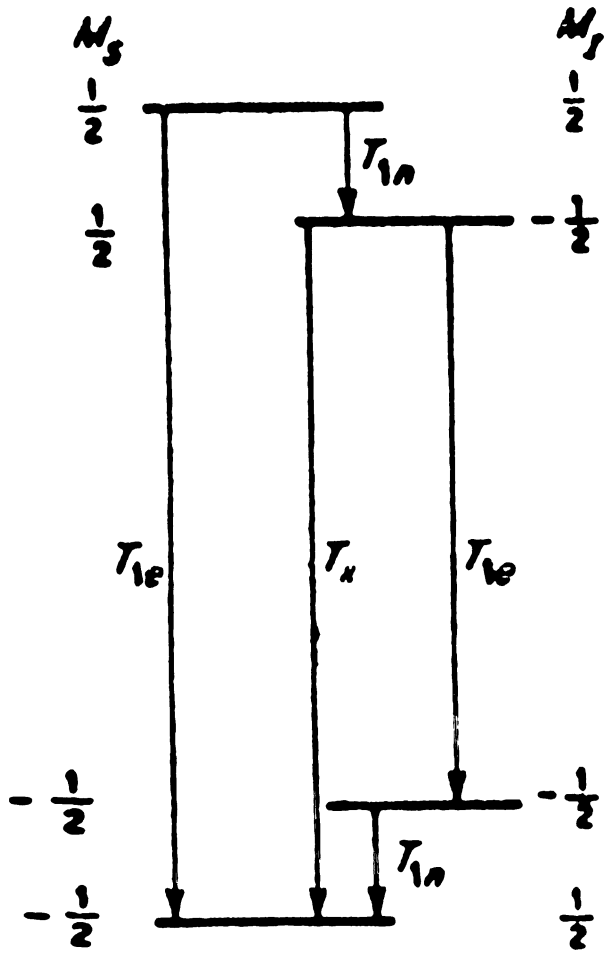
M_S
M_I
$\frac{1}{2}$
$\frac{1}{2}$
T_{1n}
$\frac{1}{2}$
$-\frac{1}{2}$
T_{1e}
T_x
T_{1e}
$-\frac{1}{2}$
$-\frac{1}{2}$
T_{1n}
$-\frac{1}{2}$
$\frac{1}{2}$

(a)

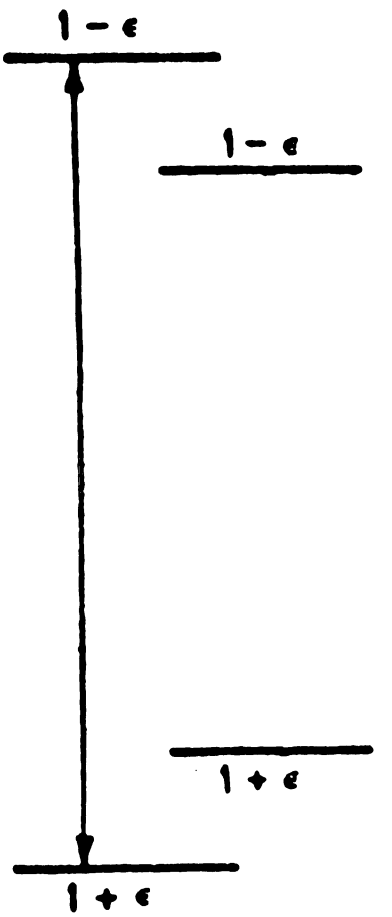
$1-\epsilon$
$1-\epsilon$
$1+\epsilon$
$1+\epsilon$

(b)

$$1/T_{2e} = k\,\gamma_e\Gamma \qquad (19)$$

where

Γ is half the linewidth at half height

k is a constant which depends on the lineshape

γ_e is the electronic magnetogyric ratio.

T_{1e} can be no shorter than T_{2e} to avoid contribution to line broadening from spin-lattice relaxation. If T_x is not too long and if the above condition holds (*i.e.*, $T_{1e} \geq T_{2e}$) one may achieve a steady-state condition.

Let us look in more detail at the steady-state ENDOR experiment described for our system with S = 1/2 and I = 1/2. The microwave field H_{1e} necessary to partially saturate the EPR signal will be at its optimum value when $\gamma_e^2 H_{1e}^2 T_{1e} T_{2e} \approx 3$ (9). The next step is to increase the power level of the rf generator and hence the amplitude of the rf magnetic field H_{1n}. This H_{1n} is set so that $N_\uparrow$, the rate of upwards transitions at ν_{n1}, is relatively large when compared to the reciprocal of T_x, that is $N_\uparrow \geq 1$. In other words a large value of H_{1n} is required to allow the transitions $\Delta M_s = 0$, $\Delta M_I = 1$ to compete with the $\Delta(M_s + M_I)$ transitions, the latter transitions correspond to cross relaxation processes. When the rf generator frequency passes through the value ν_{n1}, an ENDOR line is observed. The ENDOR line corresponding to ν_{n2} will be also observed when the rf generator goes through the frequency ν_{n2}. If the only effective relaxation pathways were those that we have just discussed, it would be

necessary to saturate the line at the H_a field after going through the frequency ν_{n1} before being able to see the ENDOR line corresponding to ν_{n2}.

The next subject that we need to consider is the relative populations of the energy levels under different conditions. If no external magnetic field is present, the population for our simple 4 level system would consist of four degenerate levels with the individual populations at each level equal to N/4, where N is the total number of unpaired electrons. If we now applied an external magnetic field, the populations of states will be:

$$M_s = +1/2 \quad N_{1/2} = \frac{N}{4} \exp\left(-\frac{g\beta H}{2KT}\right) \approx \frac{N}{4}(1-\epsilon) \qquad (20a)$$

$$M_s = -1/2 \quad N_{-1/2} = \frac{N}{4} \exp\left(+\frac{g\beta H}{2KT}\right) \approx \frac{N}{4}(1+\epsilon) \qquad (20b)$$

where $\epsilon = g\beta H/2kT$, k is the Boltzman constant and T is the absolute temperature. To avoid repeating the use of the factor N/4 all population numbers will be divided by it, therefore Equations 20a and 20b will become $1 - \epsilon$ and $1 + \epsilon$, respectively. These populations are schematically represented in Figure 2.6b. If for example the $M_{1/2}$ transition is induced by a microwave field, the only relaxation path will be T_{1e} (Figure 2.6b) because the relaxation through T_x will be too slow since T_{1n} is in series with it and $T_{1e} << T_x << T_{1n}$.

Although the ENDOR experiment only involves partial saturation of the electron spin transitions let us assume, for the sake of simplicity, total equalization of populations of states $M_I = 1/2$ and $M_I = -1/2$, these are shown

in Figure 2.7a and 2.7b, respectively. To be able to saturate the $M_I = 1/2$ transition we should note that the $|1/2,1/2>$ and $|1/2,-1/2>$ states have a population difference equal to ϵ, but in the absence of microwave saturation the difference is equal to $\epsilon_n = g_n\beta_n H/2kT$. Therefore, if a short circuiting path is provided, there could be a partial depopulation of the $|1/2,1/2>$ state as compared to the $|1/2,-1/2>$ state. This short circuiting path is provided by the rf field at the ν_{n1} frequency. The rate of transition between the $|1/2,1/2>$ and the $|1/2,-1/2>$ states must be at least equal to T_x^{-1}. If, on the other hand, the $M_I = -1/2$ transition is to be saturated, it will be the $|1/2,-1/2>$ and the $|-1/2,1/2>$ states which will go through the "depopulation" process. The difference in population will be again ϵ, and the rf field at ν_{n1} will induce the nuclear transition and therefore an ENDOR line.

It can be seen that the magnitude of the "ENDOR effect" depends upon the relative magnitudes of the relaxation times, T_{1e}, T_{1n} and the cross relaxation time T_x. Optimum ENDOR signals are obtained when T_{1e} and T_{1n} are comparable.

Anisotropic Hyperfine Interaction

As discussed above when a radical is tumbling fast in solution all the anisotropic interactions are averaged to zero but when the motion is slowed down this is no longer true. We have to understand these anisotropic interactions to be able to analyze the ENDOR spectra of powders and non-oriented solids.

Figure 2.7. Relative populations of levels in a system in which the ENDOR behavior is governed by T_{1e} and T_x. Upon saturation of the low field EPR line, only the lower frequency ENDOR lines is observed (a). Upon saturation of the high field EPR line, only the high frequency ENDOR line is observed (b). From reference 11.

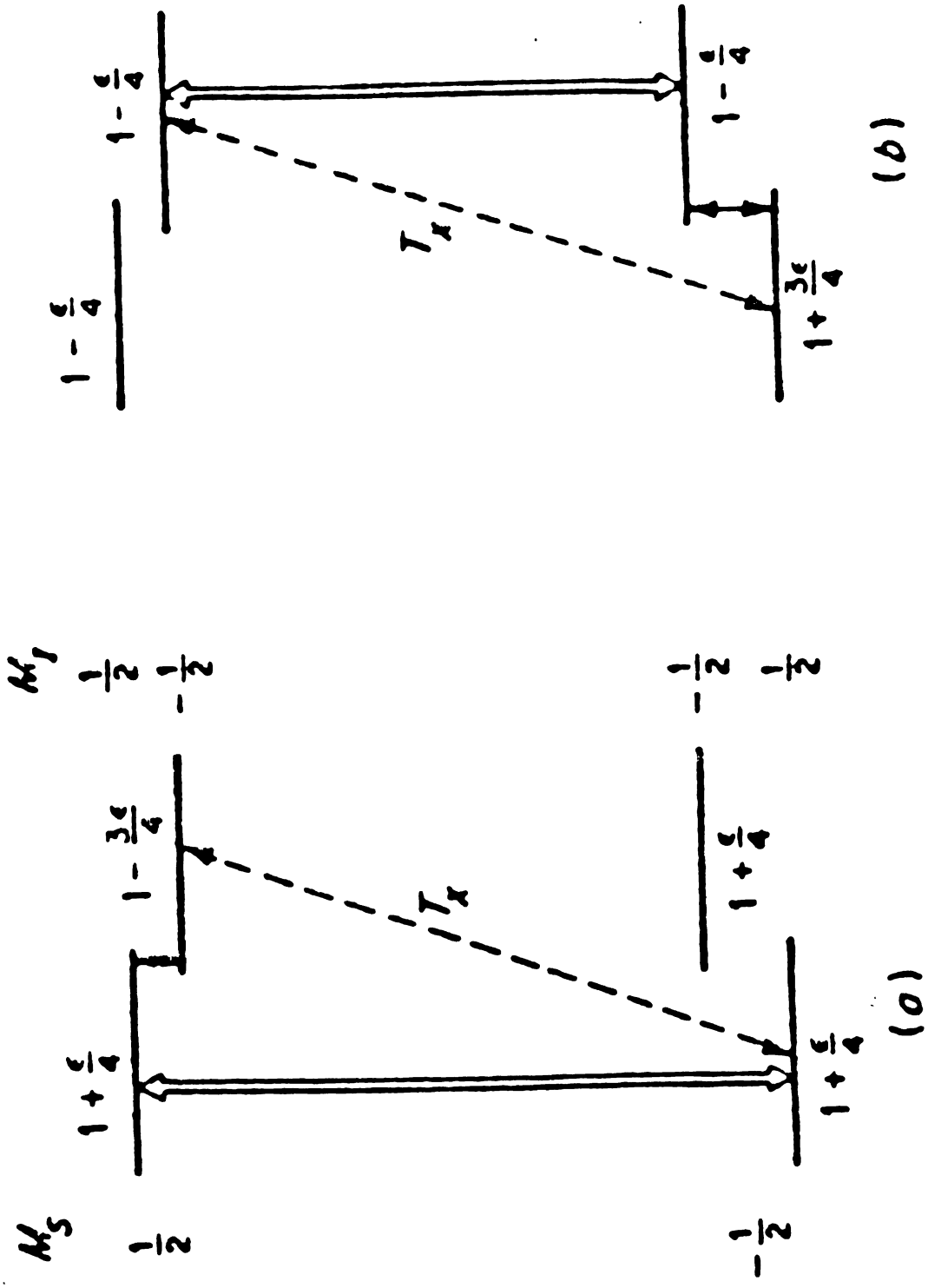
$1-\frac{\epsilon}{4}$
$1-\frac{\epsilon}{4}$
T_x
$1-\frac{\epsilon}{4}$
$1+\frac{3\epsilon}{4}$
(0)
M_1
$-\frac{1}{2}$
$-\frac{1}{2}$
$-\frac{1}{2}$
$-\frac{1}{2}$
$1-\frac{3\epsilon}{4}$
$1+\frac{\epsilon}{4}$
T_x
$1+\frac{\epsilon}{4}$
$1+\frac{\epsilon}{4}$
(0)
M_5
$-\frac{1}{2}$
$-\frac{1}{2}$

Let us consider the case of an organic radical in a single crystal. To simplify the explanation we are going to assume that the g-tensor is isotropic but $\hat{\bar{A}}$, the hyperfine coupling tensor is not. The spin Hamiltonian describing such a system will have the following form:

$$H = g\beta\bar{H} \cdot \hat{S} - g_N\beta_N\bar{H} \cdot I + h\hat{S} \cdot \hat{\bar{A}} \cdot \hat{I} \qquad (21)$$

where $\hat{\bar{A}}$ is composed of nine cartesians components representing the coupling between the tensors $\hat{S}$ and $\hat{I}$ each of which consist of three vector components (9). If we choose a set of laboratory axes x' y' z', and take the direction of the magnetic field along the z' direction and use the strong field approximation, *i.e.*, that the electron Zeeman interaction dominates, we can rewrite Equation 21 as

$$H = g\beta H_{z'}S_{z'} - g_N\beta_N H_{z'}I_{z'} + h(S_{z'}A_{z'x'}I_{x'} + S_{z'}A_{z'z'}I_{z'}) \qquad (22)$$

Since we took the magnetic field along the z' direction all the $S_{x'}$ and $S_{y'}$ terms in Equation 22 are eliminated. Then if we take S = 1/2 we will have the following expression for the ENDOR frequency:

$$\nu_{ENDOR} = |\nu_N \pm R/2| \qquad (23)$$

which is analogous to the expression:

$$\nu_{ENDOR} = |\nu_N \pm A/2| \qquad (24)$$

which is the general form of the "ENDOR resonance condition". R in equation 23 is equal to:

$$R = (A^2_{z',x'} + A^2_{z',y'} + A^2_{z',z'})^{1/2} \qquad (25)$$

If the crystal is oriented in such a way that the tensor is diagonal to the laboratory x' y' z' axes system, then $R = A_{z',z'}$. R can be considered as an effective hyperfine coupling for each particular orientation of the radical with respect to the magnetic field. As can be seen R depends on the orientation of the radical with respect to the field and in general involves contributions of the different components of the hyperfine tensor. From a study of R versus the rotation angle of the external magnetic field around the axes of the single crystal, all the components of A can be obtained. Let us briefly see how this is accomplished. First the crystal is oriented by either its external morphology or by X-ray analysis. Then orthogonal crystal axes are chosen, let us call them xyz. In general for molecular crystals one must pick orthogonal axes that are not symmetry axes of the radical or molecules in the crystal. The direction of the external magnetic field relative to our xyz axes can be obtained by using the direction cosines; l_x, l_y, l_z (9). Therefore we measure R from the ENDOR spectra which in a general way is given by (9,10)

$$R = [\ l^2_x\ (A^2_{xx} + A^2_{xx} + A^2_{xz}) + l^2_y(A^2_{yx} + A^2_{yy} + A^2_{yz})$$

$$+ l_z^2 (A_{xx}^2 + A_{zy}^2 + A_{zz}^2) + 2l_x l_y (A_{xx}A_{xy} + A_{xy}A_{yy} + A_{zx}A_{zy})$$

$$+ 2l_x l_z (A_{xx}A_{xz} + A_{xy}A_{zy} + A_{xz}A_{zz})$$

$$+ 2l_y l_z (A_{xy}A_{xz} + A_{yy}A_{yz} + A_{yz}A_{zz})]^{1/2} \qquad (26)$$

Equation 26, can be rewritten as (17):

$$R = [l_x^2 T_{xx} + l_y^2 T_{yy} + l_z^2 T_{zz} + 2l_x l_y T_{xy}$$

$$+ 2l_x l_z T_{xz} + 2l_y l_z T_{yz}]^{1/2}$$

where T_{ij} are the elements of a symmetric tensor, that is, the square of the hyperfine tensor. Therefore if we can obtain the T_{ij} elements, then we can also obtain the A_{ij} elements.

To obtain the T_{ij} elements we take data with each individual xyz component perpendicular to the external magnetic field, then we calculate R by using the direction cosines and Equation 26. Next the T matrix is rotated to a new XYZ coordinate system and diagonalized. In its diagonal form $T_{xx} = A_{xx}^2$ so the principal values of the diagonalized A tensor in the new coordinate system

XYZ are determined. We can now separate the isotropic components from the anisotropic components in the A tensor. The isotropic part is given by:

$$A_{iso} = \frac{1}{3}(A_{XX} + A_{YY} + A_{ZZ}) \tag{27}$$

and the anisotropic components are given by:

$$B_{XX} = A_{XX} - A_{iso} \tag{28a}$$

$$B_{YY} = A_{YY} - A_{iso} \tag{28b}$$

$$B_{ZZ} = A_{ZZ} - A_{iso} \tag{28c}$$

We should note that the dipolar tensor is traceless, *i.e.*, the anisotropic components add to zero. Finally, we must relate the principal axes of the total hyperfine tensor in the new XYZ coordinate system to our laboratory axes system xyz. This is done by calculating the direction cosines of the XYZ axes relative to the xyz axes.

Unfortunately many radicals cannot be studied in single crystals because the crystals are too small or no crystal can be obtained. The latter is particularly true for biological systems. When studying a powder sample, where the molecules are randomly oriented with respect to the external magnetic field, *e.g.*, frozen radicals, biological samples, important information can still be obtained. The concepts introduced in this chapter will be seen again in Chapters 4 and 5 where treatment of experimental ENDOR data will be discussed.

References

1. Norris, J.P., Scheen, H. and Katz, J.J. (1979) in: The Porphyrins, Vol. 4, Chapter 3, Academic Press, Inc.

2. Feher, G. (1979) Phys. Rev. 103, 834.

3. Hyde, J.S. and Maki, A.H. (1964) J. Chem. Phys. 40, 3117.

4. Carrington, A., and McLachlan, A.D. (1969) in: Introduction to Magnetic Resonance, Harper and Row, New York.

5. Inui, T. Harasawa, S. and Obata, Y., (1956) J. Phys. Soc. Japan, 11, 612.

6. McConnell, H.M. and Robertson, R.E. (1957) J. Phys. Chem. 61, 1018.

7. Fermi, E. (1930) Z. Physik, 60, 320.

8. Wertz, J.E. and Bolton, J.R. (1986) in: Electron Spin Resonance, Chapman and Hall.

9. Kevan, L. and Kispert, L.D. (1976) in: Electron Spin Double Resonance Spectroscopy, John Wiley and Sons.

10. Atherton, N.M. (1973) in: Electron Spin Resonance, Halsted, London, Chapter 4.

11. Kurreck, H. Kirste, B. and Lubitz, W. (1984) Angew. Chem. Ing. Ed. Engl. 23, 173.

CHAPTER 3
PLASTOQUINONE QUANTITATION IN PHOTOSYSTEM II MEMBRANES

Introduction

In 1959 Kofler and co-workers (1) isolated plastoquinone (PQ, Figure 3.1a) from dried lucerne. Interest in its physiological function arose after the realization that a related substance, ubiquinone (Figure 3.1b), was involved in mitochondrial electron transport. Plastoquinone, so named because of its localization in the plastids of plant cells, and to avoid confusion with ubiquinone, was found to occur exclusively in oxygen-evolving material: algae, including blue green algae, and higher plants (2-5). It soon became apparent that plastoquinone is not a single substance but a series of related substances that can be isolated from green plant material. The most abundant and probably the most important is plastoquinone 9 or PQ_9 (6), also known as plastoquinone A. Its structure was elucidated by Trenner *et al.* (7) and by Kofler (1). Studies of photosynthetic reactions (8-11) indicated the importance of this species in serving in several functions in Photosystem II (PSII).

The first demonstrated protein bound quinone in photosynthetic systems was the primary acceptor quinone of reaction centers from the photosynthetic bacterium *Rhodobacter spheroides* (12-16). The electron acceptor system of these reaction centers is now recognized as a complex containing two ubiquinones (Q_A and Q_B) acting in series as primary and secondary acceptor quinones (16-18). An

Figure 3.1. Structure of plastoquinone-9 (a) and ubiquinone-9 (b).

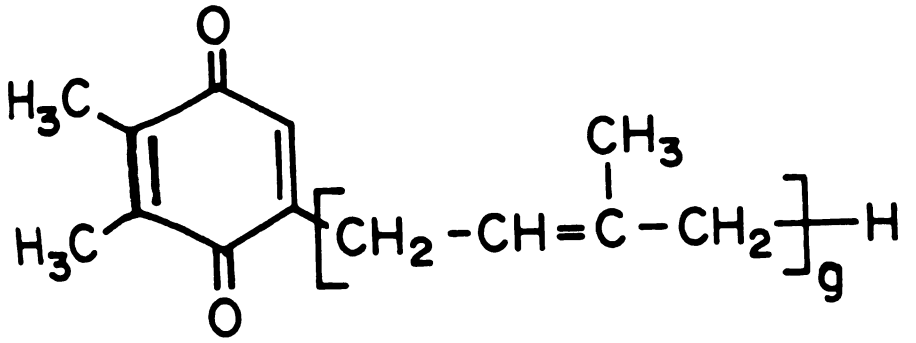

PLASTOQUINONE

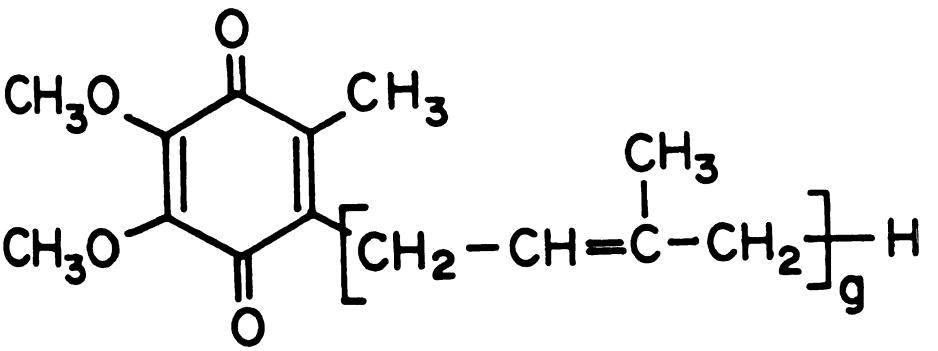

UBIQUINONE

iron atom (Fe^{2+}) is located close enough to interact magnetically with semi-reduced forms of both acceptor quinones (18-21), but is not directly coordinated to them (22). Although iron may be involved in electron transfer between them (23), this function is not certain (24). Klimov *et al.* (25) demonstrated that a similar iron-PQ acceptor complex was present in PSII. The iron does not undergo changes in oxidation state during the electron transfer reactions. In photosynthetic bacteria, as in PSII, iron is coupled to Q_A and Q_B (26). Replacement of this metal by other divalent cations, *e.g.*, Mn^{2+}, Co^{2+} Cu^{2+}, did not show any changes in the electron transfer characteristics of the iron-depleted reaction centers; however, the presence of a metal ion is necessary to establish the native electron transfer properties of Q_A (27). DeVault has suggested that the role of the iron is primarily electrostatic (28).

Besides Q_A and Q_B, plastoquinone has also been implicated as playing a role on the donor side of PSII. EPR and optical data, as well as extraction/reconstitution results, had been interpreted to indicate that the radicals that give rise to characteristic Signal II EPR spectra, Y_Z^+ and Y_D^+ were plastoquinone cation radicals (29-32). The Y_Z^+ species acts on an intermediate electron carrier between the oxygen-evolving complex and the reaction center of PSII, P_{680} (35). The Y_D^+ species has an EPR spectrum essentially identical to Y_Z^+ but its function has yet to be elucidated. A donor side specific plastoquinone requirement was also suggested by the results of electron transfer assays in membranes that had been extracted and reconstituted with a variety of variously substituted quinones (9). Although recent work now strongly indicates that

Y_D^+ and Y_Z^+ are tyrosine radicals, the possibility that an additional quinone requirement occurs on the donor site of PSII remains. Quinone quantitation is a means by which to assess this possibility and, in fact, played an important role in casting doubt on the assignment of Y_Z^+ and Y_D^+ as plastoquinone species (23,24,33,51).

There have been several determinations of the concentration of quinones in PSII membranes (23,24,33). In these studies between one and two quinones per reaction center were found. These groups used organic solvents to extract the quinones from the membranes without any chemical treatment prior to the extraction. Under these conditions quinones from acceptor side (*i.e.*, Q_A and Q_B) are most likely to be extracted, because they appear to be fairly loosely bound and probably close to the surface of the membrane (16). If PQ species are also functional on the donor side of PSII, they might be deeper in the membrane structure and therefore more difficult to extract. If there are quinones buried in the membrane protein, denaturation by organic solvent addition could cause the membrane to collapse around the quinones and physically trap them before they are released into solution and hence before the extraction is completed. By disrupting or digesting the membranes with, for example, urea or chymotrypsin prior to the extraction with organic solvents, the possibility of the quinones being trapped by the membranes is likely to be reduced.

In the experiments reported here we have used high pressure liquid chromatography (HPLC) to determine the amount of plastoquinone present in PSII membranes. Different chemical and enzymatic treatments were used prior

to the extraction of the membranes with organic solvents. The release of quinones as a function of the incubation time under these various treatments was also studied. An average of 1.52 ± 0.23 quinones per reaction center was found. This number is in agreement with those previously reported (23,24,33). This suggests that there are no PQ molecules deeper in the membrane structure of PSII membranes.

Materials and Methods

Isolation and Purification of Plastoquinone

Market spinach was used for preparing chloroplasts. Leaves were kept in the dark at 4°C prior to use, then washed in cold distilled water and deveined under low light conditions. They were broken in a Waring blender for 12 s in a standard reaction solution containing 0.4 M NaCl, 20 mM HEPES, 2 mM $MgCl_2$, 1 mM EDTA and 2 mg/ml bovine serum albumin, pH adjusted to 7.5. The homogenate was then strained through 8 layers of cheese cloth and centrifuged for 2 minutes (5,000 rpm, SS - 34 Sorvall rotor) at 4° C. The pellets were resuspended in a medium consisting of 0.5 M sucrose, 2 mM phosphate, pH adjusted to 7.5. Chlorophyll concentration ranged between 1-2 mg chlorophyll/ml as determined by the Sun and Sauer method (36).

The extraction and purification of PQ_A from these chloroplasts is based on modifications to procedures described by Barr *et al.* (37). The chloroplast preparation (100 ml) was mixed with H_2O (400 ml), isopropanol (500 ml), and heptane (500 ml) in a ratio of 2:2.5:2.5. The mixture was divided into three equal aliquots, separated in erlenmeyer flasks and protected from light. The

flasks were shaken on a reciprocal shaker for about 5 hours, after which the contents of each flask was transferred to a separatory funnel and stored overnight protected from light at about 12° C to allow phase separation to proceed. The dark green epiphase (*i.e.*, organic phase) that formed was washed with a mixture of methanol:water (1:1). The hypophase (*i.e.*, aqueous phase) of this mixture was discarded and the epiphase was stored protected from the light at about 12° C. Under these conditions additional hypophase was formed and discarded. The epiphase was washed with heptane and anhydrous sodium sulfate (Na_2SO_4) was added. Then the mixture was filtered and rotovapped to dryness.

Column chromatography was carried out with silica gel (60-200 mesh, Grade 950; MCB chemicals). The organic extract from the previous step was dissolved in about 7 ml of heptane and added to the top of the column with a pipet. After allowing this aliquot to soak evenly in the column, a solvent mixture of ether:CH_2Cl_2:hexane(1:15:84) was used as a mobile phase. Most of the carotenoids and chlorophyll were removed by this chromatography. The fraction that eluted following these two components was collected and rotovapped to dryness. A second chromatography was performed on the concentrate collected in the previous separation by following the same protocol but using CH_2Cl_2:hexane(15:85) as the solvent mixture. Plastoquinones were absorbed and held by the column while some of the other components (xantophylls, chlorophyll and carotenoids) in a yellowish fraction were eluted. After the yellowish fraction was eluted the solvent mixture was gradually changed to a final mixture that consisted of ether:hexane(50:50). The fraction collected with this last solvent mixture was

concentrated by evaporation and redisolved in about 7 ml of heptane. A final chromatographic separation was performed on this fraction. The solvent composition used for this step was ether:CH_2Cl_2:hexane (3:12:85). The first fractions eluting from the column were rich in plastoquinones. The plastoquinones obtained were then recrystalized from ethanol (200° proof). The absorption spectra in Figure 3.2 show the UV optical characteristics of the plastoquinones obtained by this method and those of a standard of plastoquinone (supplied by Dr. P.F. Sorter from Hoffman-LaRoche, Nutley, NJ). The agreement is clear.

Analysis of PSII Membranes

PSII particles were isolated from spinach by following the procedures in (38). The samples were treated at room temperature by using one of the following before extracting with organic solvents: a) 1M NaCl, b) 8M urea, or c) chymotrypsin (2 mg/mg chl at pH = 6.0). A control sample was used where no treatment was given prior to extraction with organic solvents. All three treatments were done as functions of incubation time. The protocols for subsequent PQ_A extraction and quantitation were based on those described by DeVitry *et al.* (24) After each treatment the membranes were extracted at room temperature by using hexane or heptane and 0.4% methanol (MeOH). The results presented here were obtained by using hexane extraction of PSII particles (270 mg of chlorophyll), although both hexane and heptane mixtures gave identical determinations of PQ_s. To oxidize any endogenous reduced quinone and to keep the quinones oxidized during extraction, the extraction was carried out in the presence of DCIP (270 μmole/mg Chl). The samples were extracted three times

Figure 3.2. Absorption spectra of oxidized (solid trace) and reduced (dash trace) of PQ_9 extracted from spinach chloroplasts (a) and of a standard of PQ_9 (b).

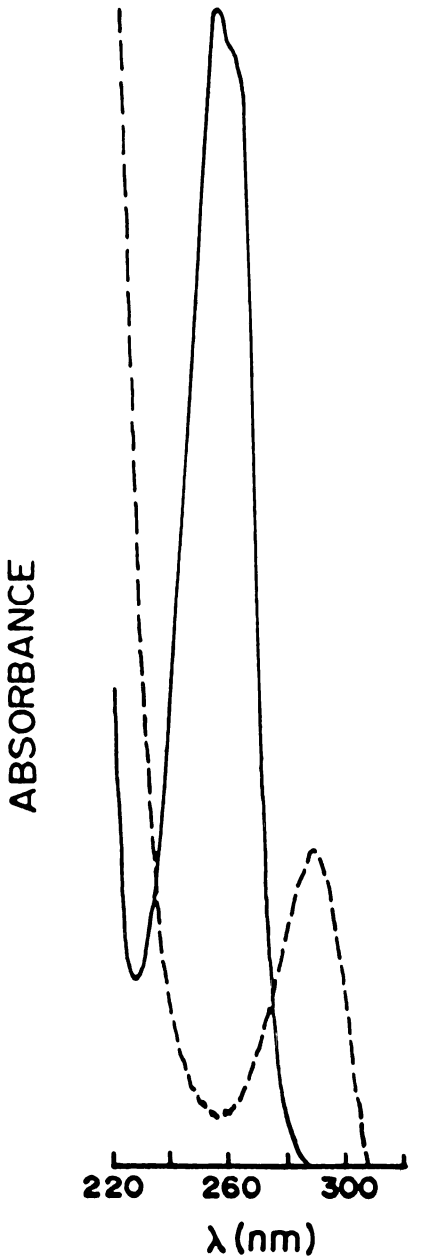
ABSORBANCE
220
260
300
λ (nm)

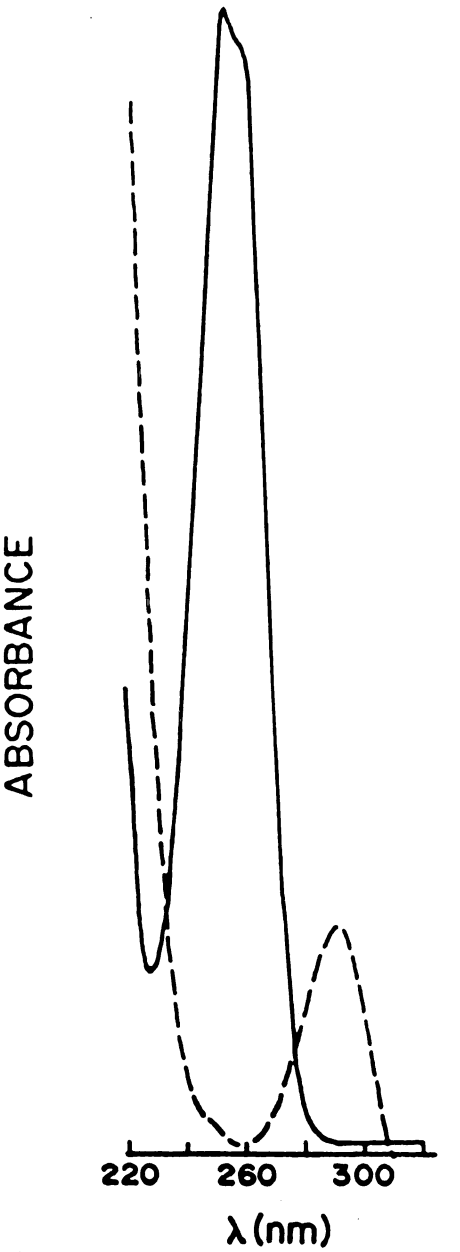
ABSORBANCE
220
260
300
λ (nm)

with the hexane/MeOH mixture (≈3-5 ml/per extraction) by shaking by hand in a separatory funnel. The organic phase was collected, evaporated to dryness, dissolved in n-heptane (≈1 ml) and filtered with a silica Sep Pak (Waters Associates). The Sep Pak was washed with benzene (≈10 ml) followed by a wash with a mixture that contained (3:2) hexane: CH_2Cl_2 (≈10 ml). The eluant was evaporated to dryness and dissolved in ethanol (Aldrich, HPLC grade) and applied to an HPLC column. HPLC was done on a Waters bondapack C-18 column (reverse phase, 3.9 x 30 mm) with methanol-isopropanol (3:1 v/v) at a rate of 1.5 ml/min. The absorbance of the mobile phase was monitored at 254 nm, which is appropriate for the 255 nm absorbance maximum for oxidized PQ_9 (Figure 2). Retention time for PQ_9 was found to be seven minutes by using a standard solution of PQ_9 previously extracted and purified from spinach chloroplasts. To determine the percent recovery for these procedures a control experiment was done with a standard of pure plastoquinone of known concentration. Under the conditions described at least 90% of the quinone was recovered.

Results

Figure 3.3 shows typical HPLC elution profiles for the PSII extracts. Figure 3.3a is the elution profile of a standard sample of purified PQ. Traces 3.3c, 3.3d and 3.3e are the analysis of the extracts treated prior to the extraction with chymotrypsin, 1M NaCl and 8 M urea, respectively. Trace 3.3b is the control sample, *i.e.*, no treatment before the extraction and trace 3.3f is a sample trace showing the background when the sample size was too large or the sample was not filtered with a Sep Pak as described in the methods section.

Figure 3.3. HPLC elution profile of a standard of PQ_9 (a). Traces c, d and e are from extracts from samples treated with chymotrypsin, 1M NaCl and 8M urea respectively. Trace b is the control sample (i.e. no pretreatment) and trace f shows the background when sample size was too large or no Sep Pack was used.

A(λ = 254)
(a)
(b)
(c)
(d)
(e)
(f)
1 2 3 4 5 6 7
RETENTION TIME (min)

Table 1 shows the levels of PQ_9 found in PSII particles isolated from spinach. Results represent an average of three measurements for each analysis. The analysis of the organic extract gives an average of 7.19 ± 1.1 nmol PQ_9/mg Chl. There are about 250 chlorophylls per reaction center in photosystem II membrane preparations (39); taking the molecular weight of chlorophyll to be 890 g/mole, this gives a ratio of PQ_9 to PSII in our analysis of 1.5 PQ_9/PSII. The amount of PQ_9 found in the samples that were chemically treated prior to the extraction with organic solvents and those samples with no pretreatment is the same within experimental error.

In our initial experiments, partial reduction of the samples was detected after the extraction. To keep all the quinones in the oxidized state DCIP was added (24) and the samples protected from light. The presence of reduced quinones gave inaccurate results for two reasons: 1) the retention time of reduced PQ_9 is expected to be different from that of oxidized PQ_9, and 2) the absorption maximum for oxidized PQ_9 is 255 nm (40) and that of reduced PQ_9 is 290(40). The eluant was monitored at 254 nm and therefore, any reduced quinones will go essentially undetected.

Figure 4 shows the time course study of release of PQ_9 from the membranes. The release of the quinones takes less than a minute. The amount of PQ_9 remains constant (with an average of 7.16 nmol PQ_9/mg chl) even after 20 minutes of incubation in NaCl, urea or chymotrypsin. Longer extraction times (more than 30 minutes) do not increase further the amount of PQ_9 found in the samples.

Table 1 LEVEL OF PQ_9 IN PSII PARTICLES

	Molar Ratio nmol/mg Chlp	(PQ_9/PSII particles)
No treatment	7.25 ± 1.1	1.61
chymotrypsin (2mg/mg Chl)	6.78 ± 1.0	1.50
1M NaCl	6.93 ± 1.0	1.54
8M urea	7.78 ± 1.2	1.74
*Tabata *et al.*	7.4	1.65
*Omata *et al.*[a]	8.3	1.85
*deVitry *et al.*[b]	5.2	1.16

*No Treatment

[a]in PSII's reaction centers ≈ 50 Chl/p_{680}

[b]from *Clamydomonas reinhardtii* reaction centers

Figure 3.4. Molar ratio (PQ/PSII particles) vs incubation time for the different treatments given to samples prior extraction.

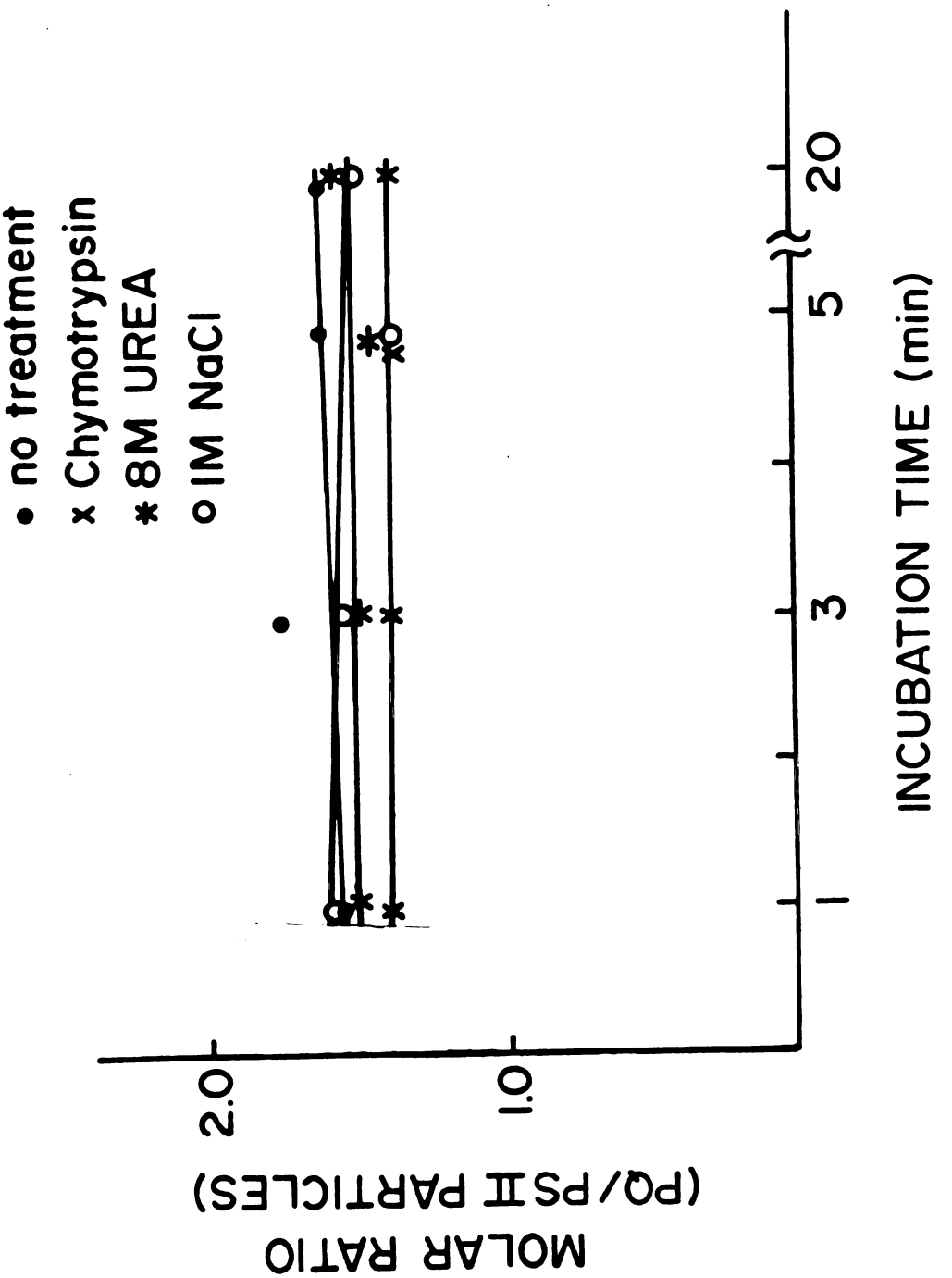
• no treatment
x Chymotrypsin
* 8M UREA
o IM NaCl
MOLAR RATIO
(PQ/PSII PARTICLES)
2.0
1.0
1
3
5
20
INCUBATION TIME (min)

Discussion

Three different methods for quantitation of plastoquinone have been reported in the literature. The first method is based on solvent extractions of plastid lipids, separation by thin layer chromatography (TLC) and spectrophotometric analysis (4). The second method uses hexane extraction combined with a separation step into a mixture of water and methanol to reduce interference from chlorophylls and carotenoids (3). The organic extract is then examined as in the previous method. The third method provides an analytical procedure to analyze quinones quantitatively and utilizes high performance liquid chromatography (HPLC) (23). The HPLC procedure is excellent for small sample analysis and requires minimal sample preparation as compared to the other two methods.

The three methods mentioned above are based on extraction of the plastoquinones from the membranes with organic solvents without any enzymatic digestion or chemical pretreatment. The rationale for disrupting the membranes before extracting with organic solvents is to reduce the possibility of quinones being trapped within the membrane when these protein/lipid structures are denatured by the addition of the organic solvents. For enzymatic digestion, chymotrypsin (2 mg/mg Chl, pH = 6.0) was used. Chymotrypsin catalyzes the hydrolysis of peptides in two distinct states (40). The first one is the combination of the substrate with chymotrypsin to form an enzyme substrate complex. The ester bond of the substrate is cleaved and water then attacks the complex and regenerates the enzyme. Tests on various synthetic peptides as substrates showed that the enzyme is an endopeptidase, *i.e.*, it can split certain types of

peptide linkages wherever they occur in a peptide chain, in contrast to the exopeptides which can split only terminal peptide bonds (42). Moreover, chymotrypsin is specific for those peptide linkages in which the carbonyl function is contributed by aromatic amino acid residues, *e.g.*, tyrosine, tryptophan, and phenylalanine; it also hydrolyzes the amides of these amino acids. The active site in chymotrypsin has two distinct features, a hydrophobic zone for binding and positioning the substrate in the active site and a catalytic portion for removing and transferring the acyl group (Figure 3.5). Figure 3.6 shows some of the compounds hydrolized by chymotrypsin (43). By treating the membranes with chymotrypsin prior to extraction with organic solvents, the polypeptides can be broken down to molecules of smaller size, thus allowing an easier diffusion of the quinones into solution upon subsequent extraction with organic solvents.

From similarities of the bacterial reaction center in function and amino acid sequence homology to Photosystem II, it was proposed that the D-1 and D-2 polypeptides carry the reaction center of PSII (44, 45). The model is based on the homology of the bacterial and plant photosystem; the X-ray structure and mutation data of the former allowed a detailed, but largely speculative, description of the Q_B and Q_A binding site of the latter (46). According to this model, amino acids from the end of transmembrane helix IV (see Figure 3.7), from the beginning of transmembrane helix V, and from the parallel helix between these two and a stretched sequence between the end of the parallel helix and the beginning of helix V make up the binding site of Q_B and herbicides on the D-1 subunit (47). Trebst has proposed that the four histidines on helices IV and V

Figure 3.5. Illustration of the active-site in chymotrypsin.

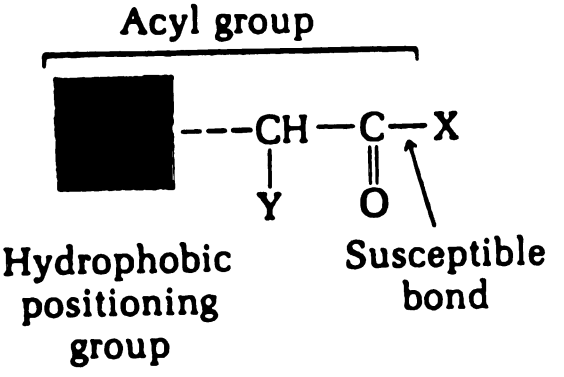
Acyl group
---CH—C—X
Y
O
Hydrophobic positioning group
Susceptible bond

Figure 3.6. Some of the compounds hydrolized by chymotrypsin.

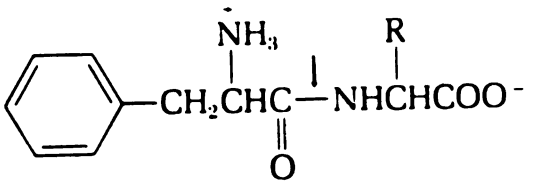

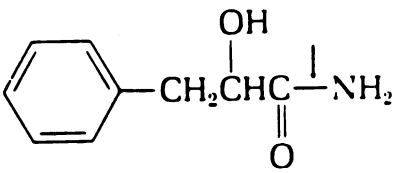

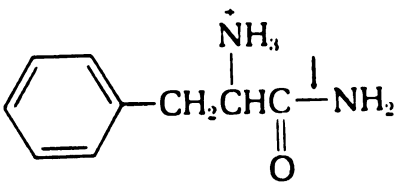

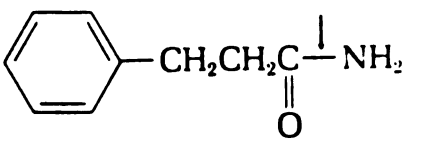

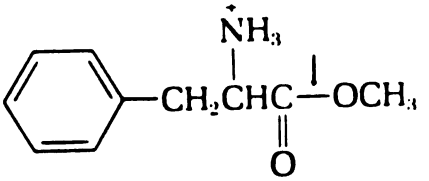

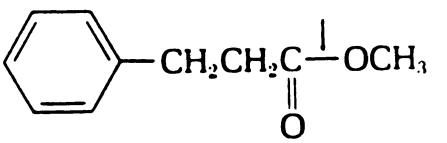

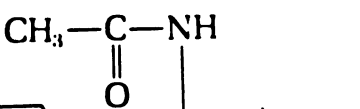

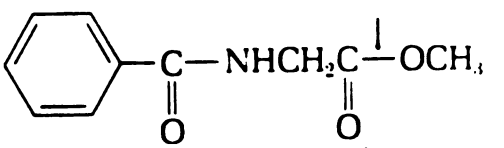

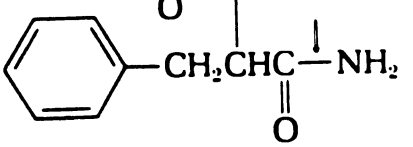

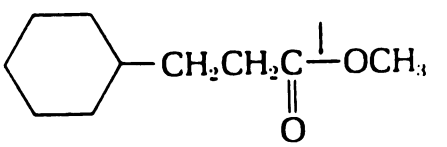

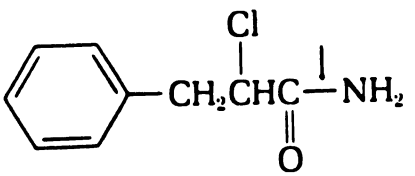

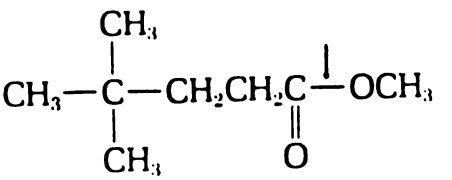

Figure 3.7. Proposed binding of Q_B and Q_A in the D-1 and D-2 subunits of PSII from reference 46.

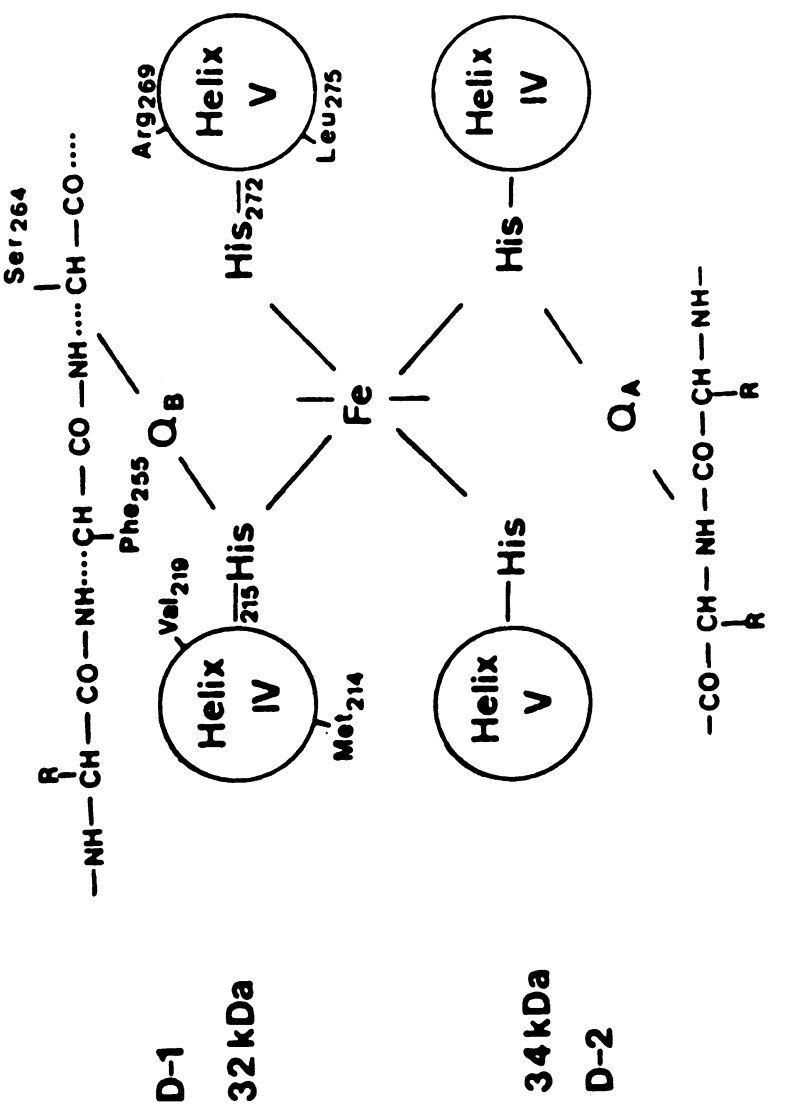
D-1
32 kDa
D-2
34 kDa
Helix IV
Helix V
Helix IV
Helix V
Fe
Q_B
Q_A
Ser_{264}
Phe_{255}
Val_{219}
His_{215}
Met_{214}
Arg_{269}
Leu_{275}
His_{272}
His
His

of both D-1 and D-2 subunits are involved in Fe binding (48). According to the model the binding site of Q_A is composed of a histidine (his), a peptide bond and a tryptophan. Chymotrypsin cleaves the C-side of phenylalanine, tryptophan, tyrosine, leucine, methionine and asparagine (see Figure 3.6). Therefore chymotrypsin should be able to release Q_A and Q_B from their binding sites. In addition, chymotrypsin should facilitate the release of any other quinone buried in the membrane structure by breaking down the protein structure and allowing the quinone to diffuse and go into solution more easily.

Another approach to release the quinones from the membranes is to unfold the membrane prior to extraction with organic solvents. 8 M urea was used for this purpose (Figure 3.8). Although the mechanism of action of urea is not fully understood, it is evident that it disrupts noncovalent interactions (42). Polypeptide chains devoid of cross-link usually assume a random coil conformation in 8 M urea (43) as evidenced by physical properties such as viscosity and optical rotatory dispersion spectroscopy. We would expect the same effect on the PSII membranes. The folding through the membrane of the plastoquinone and herbicide binding protein subunits of Photosystem II has been described by Trebst (48). The model folding of the D-1 and D-2 polypeptides, in homology to the L and M subunit of bacterial reaction centers predicts five transmembrane helices and three parallel helices. The proposed folding of D-1 and the D-2 polypeptides is shown in Figures 3.9a and 3.9b, respectively. Unfolding the polypeptides in Photosystem II should make the membrane more accessible to the solvent, permitting the quinones to be more easily extracted.

Figure 3.8. Schematical representation of the effect of 8M urea on proteins.

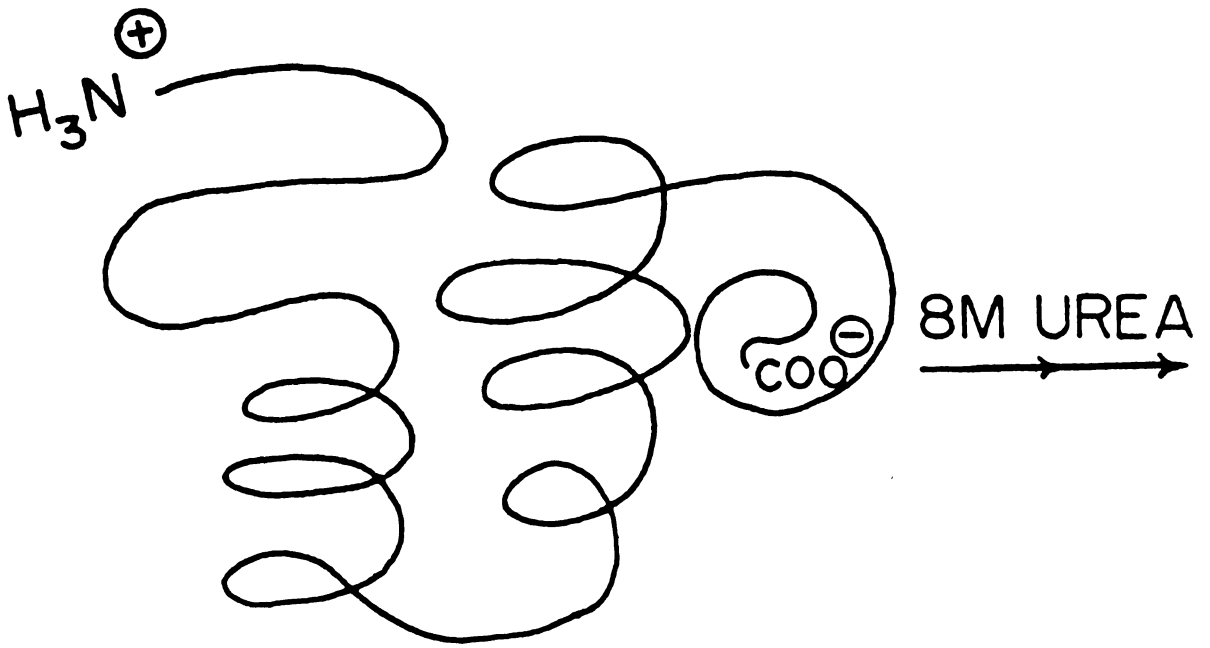
$H_3N^{\oplus}$
$COO^{\ominus}$
8M UREA

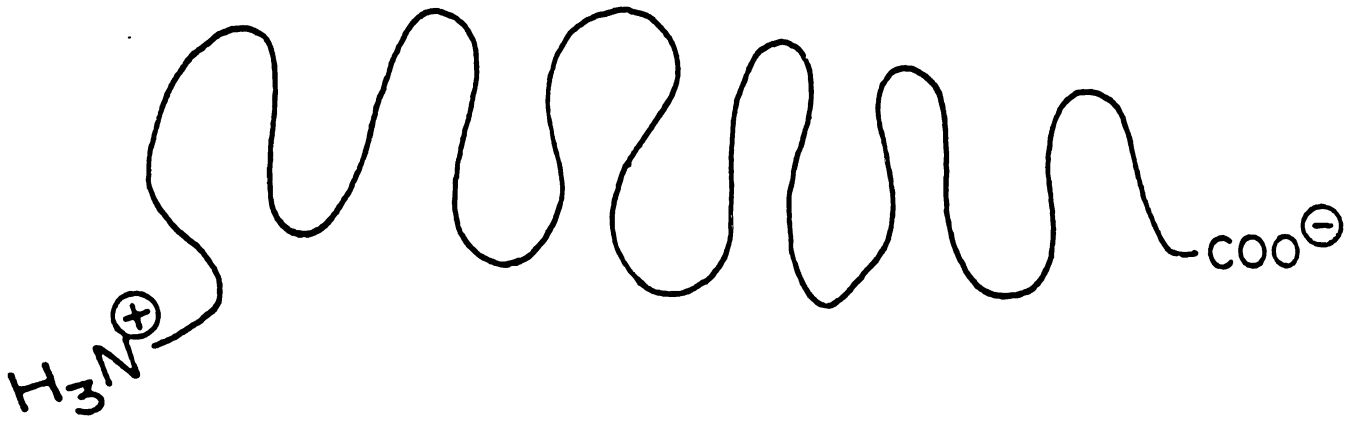
$H_3N^{\oplus}$
$COO^{\ominus}$

Figure 3.9a. Predicted folding of the amino acid sequence of the D-1 subunit of PSII (from 46).

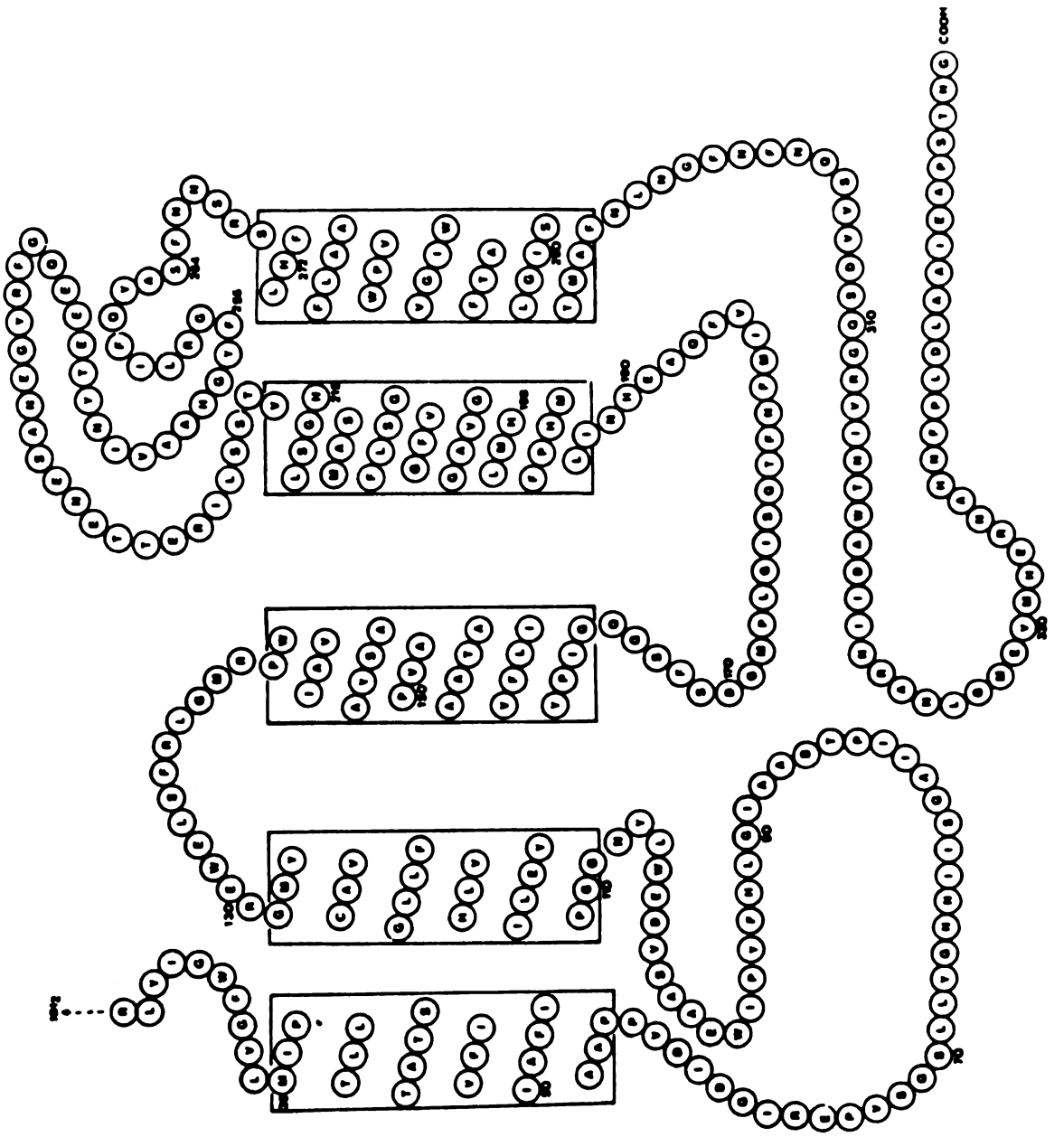

Figure 3.9b. Predicted folding of the amino acid sequence of the D-2 subunit of PSII (from 46).

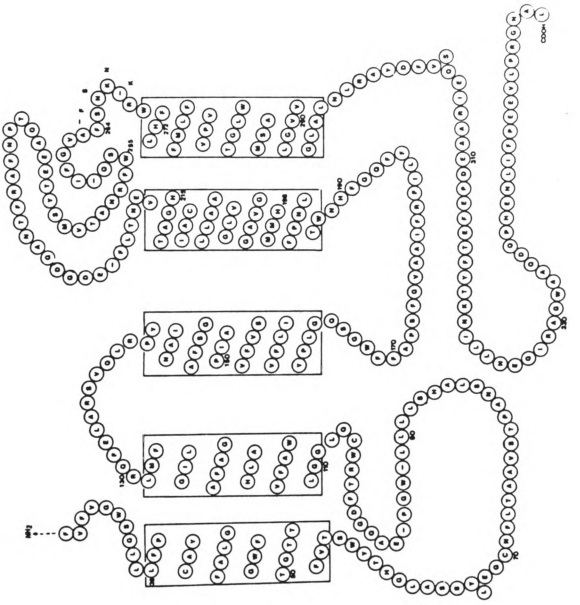
COOH
NH2
S1
S2
S3
S4
S5
S6
H1
H2
H3
H4
H5
H6

A third way to facilitate the extraction of quinones from Photosystem II particles is to shock the membranes by a change in the ionic strength of the medium. High salt concentration removes the extrinsic polypeptides in PSII particles (49) making the system more accessible (50). Again, by making the system more open, the possibility of physically trapping the quinones and therefore the possibility of incomplete extraction due to a well shielded site for the quinones is reduced.

Despite these precautions, in all cases (no pretreatment or pretreatment with 1 M NaCl, 8 M urea and chrymotrypsin) the amount of quinone found was essentially the same. Moreover, if we examine the amount of plastoquinone released as a function of the incubation time in the different media, we see that it is released relatively quickly (≈1 minute) and that the process is independent of the treatment. If the PSII membranes are incubated for longer periods of time the amount of quinone remains constant and equal to about two plastoquinone molecules per reaction center. This result suggests that there are no quinones buried deep in the membrane structure and inaccessible to simple solvent extraction. It also suggests that the quinones present in the system are relatively easily extracted, probably close to the surface in the protein structure. These results are in agreement with those reported previously, *i.e.*, about 2 plastoquinones per reaction center (see Table 1) in PSII particles where no chemical or enzymatic treatment was given to the samples prior to the extraction.

O'Malley *et al.* suggested that the Y_z^+ and Y_D^+ species where cations of plastoquinone (32). If Y_z^+ and Y_D^+ are both plastoquinone molecules we should obtain four plastoquinone molecules per reaction center. The fact that we find only 2 suggests that Y_z^+ and Y_D^+ are not plastoquinone molecules. Recently Barry and Babcock have proposed that Y_D^+ and probably Y_z^+ are tyrosine radicals (51). Our results show that there is only about 2 quinones per reaction center, which correspond to Q_A and Q_B, giving support to the tyrosine structure proposed for Y_D^+ and Y_z^+. It seems unlikely that the suggestion by Sadawasser and Dilley (9) that functional PQ_9 are present in the oxidizing site is correct. The effect observed upon extraction of the quinones on their experiments is likely to be due to removal of some other component from the chains of electron carriers or to the removal of Q_A or Q_B themselves. Although it is possible that there might be quinones covalently bound to the membrane, making their extraction and detection more difficult, there is no evidence in any similar system to suggest that this is likely.

References

1. Kofler, M., Langemann, A., Ruegg, R., Chopart-Dit-Jean, L. H., Rayround, A., Isler, O. (1959) Helv. Chim. Acta 42, 1283.

2. Lester, R. L., Crane, F. L. (1959) J. Biol. Chem. 254, 2169.

3. Fuller, R. G., Smillie, R. M., Rigopoulos, N., Yount, V. (1961) Arch. Biochem. Biophys. 95, 197.

4. Bark, R., Crane, F. L. (1967) Plant Physiol. 42, 1255.

5. Sun, E., Barr, R., Crane, F. L. (1968) Plant Physiol. 43, 1935.

6. Amesz, J. (1973) Biochim. Biophys. Acta 301, 35.

7. Trenner, N. R., Arison, B. H., Erickson, R. H., Shunk, C. H., Walf, D. E., Folkers, K. (1950) J. Am. Chem. Soc. 81, 2026.

8. Okoyama, S. (1974) Plant Cell Physiol. 15, 95.

9. Sadewasser, D. A., and Dilley, R. A. (1978) Biochim. Biophys. Acta 501, 208.

10. Clayton, R. K., and Straley, S. C. (1972) Biophys. J. 12, 1221.

11. Clayton, R. K., and Yau, H. F. (1972) Biophys. J. 12, 967.

12. Feher, G., Okamura, M. Y., and McElroy, J. D. (1972) Biochim. Biophys. Acta 267, 222.

13. Cogdell, R. J., Brume, D. C., and Clayton, R. K. (1974) FEBS Lett. 45, 344.

14. Okamura, M. Y., Isaacson, R. A., and Feher, G. (1975) Proc. Natl. Acad. Sci. USA 72, 3491.

15. Vermeglio, A. (1977) Biochem. Biophys. Acta 459, 516.

16. Wraight, C. A. (1977) Biochem. Biophys. Acta 459, 525.

17. Feher, G. (1971) Photochem. Photobiol. 14, 373.

18. Leigh, J. S., and Dutton, P. L. (1972) Biochim. Biophys. Res. Commun. 46, 414.

19. Wraight, C. A. (1978) FEBS Lett. 93, 283.

20. Eisenberger, P. M., Okamura, M. Y., and Feher, G. (1980) Fed. Proc. Fed. Am. Soc. Exp. Biol. 39, 1802.

21. Blankenship, R. E., and Parson, W. W. (1979) Biochim. Biophys. Acta 545, 429.

22. Okamura, M. Y., Feher, G., and Nelson, N. (1982) in "Photosynthesis" (Govindjee ed.), Vol. 1, Academic Press, New York.

23. Omata, T., Murata, N., and Satoh, K. (1984) Biochim. Biophys. Acta 765, 403.

24. de Vitry, C., Carles, C., and Diner, B. A., (1986) FEBS Lett. 196, 203.

25. Klimov, V. V., Dolan, E., Shaw, E. R., and Ke, B. (1980) Proc. Natl. Acad. Sci. USA 77, 7227.

26. Rutherford, A. W. (1986) Biochem Soc. Trans. 14, 15.

27. Debus, R. J., Feher, G., and Okamura, M. Y. (1986) Biochem. 25, 2276.

28. DeVault, D. (1986) Photosyn. Res. 10, 125.

29. O'Malley, P. J., Babcock, G. T., and Prince, R. C. (1984) BBA 766, 283.

30. Kohl, D. H., and Wood, P. M. (1969) Plant Physiology 44, 1439.

31. Hales, B. J., and Das Gupta, A. (1981) Biochim. Biophys. Acta 637, 303.

32. O'Malley, P. J., and Babcock, G. T. (1984) Biochim. Biophys. Acta 765, 370.

33. Tabata, K., Itoh, C., Yamamoto, Y., Okamura, S., and Nishimura, M. (1985) Plant Cell Physiol. 26, 855.

34. Dekker, J. P., Van Gorkom, H. J., Brok, M., and Ouwehand, L. (1984) Biochim. Biophys. Acta 764, 301.

35. Hoganson, C. W., Demetriou, Y., and Babcock, G. T. (1987) in: Progress in Photosyn. Res. (Biggins, J., ed.) Vol. 1, p. 479, Martinus Nihoff, Dordrecht.

36. Sun, A.S.K. and Sauer, K. (1973) Biochim. Biophys. Acta 325, 483.

37. Baer, R., Henninger, M.D. and Crane, F.L. (1967) Plant Physiol. 42, 1246.

38. Berthold, D. A., Babcock, G. T., and Yocum, C. F. (1981) FEBS Lett. 134, 231-234.

39. Blankenship, R. E., Babcock, G. T., Warden, J. T., and Sauer, K. (1975) FEBS LETTS 51, 287.

40. Stryer, L. (1975) in: Biochemistry, (Freeman ed.) pp. 182.

41. Lominski, A., and Rienets, K. G. (1981) Photochemistry 20, 993.

42. Lehninger, A. L. (1978) in: Biochemistry, (Worth ed.) pp. 218.

43. Bruice, T. C., and Benkouic, S. J. (1969) in: Biorganic Mechanisms and Comprehensive Review of Organic Model Reactions for Various Types of Enzymes, (Benjamin ed.) Menlo Park, CA.

44. Deisenhofer, J., Epp, O., Miki, K., Huber, R. and Michel, J., (1984) J. Mol. Biol. 180, 385.

45. Trebst, A., and Depka, B. (1985) in: Antennas and Reaction Centers of Photosynthetic Bacteria - Structure, interactions and Dynamics (M. E. Michele-Beyerle, ed.) pp. 216 Springer Verlag, Berlin, Heidelberg.

46. Trebst, A. (1986) Z. Naturoforsch 40 c, 237.

47. Trebst, A. (1986) Z. Naturoforsch 40 c, 240.

48. Trebst, A. (1987) Z. Naturoforsch 42 c, 742.

49. Ghanotakis, D. F., Topper, J. N., Babcock, G. T., and Yocum, C. F. (1984) FEBS Lett. 170, 169.

50. Dekker, P. J., Ghanotakis, D. F., Plijter, J. J., Van Gorkom, H. J., and Babcock, G. T. (1984) Biochim. Biophys. Acta 767, 515.

51. Barry, A., and Babcock, G. T. (1987) Proc. Natl. Acad. Sci. USA, 84, 7099.

CHAPTER 4
CHARACTERIZATION OF THE ELECTRON DONOR TO THE REACTION CENTER IN PHOTOSYSTEM II BY ENDOR SPECTROSCOPY

Introduction

In Photosystem II (PSII) of green plants, two tyrosine free radicals are involved in the oxygen evolving process, along with the reaction center chlorophyll, P_{680}. The first of those two radicals, $Y_Z^{\bullet}$ functions as an electron carrier between the oxygen evolving complex (OEC) in PSII and P_{680} (1). $Y_D^{\bullet}$ the other tyrosyl radical present in this photosystem, has an unknown function in the photosynthetic apparatus, although Rutherford *et al.* (2) suggested that it may play a role in maintaining the integrity of the manganese complex in the OEC. A characteristic, partially resolved EPR signal first observed by Commoner *et al.* in 1956 for $Y_D^{\bullet}$ (3) and in 1975 by Babcock and Sauer for $Y_Z^{\bullet}$ (1), is a common feature for both of these radicals. Even though $Y_Z^{\bullet}$ and $Y_D^{\bullet}$ are functionally different, their chemical structure and orientation in the membrane appear to be essentially the same. Only in their EPR power saturation behavior do $Y_Z^{\bullet}$ and $Y_D^{\bullet}$ show a difference (4,5), which has been attributed to a magnetic interaction between $Y_Z^{\bullet}$ and the manganese of the water splitting complex that does not occur for $Y_D^{\bullet}$.

Tyrosine radicals are not exclusive to photosynthetic material. For example, they are also found in the enzyme ribonucleotide diphosphate reductase

(RDPR), which catalyzes the formation of deoxyribonucleotides from ribonucleotides, a reaction essential for DNA synthesis in living cells (6,7). A characteristic EPR signal was reported for the bacterial enzyme in 1972 (8). Even though the radicals in the RDPR enzyme and the Y_D^+ species in PSII are both tyrosine molecules, the lineshape of the Y_D^+ EPR spectrum differs from that observed for the radical in the RDPR enzyme. One explanation for this difference is that the β-CH_2 protons in the two radicals have different orientations with respect to the phenol ring (9).

The EPR lines of these protein bound radicals are broadened owing to unresolved hyperfine structure, making it difficult to extract information from these poorly resolved spectra. When radicals are tumbling fast in solution, all anisotropic interactions are averaged out and an isotropic spectrum is observed. But when radicals are immobilized, as in the case of biological samples, the anisotropic interactions no longer average to zero and a powder type spectrum is obtained. Under these conditions additional spectroscopic techniques, such as electron nuclear double resonance (ENDOR), may be used to extract the different proton hyperfine tensor components that contribute to the EPR spectrum. An ENDOR approach to these immobilized radicals, therefore, has the potential to provide both isotropic and anisotropic tensor components and thus to provide significant information on radical spin distribution and structure that is not available from the EPR spectrum alone (10).

An additional advantage of ENDOR is that it can specifically detect different classes of protons. In the tyrosine model for the Y_D^+ radical there are 4

Figure 4.1. **Different** classes of protons in the tyrosine model for the Y_D^+ radical.

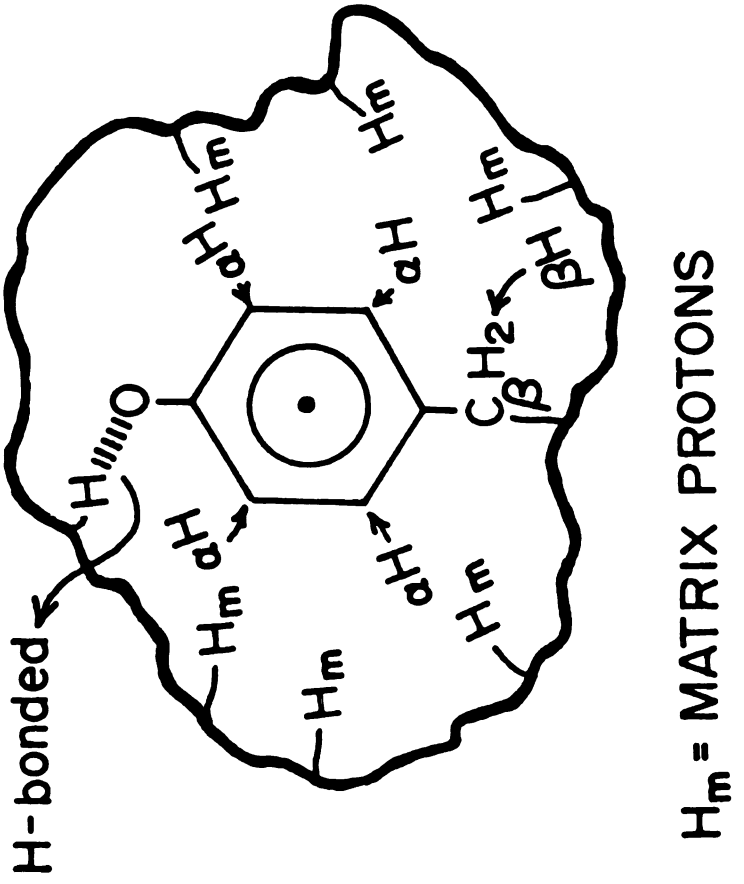
H-bonded
H_m
H_o
O
H_o
H_m
H_m
H_o
H_m
H_o
H_m
H_m
CH_2
βH
H_m
H_m
$H_m = MATRIX PROTONS$

kinds of protons: matrix protons, hydrogen-bonded protons, α-protons and β-protons (see Figure 4.1). With the help of H_2O/D_2O exchange the matrix protons and hydrogen-bonded protons have been investigated for Y_D^+ in the PSII membrane fragments, the studies are discussed in detail in the following chapter. Although the unpaired spin density distribution for the Y_D^+ radical needs to be established, in general for the tyrosine and phenoxy radicals it is mainly localized at the 1, 3 and 5 positions (6,12-15). Therefore, we expect the largest hyperfine couplings from the protons or groups (*e.g.* $-CH_2-$) interacting directly with the unpaired spin density at these positions.

There has been some solution EPR work done on tyrosine radicals (12,16-18) and tyrosine radicals in single crystals have been studied by EPR (12) and by ENDOR (13). All of these groups reported a triplet splitting of about 7 G from the α-protons at the 3-5 positions and a major doublet splitting of 15-19 G from one of the β-methylene protons or as representing the sum of the splittings of both of these protons with the center line of the expected triplet being broadened by restricted rotation. In the work reported here we have used powder ENDOR techniques to measure the hyperfine coupling for the Y_D^+ species and have assigned the major hyperfine interactions in the radical.

The hyperfine coupling constant corresponding to the β-proton is used to determine the geometry of the $-CH_2-$ at the 1 position (6,12,17). The ring protons at the 2,6 and 3,5 are more difficult to measure owing to their large anisotropies, but by using two-dimensionally oriented samples we were able to determine their hyperfine tensor components. The hyperfine couplings for the

different sets of protons measured from the Y_D^+ ENDOR spectrum provide a way to calculate the unpaired spin density distribution for the tyrosine radical in PSII. We have also been able to determine the orientation of the tyrosine ring plane with respect to the membrane plane by using oriented PSII membranes, chemical models and EPR simulations.

Materials and Methods

Oxygen evolving PSII particles were isolated from spinach and tris washed when required by using procedures based on those in (19). Oriented membranes were prepared by resuspending the PSII particles at approximately 8 mg Chl/ml in a buffer contained 20 mM Mes (pH = 6.0) and 10 mM NaCl. The suspension of membranes was painted onto Mylar sheets and dried at 12°C for 48 hours in a closed dark container. By drying the strips in the presence of a saturated solution of $ZnSO_4$ the relative humidity was kept at 90%. The EPR and ENDOR of these samples were recorded in such a way that the external magnetic field was either parallel (*i.e.*, 0°) or perpendicular (*i.e.*, 90°) to the membrane plane. The X-band EPR and ENDOR spectra were recorded on a Bruker ER 200D spectrometer equipped with a Bruker ENDOR accessory(20) operating at temperatures and instrument setting indicated in the figure captions.

Results

Figure 4.2 shows the Y_D^+ ENDOR spectrum of a powder PSII sample recorded at 10K. In the low frequency region of the Y_D^+ spectrum (Figure 4.2a) a complex structure, particularly in the region around the free proton frequency, ν_H = 14.7 MHz at X-band in our instrument (matrix ENDOR), is observed.

Figure 4.2. Y_D^+ ENDOR spectrum in the low (a) and high (b) frequency region. T = 10K; microwave power 6.3 mW rf power at 10 MHz, 150W, fm deviation 50KHz (a) and 150KHz (b).

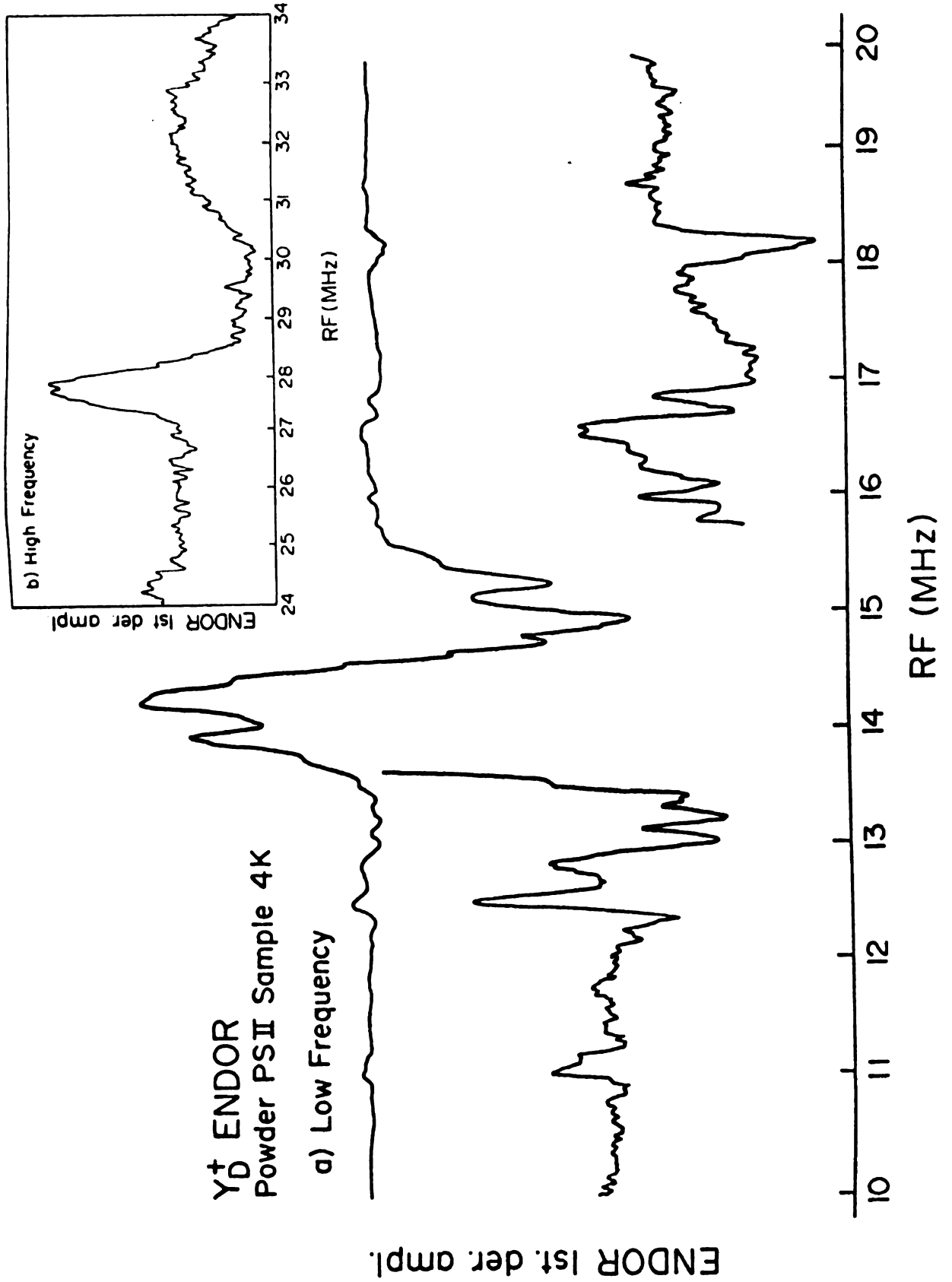
Y_D^+ ENDOR
Powder PSII Sample 4K
a) Low Frequency
b) High Frequency
ENDOR Ist. der. ampl.
RF (MHz)
10
11
12
13
14
15
16
17
18
19
20
24
25
26
27
28
29
30
31
32
33
34

These bands arise from dipolar coupling between the immobilized radical and its surrounding protein environment as discussed in detail in the following chapter. In addition to the matrix there are at least six other resonances. In the high frequency region (Figure 4.2b) two bands are observed. In the analysis that follows we begin with the larger couplings, proceed to the weakly coupled protons, and then present data on the orientation of the radical in the photosynthetic membrane.

Based on EPR and ENDOR studies, O'Malley and Babcock proposed a plastoquinone cation radical origin for Y_D^+ (21,22). In their interpretation they assigned the two bands at 28.1 and 30.3 MHz in Figure 4.2b to the hyperfine components of the methyl group at position 2 in the plastoquinone cation radical. However, in the proposed tyrosine model there are no methyl groups but a methylene at the 1 position. For this type of $-CH_2-$ group we do not expect the dihedral angle to be the same for both protons. A difference in this angle will produce different hyperfine couplings for the two β-protons; the smaller the dihedral angle between the β-proton and the p_z orbital at carbon 1, the stronger the interaction between the unpaired spin density at this position and hence the larger the coupling (see Equations 1, 2, and 3 below).

For β-protons axial symmetry is expected with the largest hyperfine tensor component lying along the $C-CH_2$ bonding direction. Because the isotropic coupling value for the β-protons is expected to be positive (23), we ascribe the largest component along this direction. For the Y_D^+ radical, the direction from carbon 1 to one of the methylene protons corresponds to the parallel hyperfine

tensor component ($a_{\|}$); we assign the resonance with a coupling of 31.4 MHz (Figure 4.2b) to this tensor element ($a_{\|}$). The other band with a hyperfine coupling of 27.2 MHz corresponds to the perpendicular hyperfine tensor component ($a_{\perp}$) The magnitude of the hyperfine coupling for this β-proton of the methylene group in the $Y_D^{\bullet}$ radical is consistent with the observation by Sjoberg *et al.*, (6) that the major splitting observed in the RDPR EPR spectrum is attributed to one of the β-protons in the tyrosine radical in this enzyme. Hence the second β-proton of the $Y_D^{\bullet}$ radical in the $-CH_2-$ group should exhibit a smaller hyperfine coupling and therefore it should resonate in the low frequency region (Figure 4.2a).

Information about the orientation of the radical ring plane with respect to the membrane plane can be obtained by using oriented PSII membranes. The $Y_D^{\bullet}$ ENDOR of oriented PSII samples in the high frequency region (23-33 MHz) is illustrated in Figure 4.3b and 4.3c. When the applied magnetic field is perpendicular to the membrane plane (Figure 4.3b) the major contribution to the $Y_D^{\bullet}$ ENDOR spectrum is a broad band at 30.1 MHz ($a_{\|}$). The situation is reversed when the field is rotated by 90° and the band at 28.1 MHz ($a_{\perp}$) is the major contribution to the spectrum. These observations indicate that the tyrosine phenol ring plane is close to perpendicular to the membrane plane.

These assignments are consistent with studies on $Y_D^{\bullet}$ in blue green algae and with models in which β-protons at the 1 position and α-protons at the 2-6 and 3-5 positions were substituted by deuterium (24). When deuterium was substituted at the 3-5 positions only a doublet with a coupling constant of about

Figure 4.3. High frequency $Y_D^{\bullet}$ ENDOR spectrum for powder (a) and oriented samples with the magnetic field applied perpendicular (b) and parallel (c) to the membrane plane. The correspondent EPR spectrra are shown in the insets: T = 4K; microwave power 6.3 MW rf power at 10MHz, 150 W; fm deviation 150 KHz.

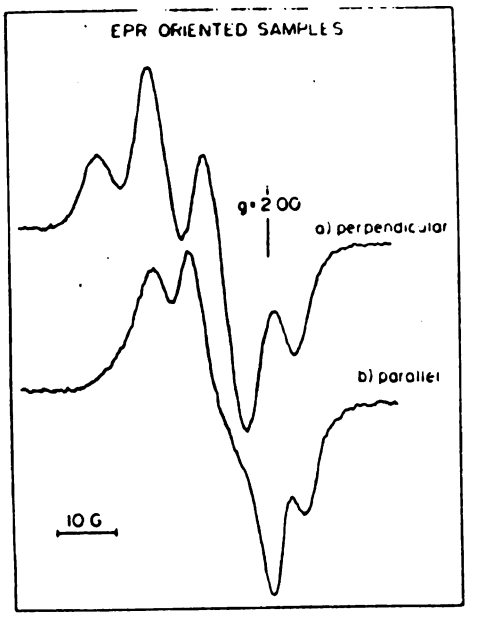

ENDOR
4K
Y_{D^+} in PS II
$-CH_2-$ proton

a) powder unoriented

$a_\perp$

$a_{||}$

b) perpendicular

$a_{||}$

$a_\perp$

c) parallel

ENDOR Ist. der. amp.

24 26 28 30 32

RF(MHz)

15 G for the immobilized tyrosine and about 12 G for the biological sample was observed. This corresponds to the coupling of one of the β-protons and supports the assignment of the large coupling observed in the Y_D^+ spectrum to one of the β-protons. When the substitution was on the β-methylene protons a set of resonances with a major coupling constant of about 6.5 G was observed for both the model and biological samples. When deuterium was substituted at the 2-6 positions little or no change was observed for either sample. EPR and ENDOR studies on the enzyme RDPR, where the same specific isotropic substitution approach was used (20) (*i.e.*, substitution of α-protons at the 3-5 positions and β-protons at the 1 position) also support our assignment for the resonances observed in the Y_D^+ ENDOR spectrum and the general idea that carbons 1, 3 and 5 in the aromatic ring carry a high unpaired spin density.

Owing to the small unpaired spin density at the 2-6 carbons in the aromatic tyrosine ring, we expect the protons at these positions to have a small hyperfine coupling and therefore to resonate in the low frequency region (Figure 4.2a). On the other hand, a larger hyperfine coupling is expected for the 3-5 α-protons due to the greater unpaired spin density at the carbons in these positions. ENDOR bands from α-proton are in general of too weak intensity to be observed in powder ENDOR. However, studies made on the benzoquinone anion radical have shown that ENDOR bands of substantial intensities may be observed from ring protons (25). In general, α-protons give rise to relatively broad ENDOR lines with principal values of the hyperfine tensor approximately equal to $0.5a_{iso}$, a_{iso}, $1.5a_{iso}$, where a_{iso} is the isotropic hyperfine coupling

(26). Hence, the ENDOR spectrum for an α-proton should exhibit a rhombic signal with a buildup of intensity at the isotropic coupling with shoulders near $0.5a_{iso}$ and $1.5a_{iso}$. For the Y_D^+ radical we could not observe the α-proton resonances at the 3-5 positions in the ENDOR powder spectrum. But by using oriented PSII membranes we have been successful in observing the ENDOR lines corresponding to these protons. Figure 4.4 shows the Y_D^+ ENDOR spectrum in oriented PSII membranes in the 20-30 MHz region recorded at 108K with the magnetic field applied perpendicular (Figure 4.4a) and parallel (Figure 4.4b) to the membrane plane. We expect α-protons at the 3-5 positions to resonate in this region. The resonances observed in these spectra show some of the characteristics expected for an α-proton.

We assign the resonance at about 27 MHz in Figure 4.4a to the a_x hyperfine tensor component of the α-protons at these positions; in our axis system the x-axis is in the ring plane and perpendicular to the y-axis which is along the C-H bond, the z-axis is perpendicular to the ring plane. When the magnetic field is applied parallel to the membrane plane (Figure 4.4b) a broad band at 22.6 MHz with an overlapping resonance at 21.7 MHz is observed. These resonances are assigned to the z ($a_z^{\alpha H(3-5)}$) and z'($a_{z'}^{\alpha H(3-5)}$) hyperfine tensor components of these α-protons. The observed splitting of the a_z hyperfine tensor component is likely to be a result of a slight inequivalence of protons 3 and 5. This inequivalence may be attributed to the fact that the tyrosine molecule is embedded in a protein matrix, making the microenvironment surrounding each proton inequivalent. A similar phenomenon has been observed by Broustolon *et al.* (26)

Figure 4.4. Oriented $Y_D^{\bullet}$ ENDOR spectra with magnetic field applied perpendicular (a) and parallel (b) to the membrane plane. T = 108K; microwave power 6.3 mW; rf power at 10 MHz, 150W; fm deviation 150KHz.

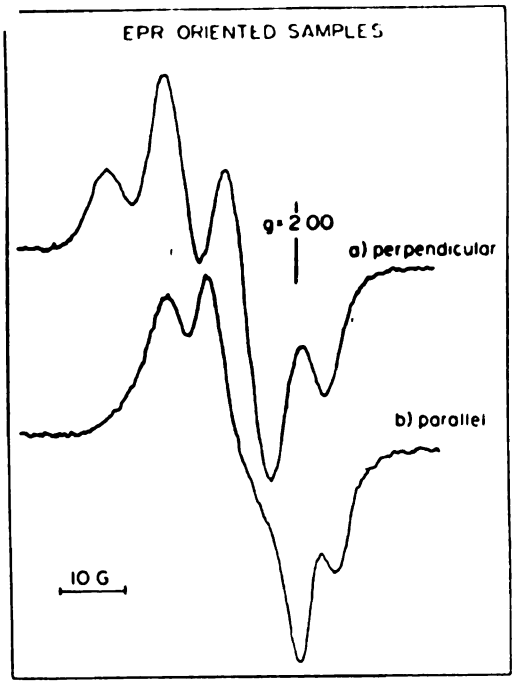

ENDOR
108K
Y_D+ in oriented PS II
3,5 ring protons

a) perpendicular

b) parallel

$a_x^{\alpha H(3-5)}$

$a_z^{\alpha H(3-5)}$

$a_z'^{\alpha H(3-5)}$

ENDOR Ist der. amp.

20 22 24 26 28 30

RF (MHz)

in γ-irradiated single crystals of potassium hydrogen glutarate. These authors attributed the observed inequivalence for the α-protons in their system to the fact that the C-H bond is not a symmetry axis. The third component of this rhombic tensor is a resonance observed at about 18.5 MHz in Figure 4.5a, this ENDOR line corresponds to the $0.5a_{iso}$ part of the hyperfine tensor ($a_y^{\alpha H(3-5)}$) This assignment is based on the studies mentioned earlier on the RDPR enzyme in which the resonances corresponding to the protons at the 3-5 positions disappeared after substitution of these α-protons with deuterium. Even though we see a weak band corresponding to the a_y component of this tensor at 4K the other two parts a_x and a_z are not observed at this temperature in either powder or oriented samples. It is only in the 103 to 114 K temperature range that we see the higher frequency resonances corresponding to the α-protons at the 3-5 positions. If we examine Figure 4.4 we see that when the magnetic field is applied perpendicular to the membrane plane (Figure 4.4a) the a_x component of the α-protons at the 3-5 position is the sole contribution to the spectrum. This suggests that the ring plane is not exactly perpendicular to the membrane plane but at an angle of about 60° (see discussion below and Figure 4.6).

Oriented PSII membranes provide a way of detecting weak ENDOR signals (*i.e.*, α-protons at the 3-5 positions) by increasing the effective spin concentration as compared to powder samples. These samples also provide a way to simplify the analysis of the weaker hyperfine couplings observed in Figure 4.2a. Figure 4.5 shows the $Y_D^{\bullet}$ ENDOR spectra for oriented PSII samples with the magnetic field applied perpendicular (Figure 4.5a) and parallel (Figure 4.5b) to

Figure 4.5. High resolution oriented Y_D^* ENDOR spectrum with magnetic field applied perpendicular (a) and parallel (b) to the membrane plane T = 4K; microwave power 6.3 mW; rf power at 10 MHz, 150 W; fm deviation. 30 KHz.

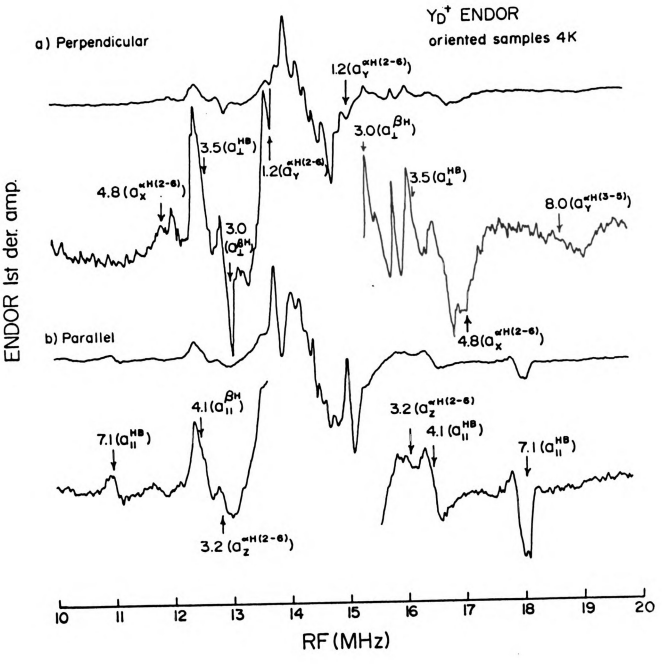
Y_D^+ ENDOR
oriented samples 4K
a) Perpendicular
b) Parallel
ENDOR Ist der. amp.
RF (MHz)
10
11
12
13
14
15
16
17
18
19
20
1.2($a_y^{\alpha H(2-6)}$)
3.0($a_\perp^{\beta H}$)
3.5($a_\perp^{HB}$)
1.2($a_y^{\alpha H(2-6)}$)
4.8($a_x^{\alpha H(2-6)}$)
3.5($a_\perp^{HB}$)
8.0($a_y^{\alpha H(3-5)}$)
3.0
($a_\perp^{\beta H}$)
4.8($a_x^{\alpha H(2-6)}$)
4.1($a_{||}^{\beta H}$)
3.2($a_z^{\alpha H(2-6)}$)
7.1($a_{||}^{HB}$)
4.1($a_{||}^{HB}$)
7.1($a_{||}^{HB}$)
3.2($a_z^{\alpha H(2-6)}$)

Figure 4.6. Experimental and simulated oriented Y_D^+ EPR spectra with the magnetic field applied perpendicular (a,b) and parallel (c,d) to the membrane plane. T = 115K.

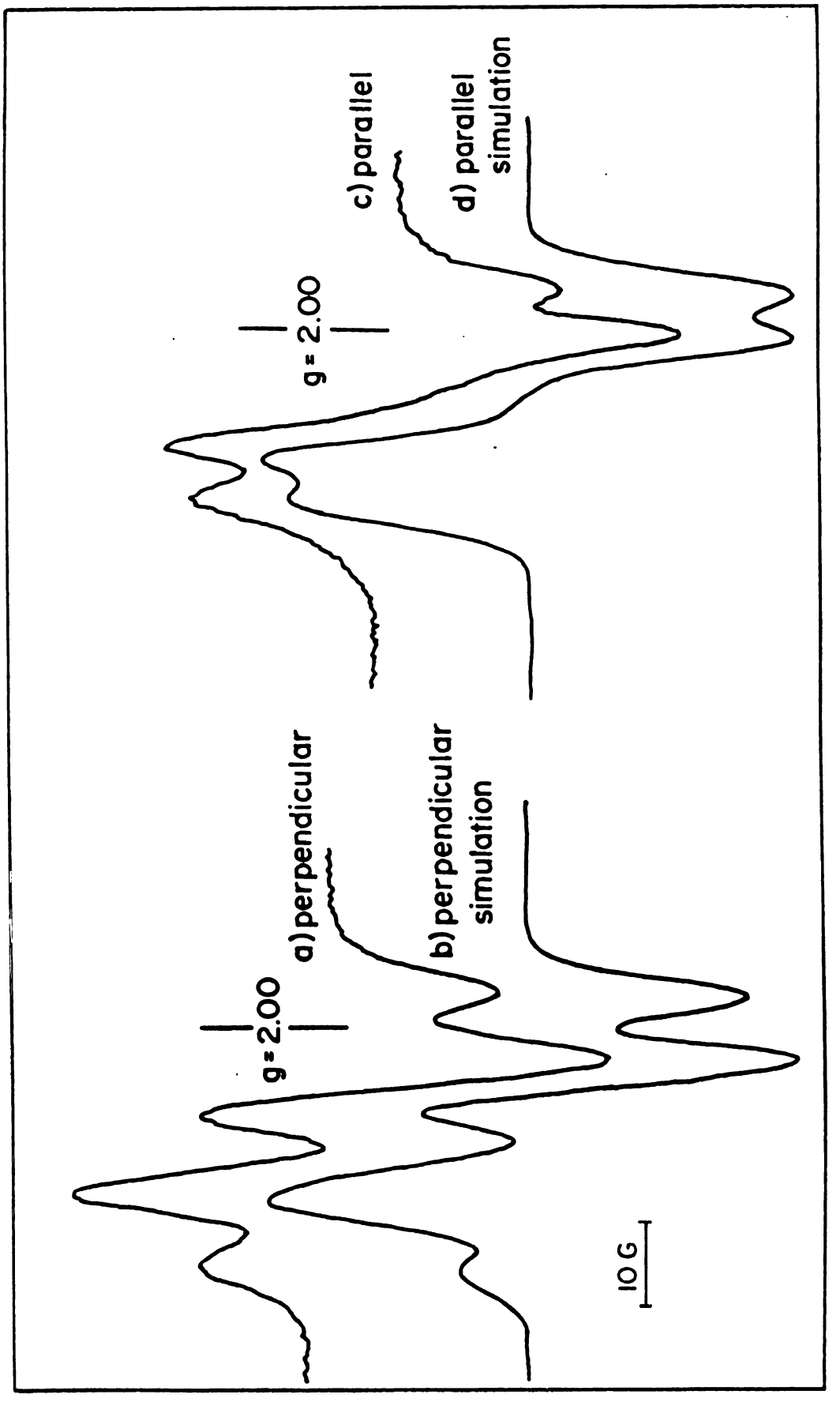
g = 2.00
a) perpendicular
b) perpendicular simulation
g = 2.00
c) parallel
d) parallel simulation
10 G

the membrane plane recorded at 10K. Couplings labeled $a_{\|}^{HB}$ (7.1 MHz) in Figure 4.5b and $a_{\perp}^{HB}$ (3.5 MHz) in Figure 4.5b have been assigned to the parallel and perpendicular hyperfine tensor components of a hydrogen-bonded proton respectively as discussed in the following chapter. Owing to the characteristic axial line shape observed for the resonances with coupling of 3.1 MHz in Figure 4.5a and 4.1 MHz in Figure 4.5b and to the fact that the second β-proton should have a relatively small hyperfine coupling as explained above, we expect this β-proton from the methylene group to resonate in this low frequency region. We assign these resonance to the perpendicular ($a_{\perp}^{\beta H}$ = 3.1 MHz) hyperfine tensor components of the second β-proton. Based on their rhombic line shape, on the small coupling values and on the ratio of hyperfine couplings which are characteristic of an α-proton, we assign the resonances with couplings of 4.8 and 1.2 MHz in Figure 4.5a and the resonance with coupling of 3.2 MHz in Figure 4.5b to the x, y and z hyperfine tensor components of the α-protons at the 2-6 positions respectively (see Table 1).

Computer simulations of the oriented $Y_D^{\bullet}$ EPR spectra (Figure 4.6) were performed by using the program developed by Brok *et al.* (27). The data used as input for these simulations were the anisotropic g-tensor components, the values of the hyperfine tensor components for α and β-protons and the Euler angles that define the orientation of these tensor components with respect to the molecular axes (see Table 2) and the orientation of the radical with respect to membrane plane. This orientation was obtained by first analyzing the $Y_D^{\bullet}$ ENDOR spectra of oriented PSII membranes, then by using a tyrosine molecular

Table 1 Assignments of $Y_D^{\bullet}$ ENDOR lines within the tyrosine model

H-bonded	CH H(1)	CH H(2)	H-alpha (2-6 pos)	H-alpha (3-5 pos)
3.5MHz($a_\perp$)[a)]	27.2MHz($a_\perp$)	3.1MHz($a_\perp$)	1.2MHz(a_y)	8.0MHz(a_y)
7.1MHz($a_\parallel$)[a)]	31.4MHz($a_\parallel$)	4.1MHZ($a_\parallel$)	3.2MHz(a_z)	16.0MHz(a_z)
			4.8MHz(a_x)	25.5MHz(a_x)
	θ_1 = 45° ± 1°		θ_2 = 76° ± 1°	

Table 2 Euler Angles.

Type of Proton	a_x	a_y	a_z	θ	ϕ	ψ
β-H[a)]	11.20	9.7	9.7	17	65.0	-30.0
α-H	9.1	2.86	5.7[b)]	-12.0	-12.0	0.0
α-H	9.1	2.86	5.0[b)]	-10.0	-10.0	0.0

[a)] small dihedral angle

[b)] splitting of the a_z component explained in text

model, the angle between the line through the C_1-C_4 carbons and the membrane plane and the angle between the direction of the g_z component and the membrane plane, that could explain the observed ENDOR spectra were elucidated. The procedure and experimental data used to obtain the latter angle is described in detail in the following chapter. Finally, these angles were used to simulate the oriented $Y_D^{\bullet}$ EPR spectra. This orientation is schematically represented in Figure 4.7.

Discussion

β-Protons

In its protein binding site, the tyrosine radical is expected to have its β-methylene group rotationally immobile. Under these conditions, the isotropic hyperfine coupling constant varies according to the following set of equations:

$$a_{\beta_1}^{iso} = \rho_{C_1} B \cos^2\theta_1 \qquad (1)$$

$$a_{\beta_2}^{iso} = \rho_{C_1} B \cos^2\theta_2 \qquad (2)$$

$$\text{and} \quad \theta_1 + \theta_2 = 120° \qquad (3)$$

where $a_{\beta_1}^{iso}$ and $a_{\beta_2}^{iso}$ are the isotropic hyperfine couplings for the methylene protons 1 and 2 respectively, B is a constant, ρ_{c1} is the unpaired spin density at the C_1 position and θ_1 and θ_2 are the dihedral angles between the p_z orbital at the ring carbon and the $C_\beta H_1$ and $C_\beta H_2$ protons, respectively (see Figure 4.8).

Figure 4.7. Proposed orientation of the Y_D^+ radical in the membrane. The parallel field ($H_0^{0\bullet}$) in perpendicular to the ring plane.

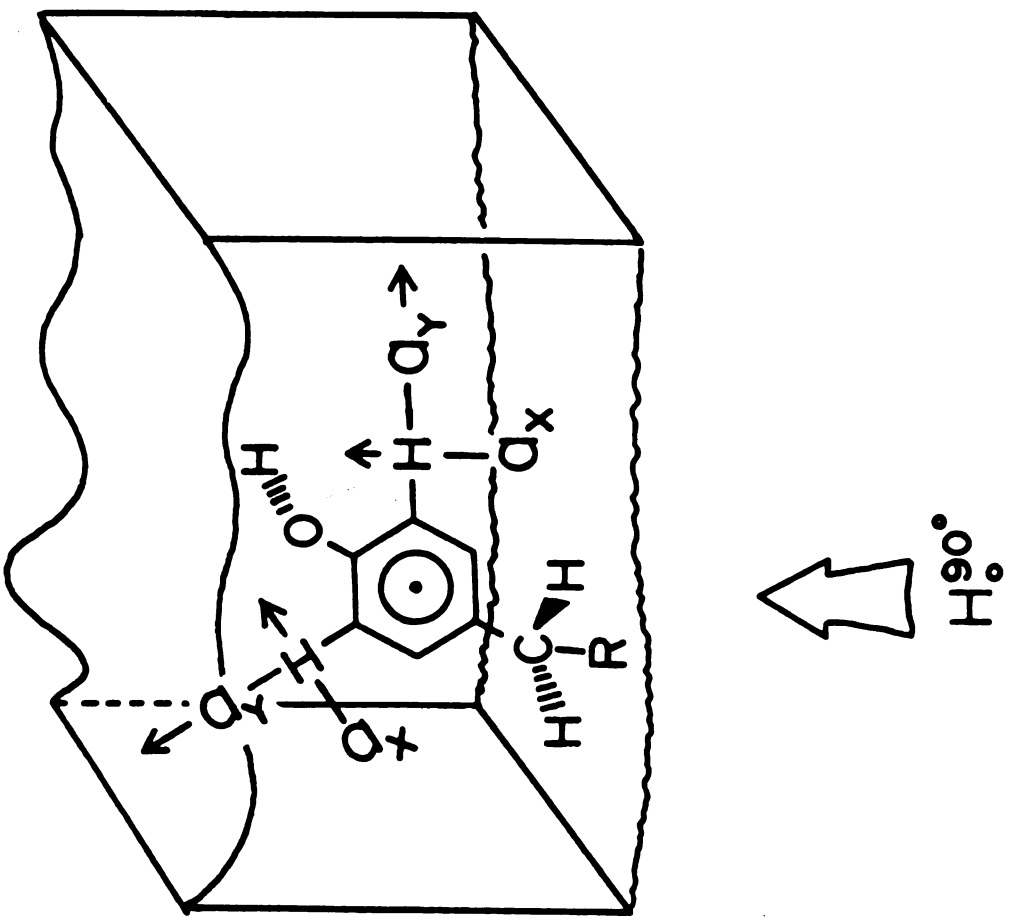
H
O
H
C
R
H
90°

Figure 4.8. Illustration of the dihedral angle (see text).

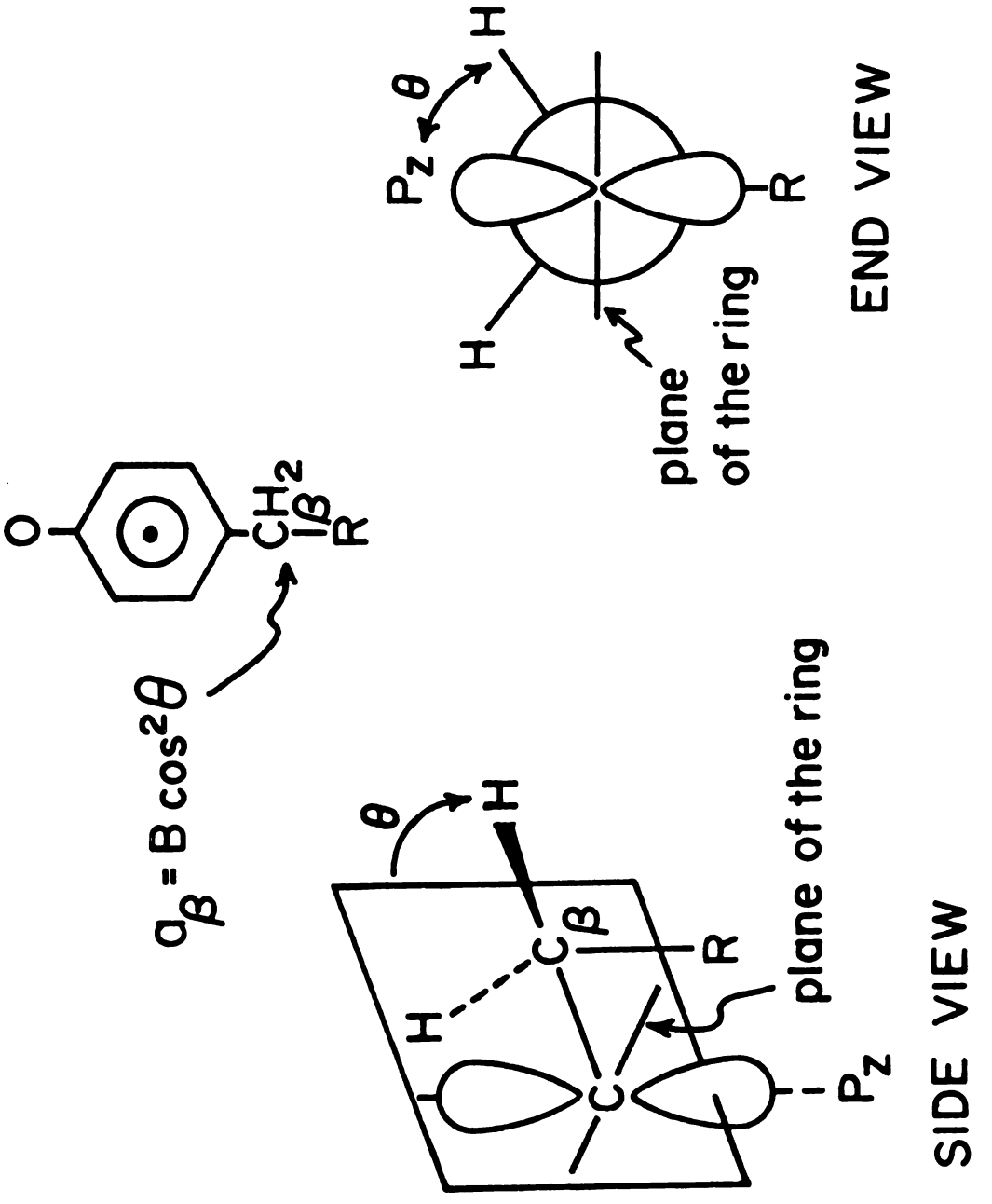
$a_\beta = B\cos^2\theta$
O
CH_2
β
R
P_z
θ
H
H
R
plane
of the ring
END VIEW
θ
H
H
C_β
R
C
P_z
plane of the ring
SIDE VIEW

Equations 1 and 2 are a modification to the semiempirical relationship proposed by Heller and McConnell (28); Equation 3 is obtained from geometrical considerations. This equation predicts that if $\theta_1 = \theta_2$ then $a_{\beta_1}^{iso} = a_{\beta_2}^{iso}$. If on the other hand $\theta_1 \neq \theta_2$, then the interactions will not be the same between the β-protons and the unpaired spin density at C_1 and the hyperfine tensor components for one proton will not be the same as the hyperfine tensor components of the second β-proton.

Equation 1 and 2 indicate that with a knowledge of ρ_{C_1}, the orientation of the methylene protons with respect to the ring can be deduced. However, reports on the spin density distribution on the tyrosine radical are in conflict. Box and co-workers (13) assigned a spin density of only 0.185 in calculations in which simple Huckel theory was used. Fasanella and Gordy (12) give an experimental value of 0.32 and SCF calculated value of 0.312 for ρ_{C_1}. Sealy and co-workers (17) assigned an unpaired spin density at this carbon of 0.5. By using the isotropic hyperfine coupling constant measured from the Y_D^+ ENDOR spectrum for the β-methylene protons, $a_{\beta_1}^{iso} = 10.2$ G and $a_{\beta_2}^{iso} = 1.2$ G, and by solving Equations 1, 2 and 3 simultaneously we can obtain a more precise value for ρ_{C_1} and the values for θ_1 and θ_2. Taking B as 50 G (18,29) we find $\rho_{C_1} = 0.40 \pm 0.02$ and $\theta_1 = 44°$ and $\theta_2 = 76°$. Table 3 shows the dihedral angles (θ_1 and θ_2) for different tyrosine radical systems. Sealy and co-workers (17) have suggested that the low energy conformation for the methylene group in the tyrosine radical corresponds to $\theta_1 = \theta_2 = \pm 60°$. But as can be seen in Table 3 this situation (*i.e.*, $\theta_1 = \theta_2$) occurs rarely. It is recognized that protein molecules

Table 3 Dihedral angles (θ_1 and θ_2) for the -CH_2- group in tyrosine radicals in different systems.

System	θ_1	θ_2	Ref.
Solution Tyrosine Radical	60°	60°	(17)
Crystal Tyrosine Radical	30°	80°	(13)
RDPR Tyrosine Radical	27°	93°	(36)
$Y_D^{\bullet}$ Tyrosine Radical	45°	76°	(this work)

are not static but in a state of constant motion (30). Torsional fluctuations of tyrosine in which the ring rotates 180° along the C_1 - C_β bond are known to occur in proteins (31,32). However, these ring "flips" rarely occur because of the large energy barrier that results from steric hinderance (33,34). A more common motion is the jiggle of the ring (*i.e.*, torsional oscillations without executing a 180° flip). This type of oscillation has been studied for tyrosine rings buried in a protein matrix (35). The average oscillation angles are typically in the range of 10-15° for isolated groups (*i.e.* near the protein center) but oscillations increase markedly near the protein surface (36). Our conclusion from the H_2O/D_2O exchange experiment that the Y_D^+ radical is in an isolated pocket deep in the membrane (11) is supported by the results of Innes and Brudvig where they found a distance of 21.4 Å from the membrane surface to the radical site (37). These results suggest that the oscillation angle should be relatively small for Y_D^+ (≈10°). Another set of conformational studies of amino acids in proteins indicates that the preferred position of the aromatic ring is parallel to the main chain on which it lies flat (38). The above conformational studies in proteins along with our own results suggest that the low energy configuration for the β-protons of the tyrosine molecule in proteins is when $\theta_1 \neq \theta_2$.

<u>α-Protons</u>

For α-protons we expect the sign of the isotropic hyperfine coupling to be negative (39). We use this to assign the three observed hyperfine tensor components of these protons as negative as follows: a_y = -8.0 MHz, a_z = -16.0 MHz and a_x = -25.5 MHz. The isotropic coupling constant (a_{iso}) is -16.5 MHz or

-5.89 G. The spectral features, rhombic line shape, and the values of the hyperfine tensor components are consistent with a C-H fragment in which the unpaired electron at the carbon interacts with the hydrogen nucleus. Stone and Walters (14) and Dixon and co-workers (15) have studied the effect of subtituents in phenoxy type radicals. These authors made the important observation that the algebraic sum of the ortho (*i.e.*, 3-5 positions) and meta (*i.e.*, 2-6 positions) isotropic hyperfine coupling constants for α-protons in a para-substituted phenoxy radical is approximately independent of the substituent. This simple rule enabled them to deduce empirically that these two coupling constants must generally have opposite signs. In the majority of cases the following relationship for para-substituted phenoxy radicals holds true:

$$|a_o + a_m| = 4.7 \pm 0.2 \text{ G} \qquad (4)$$

where a_o is the hyperfine coupling constant for the α-protons at the 3-5 positions and a_m is the hyperfine coupling constant at the 2-6 positions. The large coupling constant (a_o) usually corresponds to a positive spin density so that the small coupling constant (a_m) usually corresponds to negative spin densities.

The assignments of the couplings for the α-protons at the 2-6 positions is not as clear as those for the 3-5 positions due to overlapping resonances in the region where these protons resonate. However, by assuming the rhombic or near rhombic tensor for the 2-6 α-protons and by applying Equation 4, we can facilitate the assignment. We have assigned the hyperfine tensor components as

being a_y = 1.2 MHz, a_z = 3.2 MHz and a_x = 4.8 MHz, which yield an isotropic hyperfine coupling constant of 3.4 MHz or 1.2 G. Therefore using our values for $a_o = a_{iso}^{\alpha H(3-5)} = 5.89$ G and $a_m = a_{iso}^{\alpha H(2-6)} = 1.2$ G and assuming that the larger coupling is negative and the smaller coupling positive, we get from Equation 5 a value of 4.7 G, providing support for our assignments for these protons.

Spin Density Distribution

By using the isotropic hyperfine couplings for the α-protons at the 3-5 and 2-6 positions and the isotropic coupling for the β-protons we can calculate the electron spin density distribution in the tyrosyl radical. Based on this unpaired spin density distribution, the anisotropic hyperfine interaction for the α-protons can be calculated. Comparison between the experimental and calculated hyperfine tensor components provides a way to investigate the spin density distribution. Our procedure for determining the hyperfine tensor components for the α-protons on the $Y_D^{\bullet}$ radical is based on the method of Heller and Cole (40). This procedure has been used to calculate the principal hyperfine tensor components for the ring protons in the p-benzoquinone anion radical (25). Due to the general characteristics of the unpaired spin density distribution for the tyrosine radical we expect that the dipole-dipole interactions between the α-protons and the spin density on C_1, C_3 and C_5 will be a major contributors to the observed net α-dipolar tensor. The tyrosine radical can be considered a seven member odd-alternate aromatic radical (39) and therefore significant spin density is exprected on the oxygen.

By using the McConnel relationship (41):

$$a_{iso} = \rho Q \qquad (5)$$

where a_{iso} is the isotropic hyperfine coupling constant for the α-protons, ρ is the unpaired spin density at the carbon directly attached to the hydrogen and Q is the McConnell constant which has a value of about 26.5 G for this type of aromatic system (42) the unpaired spin density distribution can be calculated. By applying Equation 5 for the α-protons and by using the hyperfine couplings listed in Table 1 we have calculated the unpaired spin density distribution for the Y_D^+ tyrosine radical. The calculated spin density distribution is schematically represented in Figure 4.9. These assignments were tested by calculating the hyperfine tensor components for the α-protons. If the spin distribution, bond distances and related bond angles are known, the total anisotropic hyperfine interactions from the nuclei and in the molecular plane can be calculated as previously described (25,40). The bond distances of carbon-carbon and carbon-oxygen were taken to be 1.4 Å and the bond distance of carbon-proton was taken as 1.088 Å (40). The related angles for each nucleus can be worked out (see Table 4). The spin density, bond distance and angle for each nucleus where the unpaired spin density is localized is used as imput for the computer program written in our lab. The output gives the hyperfine tensor components a_{xx}, a_{yy} and a_{zz} and the angle between the principal anisotropic hyperfine tensor and the chosen axis system.

Figure 4.9. Calcualted unpaired spin density distribution in the phenyl moiety of tyrosine in the $Y_D^{\bullet}$ radical.

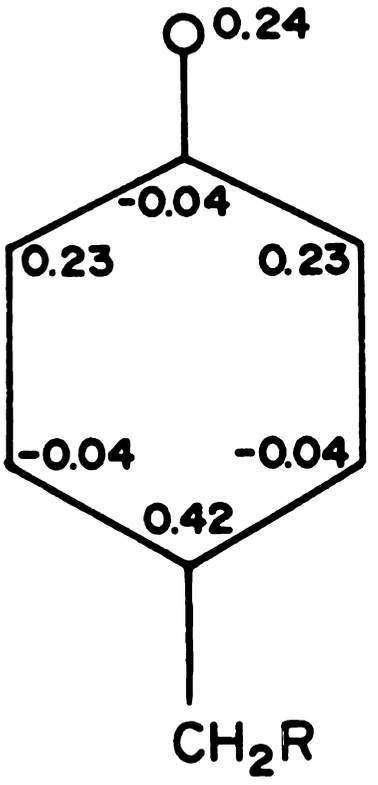
0.24
-0.04
0.23
0.23
-0.04
-0.04
0.42
CH2R

Table 4 Bond distance in Å and related bond angle in degrees

nuclei	C_1	C_2	C_3	C_4	C_5	C_6	0
bond distance	2.16	1.088	2.16	3.4	3.9	3.4	2.66
related bond angle	-34.1	0.0	34.1	21.0	0.0	-21	-65.6

To obtain the best fit between experimental and calculated hyperfine tensor components for the α-protons, we first held constant the spin density at $C_2(\rho_{c2})$, $C_3(\rho_{c3})$, $C_5(\rho_{c5})$, $C_6(\rho_{c6})$ by using the "average" Q value for these type of protons of 26.5 G (42). We then proceeded to change the spin density at $C_4(\rho_{c4})$ and at the oxygen (ρ_0), while holding the spin density at $C_1(\rho_{c1})$ constant at 0.44. We found that by changing ρ_0 from 0.20 to 0.28 and ρ_{c4} from 0 to -.08 the error in the calculated hyperfine coupling was between 8 and 12%. We choose to use an intermediate value of $\rho_0 = 0.24$ and $\rho_{c4} = -0.04$. Next we proceeded to see the effect of changing the Q value for the α-protons and therefore changing ρ_2, ρ_{c3}, ρ_{c5}, and ρ_{c6}. For these we hold ρ_{c1}, ρ_{c4}, and ρ_0 constant and equal to 0.44, -0.04 and 0.24, respectively. The Q value in these type of aromatic systems usually ranges from approximately 20 G to 33 G (42-44). We performed our calculations over a range of Q values between 18.6 G and 34 G, therefore changing $\rho_{c3} = \rho_{c5}$ from 0.32 to 0.17 and $\rho_{c2} = \rho_{c6}$ from -.06 to -.03. We found that the best fit was obtained when Q = 25.6 G. But when Q was 30 G or even 22 G the results obtained were quite reasonable and within a relatively small error (less than 20%).

Finally, we investigated the effect of changing ρ_{c4}. This was done by keeping constant ρ_{c2}, ρ_{c3}, ρ_{c5}, ρ_{c6}, and ρ_0, and changing ρ_{c1} and ρ_{c4}. The value of ρ_{c1} and ρ_{c4} that best fit our data were 0.42 and -.04, respectively. The spin density distribution illustrated in Figure 4.9 has an estimated error of approximately $\pm$11%. Our calculated hyperfine tensor components for the α-protons at the 3-5 positions are shown in Table 5.

Table 5 Experimental and calculated hyperfine tensor components for α-protons at the 3,5 positions in the Y_D^+ radical

Experimental (MHz)	Calculated (MHz)	% Error
25.5	23.0	9.8
16.0	17.8	11.3
8.0	8.5	6.3

One of the calculated hyperfine tensor components for the α-protons at the 2-6 position (a_x) shows a relatively large error, 41% (Table 6). The agreement is not as good for the hyperfine tensor components of these protons because of the incomplete resolution of the ENDOR lines for both orientations (Figure 4.4). The ENDOR determination of this tensor is affected by a large error that prevents a reliable comparison between experimental and calculated values. Also, these couplings are relatively small and even a difference of less than 1 MHz between the calculated and experimental values will be reflected as a large error. Another explanation for this large error may be the difference in dipolar interaction for the α-protons at the 2-6 positions when compared to the dipolar interaction of the α-protons at the 3-5 positions. O'Malley *et al.* (25) have done similar calculations for the anion radical benzoquinone. They found that the hyperfine tensor components of the α-protons depend critically on the nearest neighbor carbon spin density value, which causes the principal hyperfine tensor components to deviate from those expected for an isolated C-H fragment. The overall effect of the unpaired electron delocalization is to drive the rhombic C-H tensor to axiality (25). Nevertheless the calculated isotropic value for the α-protons at the 2-6 position is very close to values found in other phenoxy type radicals (14,39). To have a more precise picture of the unpaired spin density distribution we need to know the unpaired spin density at the oxygen and carbon 1. For all the other carbons (C_2, C_3, C_4, C_5 and C_6) we have a direct way of calculating the unpaired spin density at these positions. This is not the case for the oxygen and C_1, however, by substituting the oxygen by one of its isotopes

Table 6 Experimental and calculated hyperfine tensor components for α-protons at the 2,6 positions in the $Y_D^{\bullet}$ radical.

Experimental (MHz)	Calculated (MHz)	% Error
4.8	6.8	41
3.2	3.4	6.3
1.2	1.1	8.3

($^{17}0$) we can directly measure the couplings (spin for $^{17}0$, $S_{^{17}0} = 5/2$) and therefore get a better estimate of the unpaired spin at these positions. Such experiments are in progress. Our calculated unpaired spin density distribution for the $Y_D^{\bullet}$ radical is in agreement with the expected unpaired spin density distribution for these types of phenoxy radicals, *i.e.*, carbons 1, 3 and 5 carry a higher unpaired spin density than carbons at the 2,6 positions.

Orientation of $Y_D^{\bullet}$ With Respect to the Membrane Plane

The orientation of the tyrosine radical, $Y_D^{\bullet}$, in the membrane is an essential parameter for the simulation of the oriented $Y_D^{\bullet}$ EPR spectra of Figures 4.6a and 4.6b. Figures 4.3b and 4.3c show the $Y_D^{\bullet}$ ENDOR spectra in the 23-33 MHz region. The two bands observed correspond to the $a_{\parallel}$ and $a_{\perp}$ components of one of the β-protons as described above. If the ring plane were parallel to the membrane plane, application of the magnetic field perpendicular to the membrane plane, and hence perpendicular to the aromatic ring plane, should pick up mainly the perpendicular component of the tensor ($a_{\perp}$). The opposite is observed, that is, when the magnetic field is perpendicular to the membrane plane the main contribution to the spectrum is the $a_{\parallel}$ component, and when the magnetic field is parallel to the membrane plane the $a_{\perp}$ component shows a greater contribution. These results suggest that the tyrosine ring plane is perpendicular to the membrane plane.

The geometry of the radical in the membrane might be further investigated by studying the $Y_D^{\bullet}$ ENDOR spectra in Figures 4.4a and 4.4b. When the magnetic field is applied perpendicular to the membrane plane the a_x component

is the sole detectable contribution to the ENDOR spectrum in this region (Figure 4.4a). When the Y_D^+ ENDOR spectrum is recorded under the same conditions as in Figure 4.4a, but in the 10-20 MHz region a small band at about 18.5 MHz is observed (data not shown but see the following chapter). This band has been assigned to the y component of the hyperfine tensor for the α-protons at the 3-5 positions (a_y = 8.0 MHz). The fact that a_x is relatively much stronger than the a_y component suggests that at least one of the α-protons at the 3-5 positions should be nearly parallel to the membrane normal (see Figure 4.7). This suggests that the angle between the membrane normal and the line through the C_1 - C_4 carbons is not equal to 0°. When the magnetic field is applied parallel to the membrane plane (Figure 4.4b) the z component (a_z) of the hyperfine tensor for the α-protons at the 3-5 positions is the major contribution to the Y_D^+ ENDOR spectrum.

We have estimated an angle of approximately 60° for the orientation of the g_x component of the Y_D^+ radical with respect to the membrane plane and an angle of about 15° for the orientation of the g_z component with respect to the membrane normal. The latter is discussed in detail in the following chapter. To test this estimation of these angles we simulated the oriented Y_D^+ EPR spectra. The simulations are shown in Figure 4.6b for the field applied perpendicular to the membrane plane and in 4.6d for the field parallel to the membrane plane. The results of this simulations support the proposed orientation of the radical with respect to the membrane (Figure 4.7).

By plotting the g-value of the zero crossing of the oriented Y_D^+ Q-band EPR spectra against the angle between the magnetic field and the normal to the membrane plane, Hoff *et al.* (45) found a similar orientation for the aromatic ring with respect to the membrane. Even though they were assuming a plasto-quinone origin for the Y_D^+ species, their results are still valid for the tyrosine model for Y_D, since the directions of the g-tensor components they assumed are the same for the plastoquinone cation radical as for the tyrosine radical. They were looking at the orientation of the g-tensor components with respect to the membrane plane, making their findings independent of the model. The proposed orientation of the Y_D^+ radical in PSII is schematically represented in Figure 4.7.

Conclusions

The Y_D^+ EPR signal in an oriented multilayer of PSII membranes provides a way of gaining more insight into the structure and orientation of the radical in the membrane. The apparent quartet structure observed in the Y_D^+ powder EPR spectrum and more noticeably in oriented membranes, can be explained in terms of an approximate degeneracy between the α-protons at the 3-5 positions and one of the β-protons. We found that the preferred geometry or low energy configuration of β-protons in Y_D^+ in PSII is when $\theta_1 \neq \theta_2$. The situation in which $\theta_1 = \theta_2$ seems to occur rarely in this type of systems. α-protons possess a large anisotropy making them hard to detect by ENDOR spectroscopy due to line broadening. The use of oriented samples facilitated the detection of these signals by increasing the relative concentration of the radical in the samples. The proposed unpaired spin density distribution for the Y_D^+ radical, in which large

spin density is localized at the 1, 3, and 5 position, is in agreement with the expected unpaired spin density for phenoxy type radicals. The orientation of the $Y_D^{\bullet}$ tyrosyl aromatic ring plane with respect to the membrane plane is such that the angle between the membrane plane and the line through the C_1-C_4 carbons is about 60° (see Figure 4.7).

References

1. Babcock, G.T. and Sauer, K. (1975) Biochem. Biophys. Acta 376, 315.

2. Styring, S., Stenbjoern, A., and Rutherford, A.W. (1988) Biochem. 27, 4915.

3. Commoner, B., Heise, J.J. and Townsend, (1956) J. Proc. Nat'l Acad. Sci. USA 42, 710.

4. Warden, J.T., Blankenship, R.E. and Sauer, K. (1976) Biochim. Biophys. Acta 423, 462.

5. Yocum, C.F. Yerkes, C.T., Blankenship, R.E., Sharp, R.R. and Babcock, G.T. (1981) Proc. Nat'l. Acad. Sci USA 78, 7505.

6. Sjoberg, B.M., Reichard, P., Graslund, A. and Ehrenberg, A. (1978) J. Biol. Chem. 253, 6863.

7. Sahlin, H. Graslund, A., Ehrenberg, A. and Sjoberg, B.M., (1982) J. Biol. Chem. 257, 366.

8. Ehrenberg, A. and Reichard, P. (1972) J. Biol. Chem. 247, 3485.

9. Barry, B.A. and Babcock, G.T. (1988) Chimica Scripta, in press.

10. Lubitz, W. and Babcock, G.T. (1987) Trends in Biochemical Sciences 12, 96.

11. Rodriguez, I.D. and Babcock, G.T., in preparation.

12. Fasanella, E.L. and Gordy, W. (1969) Proc. Nat'l. Acad. Sci. USA 62, 299.

13. Box, H.C., Bodzinski, E.E. and Freund, H.G. (1974) J. Chem. Phys. 61, 2222.

14. Stone, T.J. and Walters, W.A. (1964) J. Chem. Soc. 37, 213.

15. Dixon, W.T., Moghime, M. and Murphy, D. (1974) J. C. S., Faraday Trans. 2, 70, 1713.

16. Tomkiewicz, M., McAlpine, R.D. and Cocivera, M. (1972) Can. J. Chem. 50, 3849.

17. Sealy, R.C., Harman, L., West, P.R. and Mason, R.P. (1985) J. Am. Chem. Soc. 107 3401.

18. Fisher, H. (1973) in Free Radicals, Vol. 2 ed. J.K. Kochi (Wiley, New York) Ch. 19.

19. Berthhold, D.A., Babcock, G.T. and Yocum, C.F. (1981) FEBS Lett, 134, 231.

20. Bender, C.J., Chandrashekar, T.K.C., Rodriguez, I.D. and Babcock, G.T. (1985) in preparation.

21. O'Malley, P.J. and Babcock, G.T. (1984) Biochem. Biophys. Acta 423, 462.

22. O'Malley, P.J., Babcock, G.T. and Prince, R.C. (1984) Biochem. Biophys. Acta 766, 283.

23. Borg, D.C. and Elmore, J.J. (1967) in: Magnetic Resonance in Biological Systems, Pergamon Press, Oxford, 341.

24. Barry, B.A., El-Deeb, M., Babcock, G.T. (1988) in preparation.

25. O'Malley, P.J. and Babcock, G.T. (1986) J. Am. Chem. Soc. 108, 3995.

26. Broustolon, M., Mariero, A.L. and Corvaja, C. (1981) J. Mag. Res. 45, 386.

27. Brok, M. Babcock, G.T. and Hoff, A.J. (1986) J. Mag. Res. 90, 368-378.

28. Heller, C. and McConell, H.M. (1960) J. Chem. Phys. 32, 1535.

29. Ayscough, P.G. (1967) Electron Spin Resonance in Chemistry, Methven, Longdon,

30. McCammon, J.A. and Karplus, M. (1983) Accounts of Chemical Research 16, 187.

31. Campbell, I.D., Dobson, C.M. and Williams R.J.P. (1978) Adv. Chem. Phys. 39, 55.

32. Gurd, F.R.N. and Rothgeb, T.M. (1979) Adv. Protein Chem. Phys. 33, 73.

33. Northrup, S.H., Pear, M.R., Lee, C.Y., McCammon, J.A. and Karplus, M. (1982). Proc. Nat'l. Acad. Sci. USA 79, 4035.

34. Gelin, B.R. and Karplus, M. (1975) Proc. Nat'l. Acad. Sci. USA 72, 2002.

35. McCammon, J.A., Wolyness, P.G. and Karplus, M. (1979) Biochem. 18, 927.

36. Northrup, S.H., Pear, M.R., Morgan, J.D., McCammon, J.A. and Karplus, M. (1981) J. Mol. Bio. 153, 1087.

37. Innes, J.B. and Brudvig, G.W. (1988) Biophys. J., 614a Abstr. W-Pos 384.

38. Janin, J. and Wodak, S. (1978) J. Mol. Bio. 125, 357.

39. Wertz, J.E. and Bolton, J.R. (1972) Electron Spin Resonance: Elementary Theory and Practical Applications, McGraw Hill: New York.

40. Heller, C. and Cole, T. (1962) J. Chem. Phys. 37, 243.

41. McConnell, H.M., Heller, C., Cole, T. and Fessenden, R.W. (1960) J. Am. Chem. Soc. 82, 766.

42. Lewis, L.C. and Singer, L.S. (1985) Magnetic Resonance in Chemistry Vol. 23, 698.

43. McConnell, H.M. (1956) J. Chem. Phys. 24, 764.

44. McConnell, H.M. and Chesnut, D.B. (1958) J. Chem. Phys., 28, 107.

45. Brok, M., Horikx, J.T.G. and Hoff, A.J. (1986) FEBS Lett. 203, 36.

CHAPTER 5
H_2O/D_2O EXCHANGE OF THE $Y_D^{\bullet}$ RADICAL IN PSII STUDIED BY ENDOR SPECTROSCOPY

Introduction

In photosystem II (PSII) the charge separation process that occurs upon light absorption involves the transfer of an electron from the reaction center P_{680} to the primary acceptor, a pheophytin molecule. To stabilize the initial charge separation to dissipative recombinaton subsequent forward electron transfer must be fast. For $P^{\bullet}_{680}$ species formed in PSII, this fast electron transfer is performed by a component Y_z (1), which donates electrons to the oxidized reaction center chlorophyll in less than 1 μs (2). The oxidized form of this donor, $Y_z^{\bullet}$ is subsequently reduced by the manganese cluster, which is the site of O_2 evolution in photosynthesis. The $Y_z^{\bullet}$ is paramagnetic and has a characteristic EPR signal with g = 2.0046 and line width of approximately 20 gauss. There is a second radical associated with PSII, $Y_D^{\bullet}$ that has the same EPR line width, g-value, and partially resolved hyperfine structure as $Y_z^{\bullet}$. These observations have lead to the conclusion that species with the same chemical structure give rise to these radicals (3). The behavior of these radicals only differ in their microwave power saturation characteristics (4,5).

Recently, Barry and Babcock have demonstrated a tyrosine neutral radical (*i.e.*, deprotonated) origin for $Y_D^{\bullet}$ and postulated a similar origin for $Y_z^{\bullet}$ (6).

With EPR alone it is difficult to extract more detailed information on hyperfine couplings, spin densities, and local protein effects, because both $Y_D^{\bullet}$ and $Y_Z^{\bullet}$ are immobilized on the EPR time scale. As a result g and hyperfine anisotropies are not averaged to zero and severe line broadening and loss of spectral resolutions occurs in the EPR spectrum.

A way to extract the information hidden in the EPR spectrum of immobilized radicals is by using electron-nuclear double resonance (ENDOR) spectroscopy, which has the capability to recover valuable information on hyperfine coupling that is usually obscured by immobilization (7). In the preceding chapter, we used ENDOR to recover isotropic and anisotropic hyperfine coupling constants for the ring and β-methylene protons on the $Y_D^{\bullet}$ radical. In these studies, we were able to extract detailed information on unpaired electron spin densities in the radical. ENDOR is also able to probe more subtle interactions that occur between the radical and its protein environment. The protons of nearby amino acids are usually weakly coupled to the unpaired spin and contribute resonances to the ENDOR spectrum of the radical near the free proton frequency, in the so-called matrix region (9). Recent work has also shown that hydrogen bonds formed between a radical and a proton donor in its immediate environment can be detected by ENDOR and that information on the orientation of the hydrogen bond can usually be obtained from the spectrum (10-14).

In the ENDOR work reported here on the $Y_D^{\bullet}$ radical, we have studied these two classes of more weakly coupled protons. The solvent accessibility of

the site has been determined by using D_2O/H_2O exchange. A hydrogen bond to the $Y_D^{\bullet}$ radical has been observed and its spatial characteristics with respect to the tyrosine ring plane has been determined by using g-anisotropy and physical sample orientation techniques. A preliminary account of some of this work has appeared (14).

Materials and Methods

Oxygen evolving PSII particles were isolated from spinach and tris-washed when required by using procedures based on those described earlier (15). D_2O/H_2O exchange was done with tris-washed PSII (t.w. PSII) particles by following several different protocols. The first method involved resuspension of pellets of t.w. PSII in a D_2O buffer that contained 50 mM Hepes and 10 mM NaCl at pD = 7.5 followed by incubation for up to 12 hours in the dark at 4°C. The second approach was to incubate t.w. PSII particles in a D_2O buffer containing 50 mM Mes and 10 mM NaCl at pD = 6.0 for three days in the dark at 4°C. The buffer was changed twice during the course of exchange. Brief periods of room light (2-3 minutes) were given at 6 hour intervals during incubation. We found that freeze-thaw cycles accelerate the exchange process; this was done three times for the samples reported here. A third way to perform the D_2O/H_2O exchange was to lyophilize t.w. PSII particles that had been resuspended in a D_2O buffer at pD = 7.5 followed by resuspension of the lyophilized material in D_2O. Exchange was also performed by combining the first method with a lyophilization step.

The Y_D^+ EPR line shape did not change following these procedures in the D_2O exchanged sample or in the H_2O control. Additional free radicals are generated in substantial amounts after long periods of dark, cold incubation (24 hours at pD = 7.5 and about 9 days at pD = 6.0). EPR and ENDOR were recorded on samples that did not show any additional free radical.

Oriented membranes were prepared by resuspending the PSII particles at approximately 8 mg Chl/ml in a buffer containing 20 mM Hepes and 10 mM NaCl at pH = 6.0 (33). The suspension of membranes was painted onto mylar sheets and dried at 4°C for 48 hours in a closed container protected from light. The relative humidity in the container was maintained at 90% by drying the strips in the presence of a saturated solution of $ZnSO_4$. If the samples were incubated for longer than 48 hours another free radical was observed. The ENDOR spectra were recorded on samples that only showed the Y_D^+ EPR spectrum and no other radical. Eight to ten PSII-coated strips were placed in quartz EPR tubes. The samples were frozen and stored in liquid N_2. The Y_D^+ EPR signal was stable over a period of about 72 hours when stored in this fashion. After this period of time only 10 to 15% of the signal had decayed as judged by comparing the Y_D^+ EPR spectra recorded immediately after illumination and after 72 hours of dark adaptation at 77K.

EPR and ENDOR spectra were recorded with samples that contained 3-6 mg Chl/ml. For oriented PSII membranes the spectra were recorded in such a way that the external magnetic field was either parallel to the membrane plane (*i.e.*, 0°) or perpendicular to the membrane plane (*i.e.*, 90°). The X-band EPR

and ENDOR spectra were recorded on a Bruker ER200D spectrometer equipped with a Bruker ENDOR accessory (16). Temperature and instrument settings used are given in the figure legends.

Results

Figure 5.1 shows the $Y_D^{\bullet}$ matrix ENDOR spectra recorded at 4K for samples incubated for three days in H_2O (Figure 5.1a) or in D_2O (Figure 5.1b) at pH/pD = 6.0. An unusual feature of these spectra when compared to matrix ENDOR spectra of model compounds is the occurrence of several well-resolved lines in this weak coupling region. This occurs because each protein site is structured and identical, as opposed to the more disordered solvent environment that occurs for radicals in frozen solution. These ENDOR matrix transitions are produced by dipolar couplings between the radical and nearby amino acid protons (within 5-6 Å) surrounding it. This interaction varies as $1/r^3$, where r is the distance between the radical and the interacting magnetic nuclei. Solvent accessibility to the radical site can be investigated by looking at the changes in this matrix region that occur upon H_2O/D_2O exchange. The most noticeable change in Figure 1 is the disappearance of the resonance labeled with an arrow (a = 0.3 MHz) after the D_2O/H_2O exchange, indicating that exchangeable protons do exist at a fairly short separation distance from the radical. The bulk of the protons in the protein environment surrounding the radical, however, do not appear to exchange under these conditions.

Hydrogen-bonded protons constitute the second set of protein bound protons that can be detected in the ENDOR spectrum of the radical. As

Figure 5.1. $Y_D^{\bullet}$ matrix ENDOR spectra of samples incubated in H_2O (a) and D_2O, (b) at pH/pD = 6.0. T = 4k; microwave power 6.3 mW, rf at 10 MHz, 150W; fm deviation 30 KHz.

Deuterium Exchange

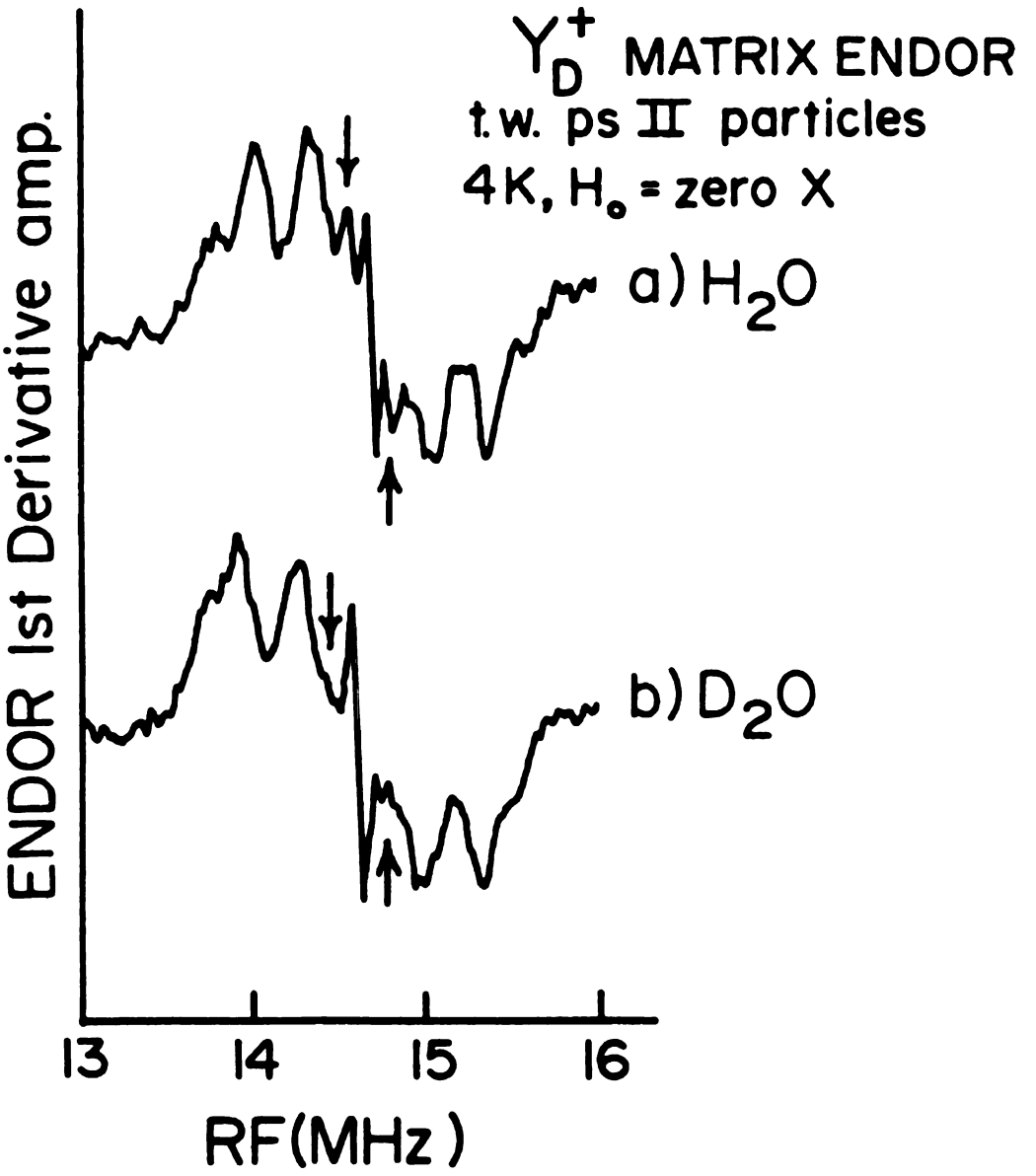

opposed to the more distant protons that contributes to the matrix, we expect the hydrogen-bonded protons to exhibit larger couplings but to retain a purely dipolar hyperfine tensor (10).

Hydrogen-bonded protons should exchange with solvent water, depending on solvent accessibility, but -CH_2- protons and α-protons on the tyrosine aromatic ring (Figure 5.2) are not expected to exchange under mild conditions. Figure 5.3b shows the ENDOR spectrum of t.w. PSII particles that were incubated for 6 hours at pD = 7.5 and subsequently freeze dried and resuspended in D_2O. The resonance with a coupling of 7.1 MHz is absent in the D_2O exchange sample as compared to that of the H_2O control (Figure 3a). Another resonance with a hyperfine coupling of 3.5 MHz is also absent in the D_2O exchanged sample and an underlying set of resonances becomes apparent. These latter resonances have been assigned to the α-protons at the 2-6 positions and to one of the β-methylene protons as described in detail in the preceeding chapter. The 3.5 and 7.1 MHz resonances that disappear upon exchange are typical of those observed for H-bonded protons in model compounds (10-12) and we assign these to perpendicular ($a_{\perp}^{HB}$) and parallel ($a_{\parallel}^{HB}$) hyperfine tensor components of an H-bonded proton, respectively. The unpaired spin in the tyrosine radical is confined to the phenol ring, the only hydrogen bond active species is the phenol oxygen, and we conclude that the hydrogen bond we observe in Y_D^+ involves this phenol oxygen. In accord with the general characteristics of hydrogen-bond interactions (10) we also conclude that the hydrogen bond hyperfine tensor

Figure 5.2. The phenol moiety of tyrosine showing the carbon numbering system used in the text.

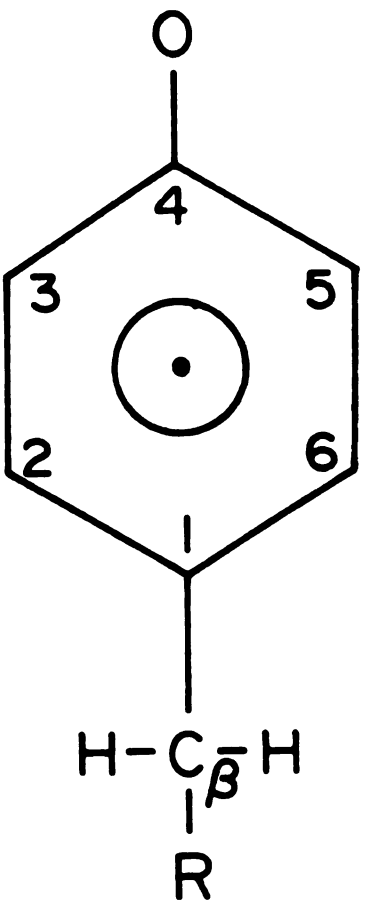
O
4
3
5
2
6
1
H-C-H
β
R

Figure 5.3. $Y_D^{\bullet}$ ENDOR spectra of samples incubated in H_2O (a) and in D_2O (b) at pH/pD = 7.5. T = 115K; microwave power 6.3 mW, rf at 10 MHz, 150 W; fm deviation 150 KHz.

H_2O / D_2O Exchange

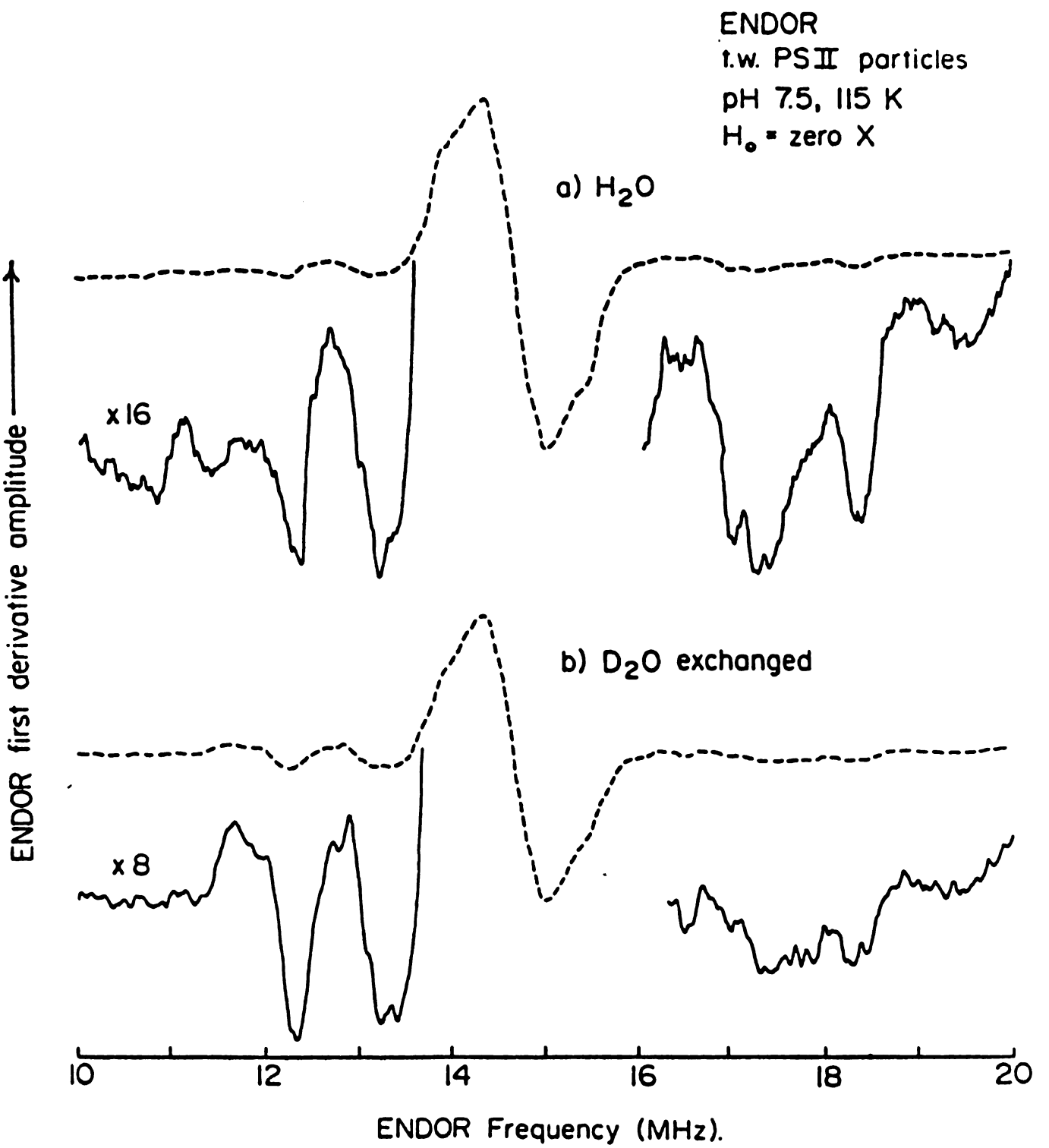

components are oriented with respect to the O···H bond with $a_{\perp}^{HB}$ along the hydrogen bond axis and $a_{\parallel}^{HB}$ perpendicular to the O···H bond direction.

Figure 5.4 shows the $Y_D^{\bullet}$ ENDOR spectra of t.w. PSII membranes incubated in D_2O (Figure 5.4b) and H_2O (Figure 5.4a), at pD/pH = 6.0 for three days at 4°C. The resonance at 7.1 MHz in the D_2O exchanged sample (Figure 5.4b) decreases in intensity as compared to that of the H_2O control (Figure 5.4a) but it is not completely absent as was the case under the exchange conditions in Figure 5.3b, where the sample was incubated at pD = 7.5. Thus at lower pD's the rate of exchange appears to be slower. It is apparent that the pD/pH has an effect on the exchange and probably on the configuration of the protein structure surrounding the radical. A similar pH effect has been observed by Volker *et al.* (17). In samples where the donor side of PSII was exposed to added trypsin the oxygen evolving capacity was only slightly affected at pH = 6.0 but was destroyed at pH = 7.5. The pH-dependence of the proteolitic activity of trypsin could not account for this effect (18). Volker *et al.* (19) showed that a trypsin treatment at pH = 6.0 did not show any effect on the $Y_D^{\bullet}$ EPR signal while at pH = 7.5 trypsin treatment resulted in complete loss of the signal.

For the $Y_D^{\bullet}$ radical Brok *et al.* (20) have determined the principal g-tensor components as follows: g_z = 2.0023, g_x = 2.0076, and g_y = 2.0044. In single crystal tyrosine radical experiments, Gordy and Fasanella (21) determined the orientation of these g-tensor axes with respect to the molecular axes and concluded that the g_z component is perpendicular to the ring plane, g_x is along the C-O bond and the g_y component is in the plane and perpendicular to g_x. The

Figure 5.4. $Y_D^{\bullet}$ ENDOR spectra of samples incubated in H_2O (a) and D_2O (b) at pH/pD = 6.0. T = 115K; microwave power 6.3 mW, hf at 10 MHz, 150W; fm deviation 150 KHz.

H_2O / D_2O Exchange

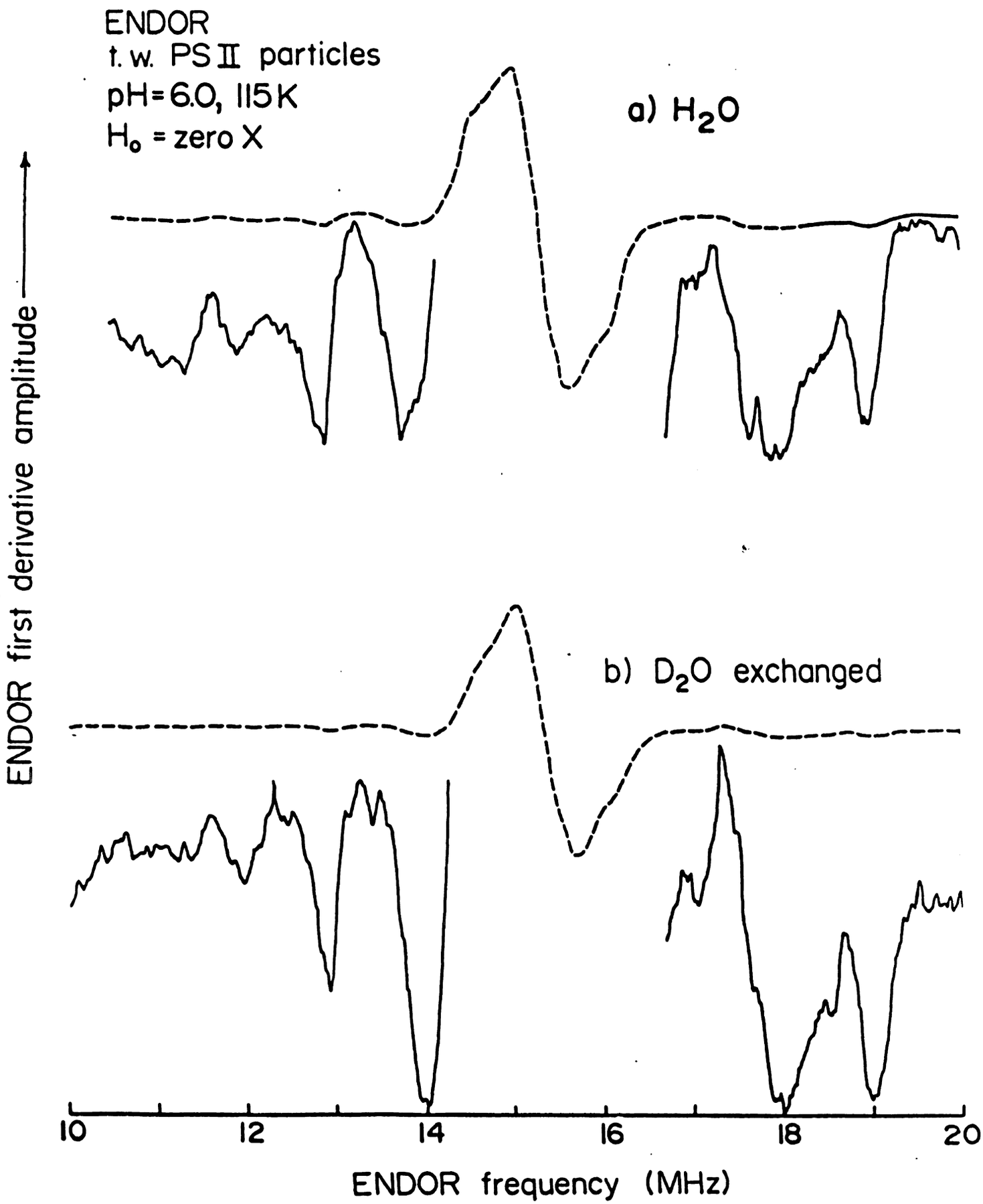

extent of g-anisotropy is fairly substantial and suggests that an orientation selection experiment that takes advantages of this g-anisotropy can be used to investigate the direction of the hyperfine tensor components, $a_{\perp}^{HB}$ and $a_{\parallel}^{HB}$, with respect to the tyrosine molecular axes. Recording the ENDOR spectrum with the magnetic field set to the high field side of the $Y_D^{\bullet}$ EPR spectrum (*i.e.*, the g_z area) should select only the molecules whose z-axis is orientated along the magnetic field; conversely x,y orientation can be selected by performing the ENDOR experiment at lower field. This approach was used by O'Malley and Babcock to investigate the orientation of the principal hyperfine tensor components for the hydrogen-bonded proton present in the p-benzoquinone anion radical (10).

Figure 5.5 shows the $Y_D^{\bullet}$ ENDOR spectrum recorded with the magnetic field set at the EPR zero crossing, g = 2.0046 (Figure 5.5a) and at the high field side, g ≈ 2.0 (Figure 5.5b). Both $a_{\perp}^{HB}$ and $a_{\parallel}^{HB}$ for the hydrogen-bonded proton are evident in Figure 5.5a, whereas $a_{\perp}^{HB}$ is the only hyperfine tensor component observed in Figure 5.5b. Since the direction of g_z is perpendicular to the ring plane, the observation of only the $a_{\perp}^{HB}$ component of hyperfine tensor when the g_z orientation is selected demonstrates that O···H axis lies in the plane of the ring, *i.e.*, that the hydrogen bond is in the ring plane.

A second approach to deconvolute the weak coupling region of the $Y_D^{\bullet}$ ENDOR spectrum is to use oriented PSII membranes. In these samples we have a single crystal type situation where orientation of the radicals with respect to the external magnetic field is constant throughout the sample, as opposed to powder

Figure 5.5. Orientation selection ENDOR spectra of $Y_D^{\bullet}$. The fields at which the two spectra were microwave power 6.3 mW, rf at 10 MHz, 150W; fm deviation 150 KHz.

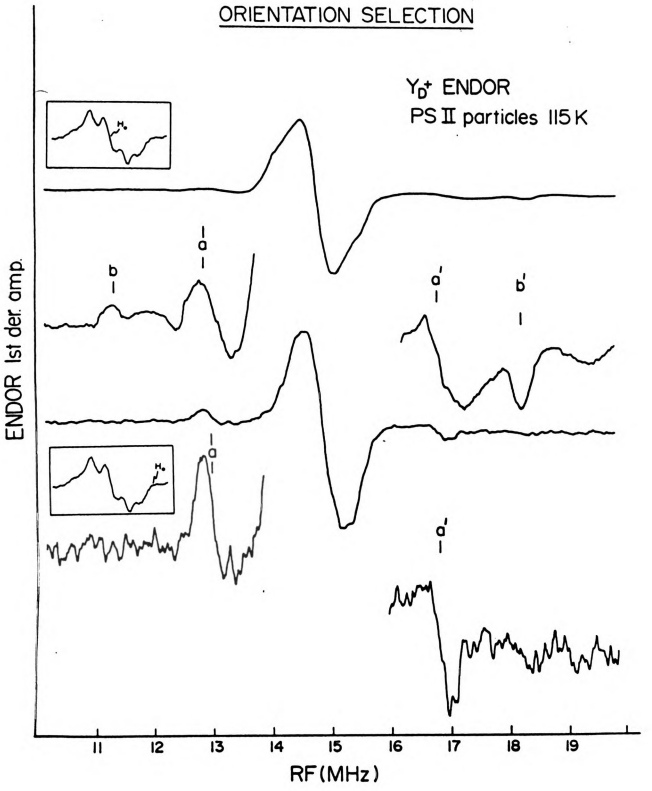
ORIENTATION SELECTION
Y_D^+ ENDOR
PS II particles 115 K
ENDOR 1st der. amp.
b
a
a'
b'
a
a'
11
12
13
14
15
16
17
18
19
RF (MHz)

sample, *i.e.*, frozen PSII membranes, where essentially all orientations are possible. We used these samples in the preceding chapter to analyze the orientation of the hyperfine tensor of the 3,5 and -CH_2- protons and here we apply this technique to the hydrogen bonded proton. Figure 5.6 shows the Y_D^+ EPR spectra for oriented PSII membranes with the direction of the magnetic field perpendicular (Figure 5.6a) and parallel (Figure 5.6b) to the membrane plane. These EPR spectra are similar to those reported for oriented PSII membranes by Rutherford (33) and indicate that we have a well oriented population. Figure 5.7 shows the Y_D^+ ENDOR spectra of these oriented PSII membranes in the 10-20 MHz region recorded at 108K. When the magnetic field is perpendicular to the membrane plane (Figure 5.7a) the intensity of the parallel hyperfine tensor component ($a_{\parallel}^{HB}$ = 7.1 MHz) is decreased as compared to Figure 5.7B where the field is parallel to the membrane plane. The situation with respect to the perpendicular hyperfine tensor component ($a_{\perp}^{HB}$ = 3.5MHz) is not as clear owing to overlap of different ENDOR lines in this region. These spectra indicate that the ring plane of the Y_D^+ tyrosine radical is tilted with respect to the membrane plane.

Another free radical is observed along with the Y_D^+ EPR spectrum if the samples are incubated for long periods of time, more than two weeks at pD/pH = 6.0 or longer than 24 hours at pD/pH = 7.5, during the D_2O/H_2O exchange experiment (Figure 5.8). This is not a result of deuterium substitution or exchange, as this radical is also observed in the H_2O control sample. When these samples are illuminated, a composite EPR spectrum with g = 2.0035 and

Figure 5.6. Oriented Y_D^+ EPR spectra with the magnetic field applied perpendicular (a) and parallel (b) to the membrane plane T = 115K; microwave power 6.34 mW, rf at 10 MHz, 150W; fm deviation 150 KHz.

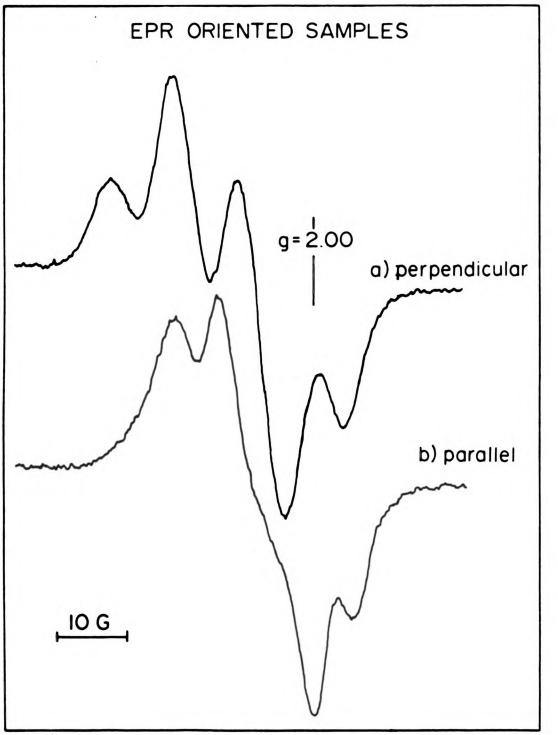
EPR ORIENTED SAMPLES
g= 2.00
a) perpendicular
b) parallel
10 G

Figure 5.7. Oriented $Y_D^{\bullet}$ ENDOR spectra with the magnetic field applied perpendicular (a) and parallel (b) to the membrane plane. The correspondent EPR are shown in the inset. T = 108K; microwave power 6.3 mW, rf at 10 MHz, 150W; fm deviation 150 KHz.

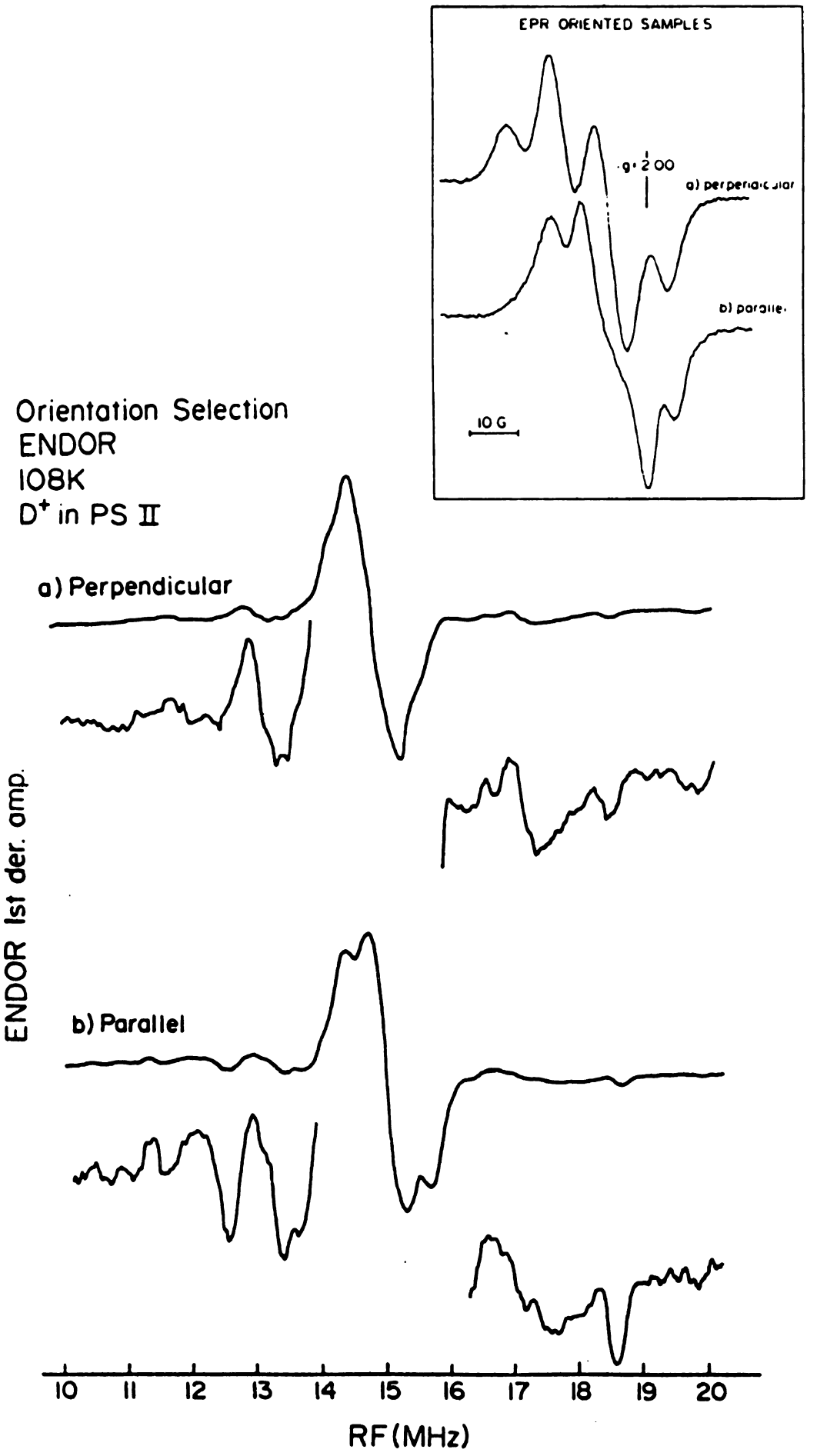
EPR ORIENTED SAMPLES
g = 2.00
a) perpendicular
b) parallel
10 G
Orientation Selection
ENDOR
108K
D+ in PS II
a) Perpendicular
b) Parallel
ENDOR Ist der. amp.
10
11
12
13
14
15
16
17
18
19
20
RF (MHz)

Figure 5.8. Y_D^+ EPR spectra of samples incubated at pD/pH = 6.0 for the time indicated in the figure. T = 298K.

t.w. PSII particles

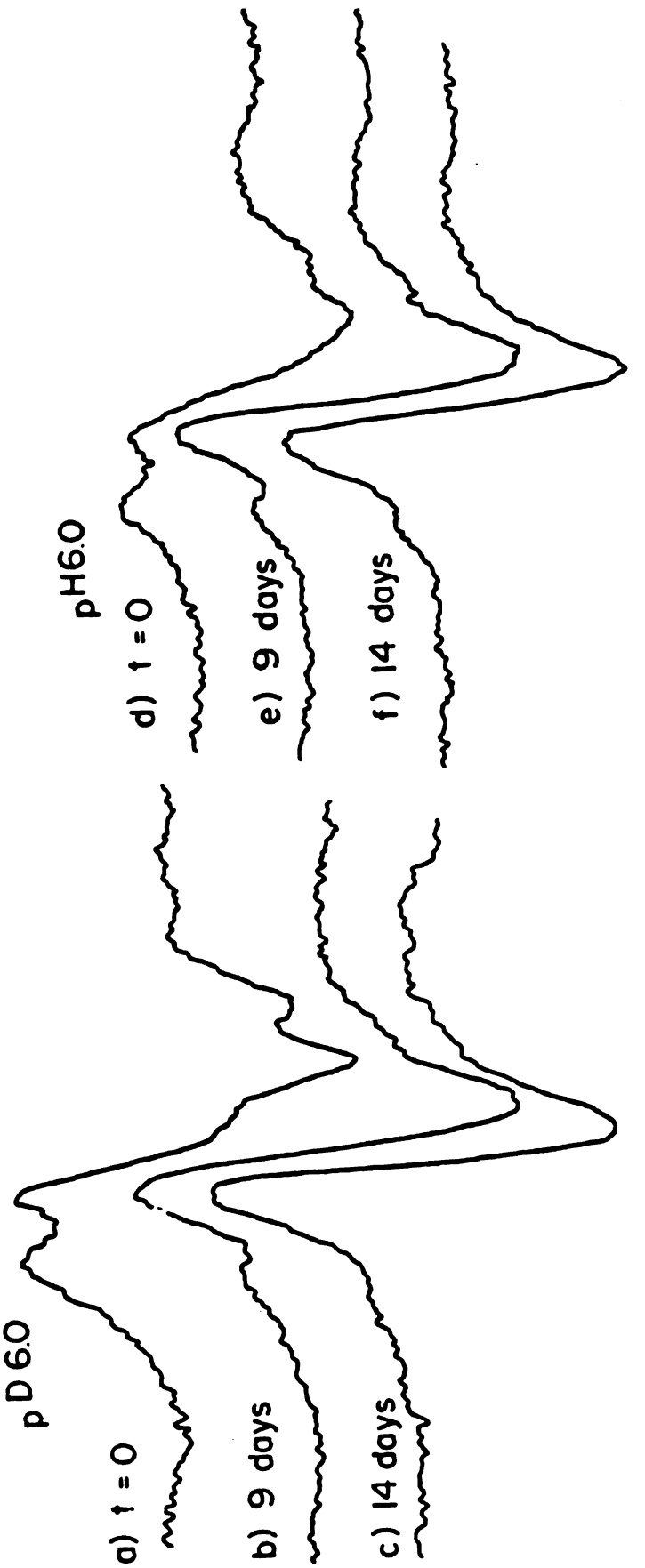

line width of 11 G is observed. If the sample is then incubated in the dark for a period of about 3 hours the contribution of the Y_D^+ EPR spectrum is absent and a signal with g = 2.0026 and line width of approximately 10 G is obtained (Figure 5.9). When preparing oriented samples, the same type of radical is observed if the drying time is too long. In both cases the characteristics of this radical correlate with those of a chlorophyll cation radical. This radical can also be formed by using high concentrations of K_2IrCl_6 (≈15mM) (22), by illuminating t.w. PSII membranes at -154°C in the presence of 5mM K_2IrCl_6 or $K_3Fe(CN)_6$ (23) and by adding 2 M urea to t.w. PSIIs.

Discussion

The protons interacting with the unpaired electron spin density in the Y_D^+ radical can be divided into two classes. Protons bonded directly to the ring or to the methylene carbon at the 1 positon have both isotropic (Fermi contact) and anisotropic (dipole-dipole) hyperfine interactions. The second class of protons derive from the protein and are not covalently bonded to the tyrosine head group. The electron-nuclear interactions of these more distant protons consist only of dipolar interactions. H-bonded and matrix protons fall under this second group.

The occurrence of matrix ENDOR lines depends on whether there are magnetic nuclei in the local environment of the unpaired spin, typically within 5 to 6 Å (9). In the protein binding site the radical is in a well-defined, highly structured environment. This situation will produce specific dipole-dipole interactions between the radical and nearby amino acid protons leading to the

Figure 5.9. EPR signal observed when samples are incubated for too long in D_2O or H_2O (a) as described in the text. EPR signal of the radical observed after $Y_D^{\bullet}$ decayed (b) T = 298K.

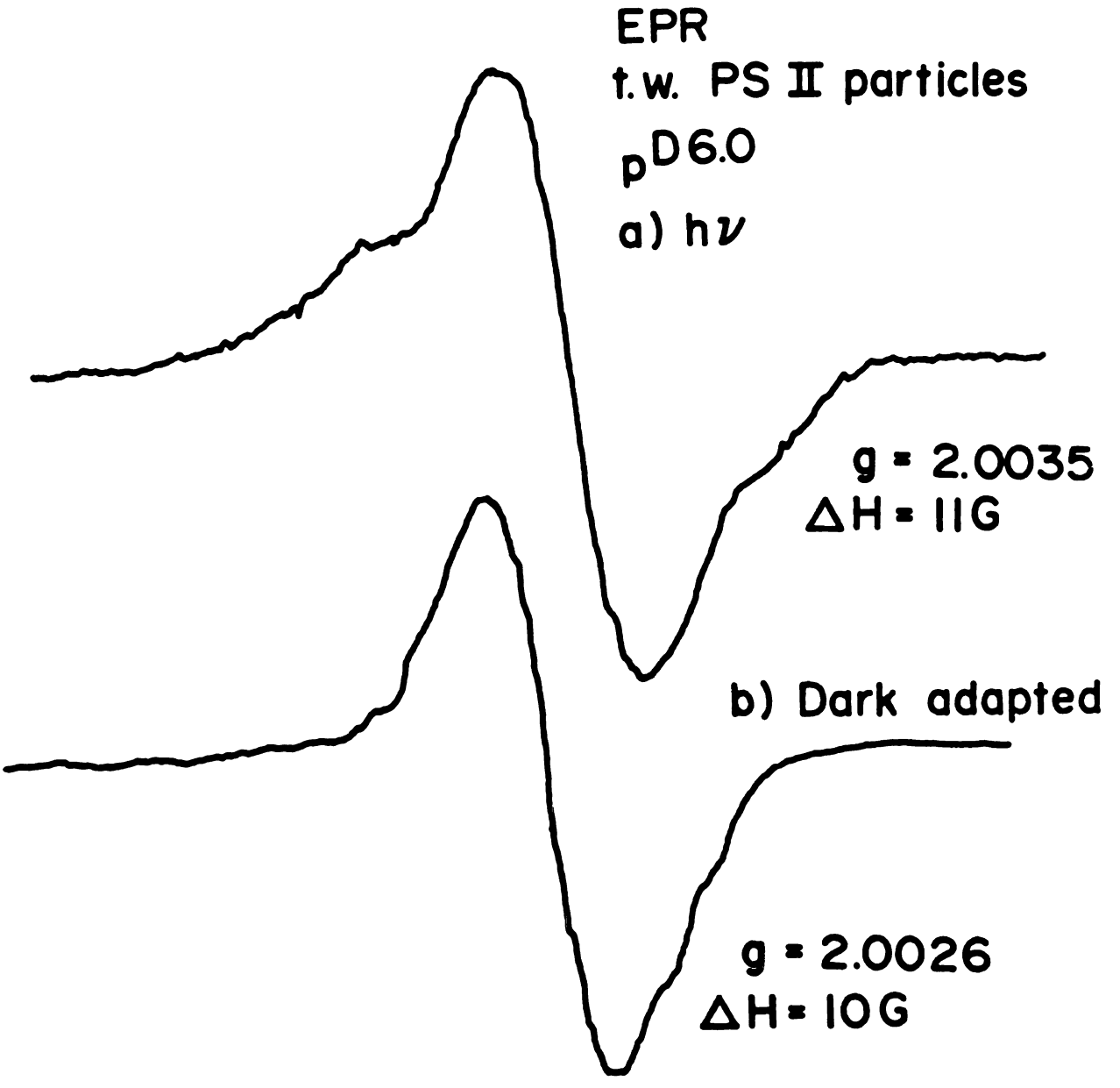
EPR
t.w. PS II particles
pD 6.0
a) hν
g = 2.0035
ΔH = 11G
b) Dark adapted
g = 2.0026
ΔH = 10G

resolved matrix ENDOR spectra observed in Figure 5.1. These spectra contrast markedly with the matrix ENDOR spectra observed in model compounds (10-12,14). In the models the solvent environment is not locally ordered, the dipole-dipole interactions vary widely, and the poorly resolved spectra commonly observed in these cases result.

Because the matrix ENDOR spectra in the $Y_D^{\bullet}$ radical is produced primarily by relatively weak interactions between the radical and nearby amino acid protons, some of which are likely to be exchangeable, the solvent accessibility of the binding site can be monitored. After three days of D_2O/H_2O exchange at pD/pH = 6.0 only a few changes where observed in the $Y_D^{\bullet}$ matrix ENDOR region (Figure 5.1) suggesting that only the most weakly coupled and more distant protons (≈5-6 Å) are exchanged. This implies that the binding site is well-shielded from solvent water but that it is slowly accessible. Under harsher conditions, incubation for 6 hours at pD/pH = 7.5 followed by freeze drying and resuspension in D_2O/H_2O, are we able to exchange the hydrogen bonded proton closer to the radical (Figure 5.3). Taken together, the results indicate that the $Y_D^{\bullet}$ radical is well shielded from the aqueous phase and is most likely buried deep in the membrane as suggested by the results of Debus *et al.* (24). This conclusion is supported by data obtained by Innes *et al.* (25) that showed that the microwave power saturation behavior of the $Y_D^{\bullet}$ EPR spectrum was dependent upon added Dy^{3+} -EDTA. From the concentration dependence they estimated a distance of 21.4 Å from the radical binding site to the membrane surface

in t.w. PSII, consistent with the idea that the radical is well-shielded from solvent water.

Our observation of a hydrogen-bonded proton to the $Y_D^{\bullet}$ radical and our conclusion that the radical is sequestred from the aqueous phase rationalize two aspects of the *in vivo* chemistry of this species. First, upon oxidation of the tyrosine phenol the pKa of the hydroxyl proton decreases from 10.1 (26) to about -1.6 (27). The occurrence of the hydrogen bond probably results from the deprotonation of this highly acidic species according to the following sequence:

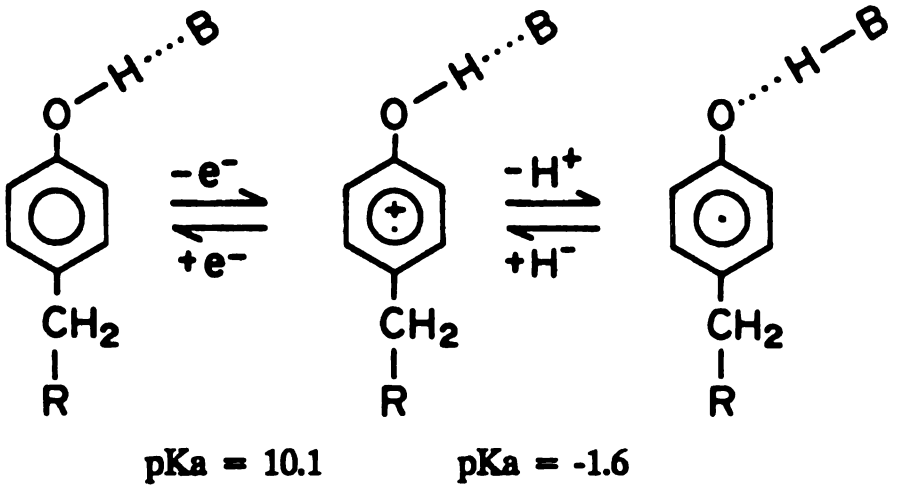

where B is a base (eq. lysine, histidine, peptide nitrogen) in the immediate vicinity. Such a sequence predicts that the tyrosine radical of the $Y_D^{\bullet}$ species is actually the neutral, *i.e.*, deprotonated form and that the formal positive charge has been transferred to the base B. This is in agreement with the g-value of the $Y_D^{\bullet}$ species, which is much more consistent with a neutral radical than with a protonated radical (6). Second our postulated location of $Y_D^{\bullet}$ in an environment

isolated from the aqueous phase may account for the unusual stability of the radical to reduction. Model compound electrochemical work on tyrosine in solution has provided a value of +0.8V at pH = 7.0 for its redox potential (28,29) in good agreement with the estimate of +0.76V for the Y_D^+ midpoint potential made by Boussac and Etienne (22). This value is characteristic of a highly oxidizing species, one that would be expected to be reduced quickly by reductants (*e.g.*, ascorbate) in the chloroplast milieu. If, however, the Y_D^+ species is isolated from the reductants, as our H_2O/D_2O exchange data indicate, then its stability to reduction becomes understandable.

Although the EPR properties of Y_D^+ and Y_Z^+ are sufficiently similar that one can sometimes infer properties of the Y_Z^+ species (6,24) from those of the stable Y_D^+ species, the hydrogen bond situation of the Y_Z^+ remains an open question. The reason for this is that the hydrogen bond influences the Y_D^+ EPR line width only slightly and ENDOR must be used to document its occurrence. To date, we have not been successful in trapping the Y_Z^+ species under conditions appropriate for ENDOR and thus we cannot comment on either the solvent accessibility or the hydrogen bonding state of this radical. Such information, of course, would be extremely useful in characterizing the role of Y_Z in transferring electrons between the site of water oxidation and the reaction center chlorophyll P_{680}.

The unusual microwave power saturation observed for the Y_D^+ EPR spectrum (30,31) was the first suggestion of a strong interaction between the Y_D^+ radical and the protein environment. This anisotropic power saturation

behavior, in which the center of the EPR spectrum saturates at lower power than the wings, has also been observed in model semiquinone systems (32). In the models this phenomenon has been explained in terms of solvent induced anisotropic spin lattice relaxation that results from hydrogen bonds to the oxygens at the 1,4 ring positions. Although the tyrosine radical $Y_D^{\bullet}$ has only a single carbonyl oxygen that participates in a hydrogen bonding interaction, it is likely that this contributes to the observed power saturation behavior of the $Y_D^{\bullet}$ EPR spectrum. In this regard a comparison of the power saturation behavior of $Y_D^{\bullet}$ to that of the tyrosine radical in ribonucleotide reductase, where the hydrogen bond interaction looks to be substantially weaker or missing altogether, may be informative.

Because the hyperfine tensor for the $Y_D^{\bullet}$ hydrogen-bonded proton is purely dipolar, we can use the principal components to estimate the O···H bond distance. Such an analysis has been carried out for the benzoquinone anion radical (10). The procedure relies upon a point dipole approximation that relates unpaired electron spin density, distance between dipoles and hyperfine coupling as follows:

$$a_i = 78.4\ \rho_o\ \left[\ \frac{3\cos^2\theta_i - 1}{r^3}\ \right] \qquad (1)$$

where a_i(i = x, y, or z) is in MHz, ρ_o is the unpaired spin density on the hydrogen-bonded atom, in this case the phenol oxygen, θ_i is the angle between the applied magnetic field and the line joining the proton and its hydrogen partner and r is the distance in Å between the two atoms (10,12). This equation

predicts that the major coupling ($a_{\parallel}^{HB}$) is along the O···H direction and that the sign of this tensor component is positive; the smaller coupling is two-fold degenerate and negative. By using equation 1, the direction of $a_{\parallel}^{HB}$ and $a_{\perp}^{HB}$, and the unpaired spin density at the oxygen for $Y_D^{\bullet}$ estimated in the preceding chapter (0.2 to 0.28), we find an O···H distance of 2.0 to 2.3 Å for the hydrogen bonding interaction.

The aromatic ring plane in the tyrosine radical lies nearly perpendicular to the membrane plane, with an angle between the C_1-C_4 axes and the membrane plane of around 60°. We can further investigate the orientation of the radical with respect to the membrane plane by looking at the directions of $a_{\parallel}^{HB}$ and $a_{\perp}^{HB}$ within the context of the $Y_D^{\bullet}$ ENDOR spectra of oriented PSII membranes. From the orientation selection experiment we know that $a_{\perp}^{HB}$ lies perpendicular to the ring plane, whereas $a_{\parallel}^{HB}$ is parallel. When the magnetic field is applied perpendicular to the membrane plane (Figure 5.7a) the intensity of $a_{\parallel}^{HB}$ is smaller as compared to the $a_{\perp}^{HB}$ component. When the field is rotated 90° with respect to the membrane plane (Figure 5.7b) the intensity of $a_{\parallel}^{HB}$ is much stronger as compared to Figure 5.7a but contributions from the $a_{\perp}^{HB}$ component remain. There are three possible explanations for the observed lack of resolution between the hyperfine tensor components of the H-bonded proton. The first explanation is poor orientation of the PSII membranes causing a large spreading of all possible angles (mosaic spread) giving rise to a situation similar to that found in a powder spectrum. A second possibility is that the H-bonded proton is not exactly co-planar with the ring plane. A third explanation would be

that the ring plane is not exactly perpendicular to the membrane plane, *i.e.*, that the angle between the g_z component and the membrane normal is not exactly 90°.

Although partial disorientation on this type of samples is expected, the mosaic spread is not so large (≈10°) that the resolution of the individual hyperfine tensor components for the various protons cannot be obtained, as shown in the preceding chapter. In addition, the Y_D^+ EPR spectra for these oriented samples demonstrated a well oriented population, eliminating the first possibility. From the orientation selection experiment we know that the H-bonded proton is in the plane of the ring, eliminating the second possibility. Therefore we conclude that the ring plane is twisted with respect to the membrane normal. We estimate a twist angle of 15° ± 5°, which is supported by EPR simulations of the Y_D^+ oriented samples. The proposed orientation of the Y_D^+ radical with respect to the membrane plane is schematically represented in Figure 5.10.

Conclusions

The ENDOR studies presented here for the Y_D^+ radical indicate that this technique is suitable for studying these type of biological systems to provide information not only on the radical itself but also on protons from amino acids in the immediate vicinity. The Y_D^+ binding site is found to be inaccessible to solvent water under most experimental conditions; only with fairly drastic treatment can protons in this site be exchanged. This observation is consistent with the stability of Y_D^+. It also suggests that the protein is labile to a certain

Figure 5.10. Proposed orientation of the Y_D^+ radical in the membrane.

extent. There is a H-bonded proton present that may play an important role in the redox chemistry of the radical. The O···H distance has been estimated to be between 2.0 to 2.3 Å. Not only is the ring plane not exactly perpendicular to the membrane plane but it is also twisted with respect to the membrane normal by about 15°.

All studies presented here were performed on Y_D^+ and, although we believed that Y_z^+ and Y_D^+ have the same structure and similar orientation with respect to the membrane, the presence of an hydrogen-bonded proton to Y_z^+ can not be tested by ENDOR at present owing to the instability of this radical. Although we do not have any evidence, it is possible that the hydroxyl proton released by the Y_D^+ and Y_z^+ species upon oxidation may be hopping on and off from the radical to a nearby base depending on the oxidation state of the tyrosine molecule. Another possibility is that it may just be a Bohr proton.

References

1. Babcock, G. T. and Sauer, K. (1973) Biochim. Biophys. Acta, 325, 482.

2. Brettel, K., Schlodder, E. and Witt, H. (1984) Biochim. Biophys. Acta 766, 403.

3. Kohl, D.H. and Wood, P.M. (1969) Plant Physiol. 44, 1439.

4. Warden, J. T., Blankenship, R. E. and Sauer, K. (1976) Biochim. Biophys. Acta, 423, 462.

5. Yocum, C. F., Yerkes, C. T., Blankenship, R. E., Sharp, R. R. and Babcock, G. T. (1981) Proc. Nat'l. Acad. Sci. USA 78, 7507.

6. Barry, B.A. and Babcock, G.T. (1987) Proc. Nat'l. Acad. Sci. USA, 84, 7099.

7. Lubitz, W. and Babcock, G. T. (1987) Trends in Biochemical Sciences, 12, 96.

8. Rodriguez, I. D. and Babcock, G. T (1988) in preparation.

9. Kevan, L., Kispert, L. C. (1972) Electron Spin Double Resonance Spectroscopy, Wiley, New York, pp. 388.

10. O'Malley, P. J. and Babcock, G. T. (1986) J. Am. Chem. Soc., 108, 3995.

11. O'Malley, P. J. and Babcock, G. T. (1984) J. Chem. Phys. 80, 3912.

12. O'Malley, P. J., Chandraskekar, T. K. and Babcock, G. T. (1985) in: Antenna and Reaction Centers of photosynthetic Bacteria (Michele-Beyerle, M. E., ed.) pp 339, Springer-Verlag, Berlin.

13. Feher, G., Isaacson, R. A., Okamura, M. Y. and Lubitz, W., in: Antenna and Reaction Centers of Photosynthetic Bacterial (Michele-Beyerle, M. E., ed.) pp. 1, Springer-Verlag, Berlin.

14. Rodriguez, I.D., Chandrashekar, T.K., and Babcock, G.T. (1987) Prog. in Photosyn. Res. 1, 471.

15. Berthold, D.A., Babcock, G.T. and Yocum, C.F. (1981) FEBS Lett 134, 231.

16. Bender, C. Barry, B.A., Chandrashekar, T.K., Rodriguez, I.D. and Babcock, G.T., (1988) in preparation.

17. Volker, M., Ono, T., Inoe, Y. and Renger, G. (1985) Biochim. Biophys. Acta, 806, 25.

18. Renger, G., Volker, M. and Weiss, M. (1984) Biochim. Biophys. Acta, 766, 582.

19. Volker, G. Renger, G. and Rutherford, A. W. (1986), Proc. Natl. Acad. Sci. USA 83, 9474.

20. Brok, M. Ebskamp, F.C.R. and Hoff, A.J. (1985) Biochim. Biophys. Acta 809, 421.

21. Gordy, W. and Fasanella, E. L. (1969) Proc. Nat'l. Acad. Sci. USA, 62, 29.

22. Boussac, A. and Etienne, L. (1984) Biochim. Biophys. Acta, 766, 576.

23. Nugent, J. H. A., Stewart, A. C. and Evans, M. C. W. (1981) Biochim. Biophys. Acta, 635, 488.

24. Debus, R. J., Barry, B. A., Babcock, G. T. and McIntosh, L. (1988) Proc. Natl. Acad. Sci. USA, in press.

25. Innes, J. B. and Bruding, G. W. (1988) Biophys. J., 53, 614a.

26. Barker, R. (1971) Organic Chemistry of Biological Compounds, Prentice-Hall, Inc. Englewood Cliffs, New Jersey.

27. Murphy, D. and Dixon, W. T. (1978) J. Chem. Soc., Faraday Trans. 2, 74, 432.

28. Steenken, S. and Neta, P. (1982) J. Phys. Chem., 86, 3661.

29. Jovanovic, S. V., Harriman, A. and Simic, M. G. (1986) J. Phys. Chem., 90, 1935.

30. Esser, A. F. (1974) Photochem. Photobiol., 20, 167.

31. Hales, B. J. and Gupta, A. D. (1981) Biochim. Biophys. Acta, 637, 303.

32. Hales, B. J. (1976) J. Chem. Phys., 65, 3767.

33. Rutherford, A. W. (1985) Biochim. Biophys. Acta, 895, 189.

CHAPTER 6
FUTURE WORK

The ENDOR studies presented here show that this is a suitable technique for studying protein bound radicals and their local environments. We were able to obtain the unpaired spin density distribution on the aromatic tyrosine ring of the $Y_D^{\bullet}$ species. We determined the geometry of the β-protons with respect to the tyrosine ring and the orientation of the radical with respect to the membrane plane. The accessibility of the radical binding site was studied and a hydrogen-bonded proton was detected on the $Y_D^{\bullet}$ radical. The spatial characteristics of this H-bonded proton were investigated and the H-bond distance was determined.

One way to strengthen our assigments of the various lines on the $Y_D^{\bullet}$ ENDOR spectrum is by using ENDOR triple resonance techniques which will allow the determination of the sign of the hyperfine coupling constant. This will be specially useful for the resonances in the low frequency region (10-20 MHz), *i.e.*, α-protons at the 2-6 positions and the β-protons with the large dihedral angle. Another way of approaching this problem is by doing ENDOR *in vivo* of samples that are specifically labeled with isotopically substituted tyrosine. By performing these experiments the ENDOR lines corresponding to the α-protons at the 2-6 and 3-5 positions and to the β-protons can be unequivocally assigned in model samples. The results of these experiments can the be extrapolated to the $Y_D^{\bullet}$ radical. Even though the unpaired spin density distribution on the model

tyrosine is expected to be slightly different than the *in vivo* samples this approach provides way of testing our assigments of the Y_D^+ ENDOR spectra.

The torsional rotations of the aromatic tyrosine ring along the C_1 - C bond discussed in Chapter 4 can be further investigated. The changes in the high frequency ENDOR region (20-30 MHz) and the low frequency region (10-20 MHz) can be monitored as a function of temperature in the tyrosine samples (*in vitro*), where the β-protons are substituted by deuterium and compared to a control sample, *i.e.*, no isotopic substitution, over the same temperature range.

The Y_D^+ matrix ENDOR lines still need to be investigated. In liquids these lines average to zero by the rapid tumbling of the radical. So matrix ENDOR can be used to probe the amount of molecular motion as a function of the temperature. Therefore, the matrix ENDOR could also be used to investigated the torsional rotations mentioned above.

We have seen that the protein enviroment surrounding the radical plays an important role in determining the function and estability of the radical. One of the interactions that is likely to influence profoundly the behavior of the radical in the binding site is the H-bond. A direct way of studying this interaction is by studying the ENDOR spectrum of perdeuterated tyrosine (*in vitro*) in protonated solvent. We have seen that this interaction is not the same in all biological systems. For example, a strong hygrogen bond is observed on the Y_D^+ radical but in the enzyme RDPR this interaction is weaker as judged by its ENDOR spectrum. The strengh of the H-bond under different conditions can

also be investigated by using perdeuterated tyrosine *in vitro* in different solvent environments and by monitoring the changes in the ENDOR spectrum.

To obtain an accurate value of the unpaired spin density at the oxygen, the phenoxy ^{16}O can be replaced by ^{17}O. Since the hyperfine interaction with the oxygen is much larger than with the protons, they should be resolvable in the EPR spectrum and there should be no need for ENDOR. One would expect that each line in the $Y_D^{\bullet}$ spectrum will be split into a sextet arising from the interaction of the unpaired electron with the nucleus I = 5/2. The hyperfine coupling for ^{17}O (a_o) in the $Y_D^{\bullet}$ radical can be estimated by using the following equation (1):

$$a_o = Q_o\rho_o + Q_{C4}\rho_{C4} \qquad (1)$$

where a_o is the hyperfine coupling in gauss, Q_o and Q_{C4} are constants for the oxygen and carbon 4 with approximate values of -40.4 and -16.7 gauss, respectively, and ρ_o and ρ_{C4} are the unpaired spin density at the oxygen and the carbon directly attached to the oxygen (*i.e.*, carbon 4). With a ρ_o = 0.24 and ρ_{C4} = -0.04 for the $Y_D^{\bullet}$ species (Chapter 4), the multiplets mentioned above should have a hyperfine coupling of about 9 gauss. Most of these lines will overlap but the lines at the low field and the high field positions (*i.e.*, the lines at the beginning and the end of the EPR spectrum) are likely to be resolvable. The individual spin densities that can be calculated from Equation 1 and the hyperfine coupling measured are substantially dependent on the choice of Q's for the oxygen and

the carbon 4. Nevertheless this experiment will provide a direct way of calculating the unpaired spin density at the oxygen. In addition it may give some insight about the H-bond interaction.

Reference

1. Gulik, W., Jr. and Geske D.H. (1966) J. Am. Chem. Soc. 88, 4119.